Univerza v Ljubljani
Fakulteta za elektrotehniko

Marija Marčan

Načrtovanje zdravljenja globoko ležečih čvrstih tumorjev s terapijami na osnovi elektroporacije

DOKTORSKA DISERTACIJA

Mentor: prof. dr. Damijan Miklavčič

Ljubljana, 2015

University of Ljubljana

Faculty of Electrical Engineering

Marija Marčan

Pre-treatment planning for electroporation-based treatments of deep-seated solid tumors

DOCTORAL DISSERTATION

Mentor: prof. Damijan Miklavčič, Ph. D.

(University of Ljubljana, Slovenia)

Ljubljana, 2015

Univerza v Ljubljani
Fakulteta za elektrotehniko

Tržaška 25
p.p. 2999
1001 Ljubljana, Slovenija
telefon: 01 476 84 11
faks: 01 426 46 30
www.fe.uni-lj.si
e-mail: dekanat@fe.uni-lj.si

Senat Fakultete za elektrotehniko Univerze v Ljubljani je na seji dne, 13.06.2013 odobril kandidatki:

MARIJA MARČAN

temo za doktorsko disertacijo z naslovom:

NAČRTOVANJE ZDRAVLJENJA GLOBOKO LEŽEČIH ČVRSTIH TUMORJEV S TERAPIJAMI NA OSNOVI ELEKTROPORACIJE

PRE-TREATMENT PLANNING FOR ELECTROPORATION-BASED TREATMENTS OF DEEP-SEATED SOLID TUMORS

Komisija za doktorski študij Univerze v Ljubljani je po pooblastilu Senata Univerze v Ljubljani temo potrdila na seji dne: 03.07.2013.

Senat Fakultete za elektrotehniko Univerze v Ljubljani je kandidatki na seji dne, 11.06.2015 priznal naslednje izvirne prispevke k znanosti:

1 Postopek razgradnje medicinskih slik za načrtovanje zdravljenja globlje ležečih čvrstih tumorjev s terapijami na osnovi elektroporacije.

2 Študija vpliva žilnih struktur in napak razgradnje na porazdelitev električnega polja v tumorju.

3 Postopek vrednotenja in popravljanja rezultatov razgradnje medicinskih slik z ročnim popravljanjem obrisov.

4 Postopek za uporabo predznanj iz baze ovrednotenih rezultatov razgradenj za izboljšavo novih primerov razgradenj.

Komisija za zagovor doktorske disertacije:

prof. dr. Igor Papič, predsednik

prof. dr. Boštjan Likar, član

prof. dr. Gregor Serša, član

prof. dr. Ratko Magjarević, član

prof. dr. Damijan Miklavčič, mentor

Fakulteta za elektrotehniko • UNIVERZA V LJUBLJANI • 2

Dekan:

prof. dr. Igor Papič

Univerza *v Ljubljani*
Fakulteta *za elektrotehniko*

I Z J A V A

Spodaj podpisani/-a, Marija Marčan, z vpisno številko 64110514 s svojim podpisom izjavljam, da sem avtor/-ica zaključnega dela z naslovom:

Načrtovanje zdravljenja globoko ležečih čvrstih tumorjev s terapijami na osnovi elektroporacije
(Pre-treatment planning for electroporation-based treatments of deep-seated solid tumors)

S svojim podpisom potrjujem:

- da je predloženo zaključno delo rezultat mojega samostojnega raziskovalnega dela in da so vsa dela in mnenja drugih avtorjev skladno s fakultetnimi navodili citirana in navedena v seznamu virov, ki je sestavni del predloženega zaključnega dela,
- da je elektronska oblika zaključnega dela identična predloženi tiskani obliki istega dela,
- da na Univerzo v Ljubljani neodplačno, neizključno, prostorsko in časovno neomejeno prenašam pravici shranitve avtorskega dela v elektronski obliki in reproduciranja ter pravico omogočanja javnega dostopa do avtorskega dela na svetovnem spletu preko Repozitorija Univerze v Ljubljani (RUL).

V Ljubljani, 18.6.2015.

Podpis avtorja/-ice:

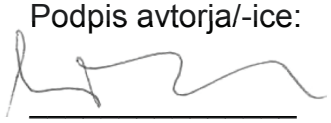

PREFACE

The present PhD thesis is a result of medical image segmentation algorithm development, phantoms research and numerical modeling carried out during the PhD study period at the Laboratory of Biocybernetics, Faculty of Electrical Engineering, University of Ljubljana. The results of the performed work have been published (or are in press) in the following international journals:

Paper 1: SEGMENTATION OF HEPATIC VESSELS FROM MRI IMAGES FOR PLANNING OF ELECTROPORATION-BASED TREATMENTS IN THE LIVER

MARCAN Marija, PAVLIHA Denis, MAROLT MUSIC Maja, FUCKAN Igor, MAGJAREVIC Ratko, MIKLAVCIC Damijan

Radiology and Oncology 48(3): 267-281, 2014.

Paper 2: EFFECT OF BLOOD VESSEL SEGMENTATION ON THE OUTCOME OF ELECTROPORATION-BASED TREATMENTS OF LIVER TUMORS

MARČAN Marija, KOS Bor, MIKLAVČIČ Damijan

PLoS ONE: 10(5): e0125591, 2015.

Paper 3: WEB-BASED TOOL FOR VISUALIZATION OF ELECTRIC FIELD DISTRIBUTION IN DEEP-SEATED BODY STRUCTURES AND FOR PLANNING ELECTROPORATION-BASED TREATMENTS

MARČAN Marija, PAVLIHA Denis, KOS Bor, FORJANIČ Tadeja, MIKLAVČIČ Damijan

Biomedical Engineering Online: in press, 2015.

Paper 4: MULTI-ATLAS SEGMENTATION OF MRI IMAGES ENHANCED WITH ATLAS SELECTION BASED ON IMAGING PROPERTIES AND RATER VARIABILITY

MARČAN Marija, MIKLAVČIČ Damijan

IEEE Transactions on Medical Imaging: submitted, 2015.

ACKNOWLEDGEMENTS

Being able to conduct this research was a true privilege, for which I am sincerely grateful to my mentor, prof. dr. Damijan Miklavčič. Thank you for making me feel like a part of the team from the very beginning, never doubting my capabilities and helping me navigate through all the rough waters of the research business.

I owe another big thank you to my MSc mentor, prof. dr. Ratko Magjarević, who had opened my path to Ljubljana in the first place.

An important factor in making this experience a privilege were the members of the Laboratory of Biocybernetics: you were my family away from home and made working with you a fun and happy experience. I am especially thankful to: Denis - for collaboration and expressing the need for an exchange student five years ago; Bor - for endless patience in teaching me numerical modeling tricks; Matej - for all discussions and thesis printing; Andraž - for being a great neighbor; Barbara - for being a true friend and keeping me sane. And to Lea.

Parts of research in this thesis would also not have been possible without the help of colleagues from the Institute of Oncology in Ljubljana, namely prof. dr. Gregor Serša who provided support in clinical matters, dr. Maja Mušič who contoured the vessels and dr. Robert Hudej, who provided prostate images - thank you all. I would also like to thank dr. Uroš Mitrović for the early discussions and advice that helped me kick start my work.

Boštjan - thank you for being right (most of the time) - especially regarding the 'you can do it' part. Your advice and support have truly carried me through the finish line.

Na kraju svega, ali nikako ne najmanje važno: dragi moji tata, mama i seka - hvala vam što ste uvijek uz mene i što nikada, nikada niste odustali, pogotovo kad je bilo najteže. Bez vas mi ovo ne bi uspjelo.

This research has been supported by Slovenian Research Agency under a Junior Research grant.

TABLE OF CONTENTS

ABSTRACT

Electroporation is a name for a phenomenon which occurs when a living cell is exposed to a sufficiently high electric field. In such a case changes occur in the cell membrane which increase its permeability. When the electric field is within well-established values, the process of electroporation is reversible and the cell membrane returns to its normal state after a period of time. The process of reversible electroporation enables molecules which normally lack membrane transport mechanisms to enter the cell. Such are some chemotherapeutic drugs for which membrane has low cellular permeability, but which have an intracellular target. Application of electroporation in combination with such chemotherapeutic drugs is successfully used to treat tumors. This tumor treating procedure has been named electrochemotherapy. Another electroporation-based treatment that is applicable in treating solid tumors relies on the process of irreversible electroporation. This procedure has been named Irreversible Electroporation and is used to destroy tumor tissue without the use of drug.

The prerequisite for a successful electroporation-based treatment is that the whole tumor is covered with a sufficiently high electric field. The electric field distribution depends on the position of electrodes relative to the tumor and the voltage applied per electrode pair. To ensure a complete coverage of a deep-seated solid tumor with sufficiently high electric field it is necessary to generate a numerical model of the electric field distribution prior to the electroporation-based procedure.

The numerical modeling procedure for electroporation-based treatment planning takes into account patient geometry obtained from medical images. The task of segmentation of medical images remains an open research topic which continues to yield new and improved methods. When applying medical image segmentation methods one must first define the

purpose of segmentation. The choice of segmentation procedure and possible parameter optimization is performed with respect to the type of tissue to be extracted and imaging modality.

This doctoral thesis presents an image segmentation framework which is intended to be used in pre-treatment planning for electroporation-based treatments of deep-seated solid tumors. The main goal of the framework is to minimize user interaction while maintaining the necessary level of robustness and accuracy in order to produce reliable treatment plans. In order to achieve this framework is designed in a form of a cycle which consists of three phases. In the first, segmentation phase, algorithms for automatic segmentation are run in order to give an initial segmentation of structures of interest. Namely, a new algorithm for automatic segmentation of hepatic vessels from MRI images was developed. The accuracy of the developed algorithm was assessed with respect to recent advances in medical image segmentation validation and having in mind the purpose of the segmentation. A part of the validation process included a sensitivity study to assess the impact of segmentation accuracy on treatment outcome and define the level of accuracy needed to ensure reliable pre-treatment planning for electroporation-based treatments.

In the second, validation phase, the users are provided with a web-based tool which enables them to validate the segmentation result of the first phase and perform corrections if necessary. The validation tool was designed so that it minimizes user interaction. Enabling the users to review, correct and validate the segmentation is a necessary step to ensure a correct segmentation while keeping the method robust regarding different image sources. The data gathered from segmentations which were validated by users provides a useful database of segmented cases. Such database can be further exploited to iteratively improve segmentation algorithms.

In the third, evolution phase, the validated segmentations from the second phase are used in order to improve the results of automatic segmentation algorithms from the first phase. The main idea of this phase is to explore how can existing images' meta-information such as imaging machine, protocol, coil type etc. along with information about rater variability be utilized in order to improve the results of automatic segmentation. This idea was implemented and tested in existing multi-atlas segmentation methods of prostate from MRI.

RAZŠIRJEN POVZETEK V SLOVENSKEM JEZIKU

UVOD

OSNOVNA NAČELA ELEKTROPORACIJE

Izpostavitev biološke celice dovolj visokemu električnemu polju povzroči povečano prepustnost celične membrane. To povečanje prepustnosti membrane omogoča prenos molekul, ki slabo ali pa sploh ne prehajajo skozi celično membrano. Opisani učinek električnega polja na celico imenujemo elektroporacija (Neumann et al. 1982; Kotnik et al. 2012). Elektroporacija se deli na reverzibilno in ireverzibilno. Reverzibilnost/ireverzibilnost elektroporacije je v korelaciji z amplitudo pulzov, njihovim trajanjem ter številom. V primeru reverzibilne elektroporacije se celična membrana po določenem času vrne nazaj v normalno stanje. V primeru ireverzibilne elektroporacije pa prihaja do celične smrti zaradi trajne porušitve strukture celične membrane ali zaradi izgube znotrajceličnih komponent (Davalos et al. 2005; Sano et al. 2010).

UPORABA ELEKTROPORACIJE V MEDICINI

V klinični praksi se elektroporacija danes uporablja kot del več različnih metod zdravljenja raka. Najpomembnejše izmed teh metod so elektrokemoterapija (Marty et al. 2006; Miklavčič et al. 2012), elektrogenska terapija (Heller & Heller 2010), cepljenje z DNA (Zhang et al. 2004) in atermična ablacija z ireverzibilno elektroporacijo (IRE) (Rubinsky et al. 2007; Garcia et al. 2011). Od teh se le elektrokemoterapija in IRE uporabljata za zdravljenje globlje ležečih čvrstih tumorjev (Edhemovic et al. 2014; Scheffer et al. 2014).

ELEKTROKEMOTERAPIJA

Elektrokemoterapija je metoda, ki združuje klasično kemoterapijo z reverzibilno elektroporacijo (Mir et al. 1991). Prednost elektrokemoterapije v primerjavi s klasično kemoterapijo je povečanje citotoksičnosti kemoterapevtikov, kot sta bleomicin in cisplatin, do katere pride zaradi povečane prepustnosti celične membrane po elektroporaciji (Serša et al. 1995; Mir et al. 2006).

Pri elektrokemoterapiji se pacientu najprej injicira citostatik, bodisi intravenozno ali neposredno v tumor. Potem se na območje tumorja preko elektrod dovedejo ustrezni električni pulzi z generatorjem pulzov posebej zasnovanim za ta namen (Reberšek et al. 2014). V primeru kožnih in podkožnih tumorjev se uporabljajo elektrode s fiksno geometrijo. Običajno gre za ploščate ali za polje majhnih igelnih elektrod, odvisno od vrste tumorja (Miklavcic et al. 2006). Čeprav obstajajo primeri, ko se igelne elektrode s fiksno geometrijo lahko uporabijo tudi za elektrokemoterapijo globlje ležečih tumorjev, je položaj in velikost globokih tumorjev običajno takšen, da zahteva uporabo več posameznih, dolgih igelnih elektrod. V primeru uporabe dolgih igelnih elektrod položaj elektrod variira glede na posameznega bolnika in geometrijo tumorja.

IREVERZIBILNA ELEKTROPORACIJA (IRE)

Povzročitev celične smrti z ireverzibilno elektroporacijo se danes uporablja kot metoda atermične ablacije tkiva (Rubinsky et al. 2007; Jiang et al. 2015). Posebnost ireverzibilne elektroporacije leži v tem, da ne povzroči bistvenega toplotnega učinka (Davalos et al. 2005), za razliko od nekaterih drugih oblik lokalne ablacije, kot sta recimo radiofrekvenčna ablacija ter krioablacija. Prav tako je dokazano, da ireverzibilna elektroporacija po terapiji ohranja zunajcelični matriks, glavne žile in druge občutljive strukture (Al-Sakere et al. 2007). Postopek izvajanja IRE terapije je zelo podoben elektrokemoterapiji, razen tega, da se pri IRE ne uporabljajo citostatiki. Ker se IRE običajno izvaja v globoko ležečih tumorjih in notranjih organih, se za dovajanje električnih pulzov uporabljajo dolge, posamične igelne elektrode. Tako kot pri elektrokemoterapiji se položaj elektrod spreminja glede na posameznega bolnika in geometrijo tumorja.

PARAMETRI ZA UČINKOVITO ELEKTROPORACIJO TKIV

Ključni pogoj, ki mora biti izpolnjen, da bi prišlo do elektroporacije, je vzpostavitev dovolj močnega električnega polja (Miklavcic et al. 1998; Miklavcic et al. 2006). V praksi se potrebna jakost električnega polja definira glede na dva praga: prag reverzibilne elektroporacije in prag ireverzibilne elektroporacije. Za doseg reverzibilne elektroporacije mora biti električno polje nad pragom reverzibilne elektroporacije, vendar manjše od praga ireverzibilne elektroporacije. V primeru ireverzibilne elektroporacije zadošča, da je jakost električnega polja nad pragom ireverzibilne elektroporacije (Kotnik et al. 2012).

Uspeh elektroporacije je na splošno odvisen od več dejavnikov. Glavni dejavniki so parametri dovedenih električnih pulzov: njihovo število, amplituda, trajanje in ponavljalna frekvenca (Pucihar et al. 2011). Ko gre za elektroporacijo tkiv, in sicer za elektrokemoterapijo in IRE, so ti parametri danes dokaj standardizirani. Drugi dejavnik, ki je zelo pomemben pri elektroporaciji tkiva, je porazdelitev električnega polja, ki pa je odvisna od električnih lastnosti tkiva, razdalje med elektrodami in parametrov električnih pulzov, predvsem njihove amplitude in števila (Miklavcic et al. 1998; Garcia et al. 2014). Prav tako so ugotovili, da se električne lastnosti tkiva, in sicer predvsem električna prevodnost, zaradi elektroporacije poveča. Ta sprememba nato posledično vpliva na porazdelitev električnega polja (Šel et al. 2005; Pavselj et al. 2005; Cukjati et al. 2007; Ivorra & Rubinsky 2007; Neal et al. 2012).

Če vzamemo v poštev vse zgoraj navedene dejavnike, postane zagotavljanje nujnih pogojev za uspešno zdravljenje globlje ležečih tumorjev s terapijami, ki temeljijo na elektroporaciji, težavno. Optimalne parametre zdravljenja za vsakega posameznega bolnika, glede na spremenljivo geometrijo tumorja in bližnjih kritičnih struktur, ni možno določiti s pomočjo standardnih postopkov in navodil. Rešitev tega problema je na voljo le v obliki bolniku prilagojenega načrtovanja zdravljenja.

NAČRTOVANJE ZDRAVLJENJA ZA ELEKTROPORACIJO GLOBLJE LEŽEČIH TUMORJEV

Načrtovanje zdravljenje je že uveljavljeno kot pomemben proces v več različnih metodah zdravljenja raka, kot so radioterapija (Lecchi et al. 2008), krioterapija (Butz et al. 2000), lasersko inducirana intersticijska termoterapija (Schwarzmaier et al. 1998), radiofrekvenčna

ablacija (Chen et al. 2009) in ostale. Pri teh načrtovanje zdravljenje ne omogoča le rutinske izvedbe zdravljenja, ampak je ključno tudi za uspešnost terapije. Skupna značilnost načrtovanja zdravljenja pri vseh zgoraj omenjenih metodah je, da se zanašajo na geometrijski model bolnika pridobljen iz medicinskih slik, na podlagi katerega se s postopki optimizacije izračunajo optimalni parametri za izvedbo zdravljenja.

Prvi koraki v smeri uporabe podobnih načel za načrtovanje terapij, ki temeljijo na elektroporaciji, so bili narejeni z razvojem numeričnih modelov elektroporacije (Pavselj et al. 2005) in spremembe prevodnosti tkiva po elektroporaciji (Šel et al. 2005). Navedeni modeli so temeljili na preprostih geometrijskih oblikah in so upoštevali le značilnosti tarčnega tkiva. Kasneje so bili v modele vključeni tudi algoritmi za optimizacijo, ki računajo napetost, ki jo je potrebno dovesti na različne pare elektrod, da bi dosegli popolno pokritost tumorja z dovolj visokim električnim poljem (Županič et al. 2008; Corovic et al. 2008). Nazadnje so bile modelom dodane še 3D geometrije drugih tkiv in struktur, ki obkrožajo tumor, pri čemer je bil postopek optimizacije parametrov prilagojen tako, da poskuša zmanjšati delež ne-tumorskih tkiv, pri katerih bi lahko prišlo do ireverzibilne elektroporacije (Županič & Miklavčič 2010; Kos et al. 2010b; Miklavcic et al. 2010). Za namen vključevanja natančne 3D geometrije bolnika v model je bilo potrebno uporabiti postopke razgradnje medicinskih slik (Pavliha et al. 2012).

SPLETNO ORODJE ZA NAČRTOVANJE ZDRAVLJENJA

Načrtovanje zdravljenja globlje ležečih tumorjev s terapijami, ki temeljijo na elektroporaciji, kot je danes v uporabi, je proces v katerem imajo tako razgradnja medicinskih slik kot numerično modeliranje enako pomembno vlogo (Zupanic et al. 2012). Ta enoten postopek načrtovanja zdravljenja je bil prvič uporabljen v klinični študiji elektrokemoterapije jetrnih metastaz raka debelega črevesa (Edhemovic et al. 2011; Edhemovic et al. 2014). Z namenom podpore tej študiji so bili razviti ter tudi ovrednoteni posebni algoritmi za avtomatsko razgradnjo medicinskih slik jeter (Pavliha, Mušič, et al. 2013). Čeprav je bila uporaba načrtovanja zdravljenja v omenjeni klinični študiji uspešna (Edhemovic et al. 2014), je kljub vsemu potrebno opraviti še nekaj ključnih korakov, preden se načrtovanje zdravljenja za terapije, ki temeljijo na elektroporaciji, lahko začne redno uporabljati tudi v kliniki. Glavni

izziv, ki ga je potrebno premagati, je zajetje celotnega inženirskega znanja v metode, ki se lahko izvajajo z minimalno interakcijo uporabnika, hkrati pa zagotavljajo potrebno raven natančnosti in robustnosti.

Ena izmed rešitev prilagajanja postopka načrtovanja zdravljenja v smeri vsakdanje rabe je spletno orodje za načrtovanje zdravljenja (Pavliha, Kos, et al. 2013). Takšno orodje je sestavljeno iz dveh glavnih delov: strežnika in vmesnika. Na strani strežnika orodje vsebuje podatkovno bazo in izvaja vse potrebne algoritme. Preko grafičnega uporabniškega vmesnika uporabnik lahko nalaga slike pacientov, izbira proces načrtovanja zdravljenja glede na organ in prejme rezultate načrtovanja.

Poleg modulov za avtomatsko razgradnjo medicinskih slik in numerično modeliranje porazdelitve električnega polja, orodje vsebuje še nekaj dodatnih modulov. Eden izmed modulov je namenjen vrednotenju in popravljanju rezultatov avtomatske razgradnje medicinskih slik. V primeru organov ali struktur, kjer avtomatska razgradnja iz medicinskih slik ni možna, ali še ni podprta, je uporabniku omogočeno ročno vrisovanje kontur. Ne nazadnje, za proces načrtovanja zdravljenja orodje potrebuje tudi vključitev elektrod v 3D model. Zaradi raznolikosti komercialno razpoložljivih elektrod in različnih možnih vstopnih poti elektrod se orodje za določitev teh parametrov zanaša na uporabnika.

RAZGRADNJA MEDICINSKIH SLIK

Razgradnja medicinskih slik je postopek razdelitve slike na objekte, oziroma organe in anatomske strukture, bodisi ročno ali pa z uporabo računalniškega algoritma. V širšem smislu in še posebej v primeru računalniško podprte razgradnje so se postopki razširili v takšni meri, da termin 'razgradnja' vključuje še različne metode pred-obdelave in lokalizacije tarčnega objekta (Wong 2005; Withey & Koles 2008).

Z vidika uporabnosti je razgradnja medicinskih slik nedvomno ključni del številnih rutinskih kliničnih metod. Te metode ne vključujejo le diagnostike, temveč tudi bolj kompleksne dejavnosti, kot sta intraoperativna navigacija ter načrtovanje zdravljenja. V klinični praksi, za zlati standard pri razgradnji medicinskih slik danes še zmeraj velja radiološko mnenje in ročno vrisovanje, vendar je tak način razgradnje izjemno dolgotrajen in naporen. Poleg tega, da je s

tem oteženo rutinsko izvajanje celotnega kliničnega postopka, prihaja pri ročni razgradnji medicinskih slik tudi do težav zaradi variabilnosti med različnimi ocenjevalci in tudi na nivoju posameznega ocenjevalca (Warfield et al. 2004). Algoritmi za avtomatsko razgradnjo medicinskih slik lahko odpravijo težave povezane z variabilnostjo in trajanjem postopka razgradnje (Klein et al. 2008).

Čeprav se na področju obdelave medicinskih slik danes pojavljajo novi, boljši algoritmi za avtomatsko razgradnjo hitreje kot kdaj koli prej, je tveganje neposredne uporabe rezultatov avtomatske razgradnje v kliniki še zmeraj visoko. Zaradi tega bi bilo koristno, morda celo obvezno, zagotoviti dodatni mehanizem vrednotenja in morebitnega popravljanja rezultatov avtomatske razgradnje s strani strokovnjakov (kirurgov in radiologov) (Warfield et al. 2004; Saad et al. 2010; Deeley et al. 2013). Če se takšen mehanizem vrednotenja združi v enotno rešitev skupaj z algoritmom za avtomatsko razgradnjo, omogoča ta združitev izgradnjo baze podatkov, ki bi vsebovala razgrajene primere, ki bi bili hkrati potrjeni s strani strokovnjakov. Navedena baza podatkov bi se potem lahko uporabila za izboljševanje samega algoritma za avtomatsko razgradnjo. Eden izmed primerov opisane enotne rešitve je tudi spletno orodje za načrtovanje zdravljenja s terapijami, ki temeljijo na elektroporaciji.

METODE

POSTOPEK RAZGRADNJE MEDICINSKIH SLIK ZA NAČRTOVANJE ZDRAVLJENJA GLOBLJE LEŽEČIH ČVRSTIH TUMORJEV S TERAPIJAMI NA OSNOVI ELEKTROPORACIJE

Metoda, ki sem jo razvila z namenom razgradnje jetrnih žil iz slik zajetih z magnetno resonanco (MRI), temelji na postopkih ojačevanja cevastih struktur in lokalnega upragovljanja. Pred osnovno metodo razgradnje najprej izvedemo zelo pomemben korak predprocesiranja, v katerem s pomočjo filtriranja odpravimo prostorsko nehomogenost sivinskih vrednosti, do katerih prihaja zaradi nehomogenosti magnetnega polja same MRI naprave (Vovk et al. 2007). Tako pripravljeno sliko maskiramo s predhodno pridobljenim rezultatom razgradnje jeter, nato pa uporabimo 3D filter, ki ojača cevaste strukture na večjih nivojih ločljivosti. Sam filter je zasnovan na analizi medsebojnih odnosov lastnih vrednosti matrike drugih odvodov slike (Frangi et al. 1998). Rezultat ojačevanja cevastih struktur je slika, kjer večja vrednost intenzitete določenega piksla pomeni, da je večja možnost, da ta piksel pripada cevasti strukturi. Z upragovljanjem rezultata ojačevanja cevastih struktur in analizo povezanih

objektov potem določimo lokacije žilnih segmentov. Končne robove žil določimo z lokalnim upragovljanjem izvirne slike na področjih okoli predhodno določenih lokacij žilnih segmentov, pri čemer vrednost praga izračunamo za vsako področje posebej z metodo, ki temelji na minimizaciji variance (Otsu 1979). Končni koraki razgradnje so namenjeni izpopolnjevanju rezultatov in vključujejo postopek rasti regij ter morfološko odpiranje za odpravo majhnih, nepovezanih komponent. Rezultati posameznih korakov razgradnje so prikazani v Sliki 1.

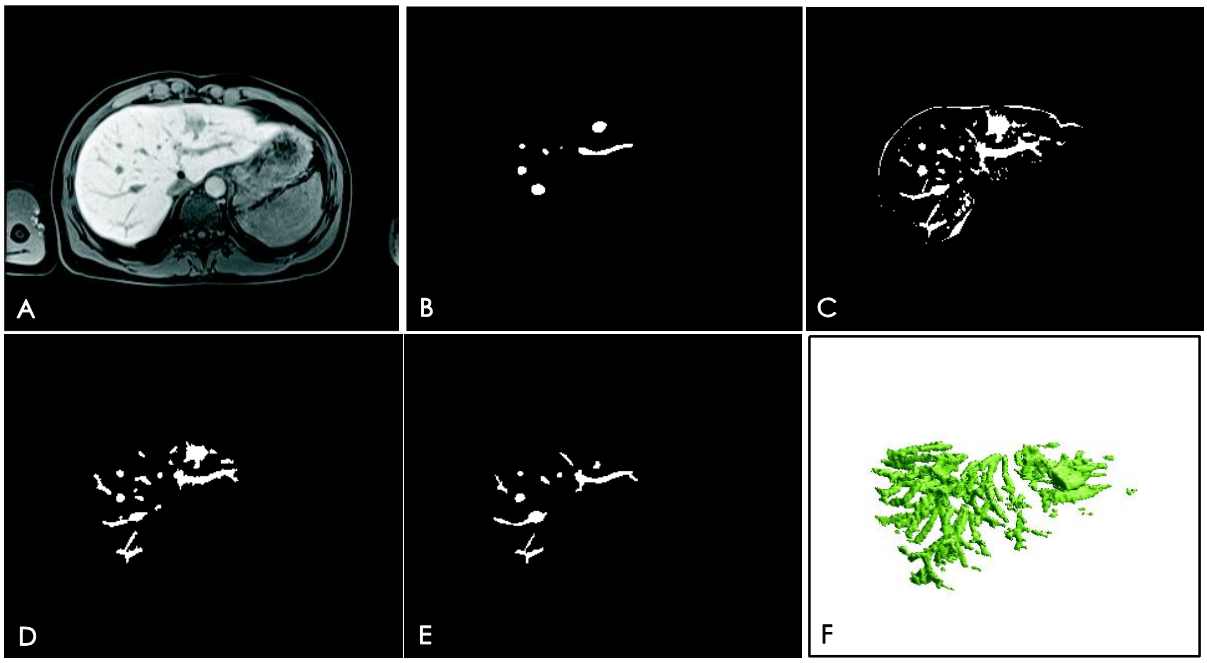

Slika 1. Rezultati posameznih korakov razgradnje jetrnih žil iz MRI slik. A. Izvirna MRI slika. B. Po odpravljeni prostorski nehomogenosti sivinskih vrednosti. C. Rezultati ojačevanja cevastih struktur. D. Po upragovljanju rezultatov ojačevanja cevastih struktur. E. Rezultati lokalnega upragovljanja. F. Končni 3D rezultat razgradnje.

Vrednotenje razvite metode razgradnje je bilo opravljeno na podlagi fantomov in slik realnih pacientov. Fantomi so bili narejeni iz plastičnih kozarcev napolnjenih z agarjem, v katere so bile v dveh različnih položajih vstavljene steklene cevke različnih velikosti (premer 4 mm, 6 mm in 8 mm) napolnjene s fiziološko raztopino (0,9% NaCl). V tem modelu je agar predstavljal jetra, medtem ko so cevke predstavljale žile. Vsi fantomi so bili slikani v MRI napravi istočasno. Primer fantoma z različnim položajem cevke je prikazan na Sliki 2.

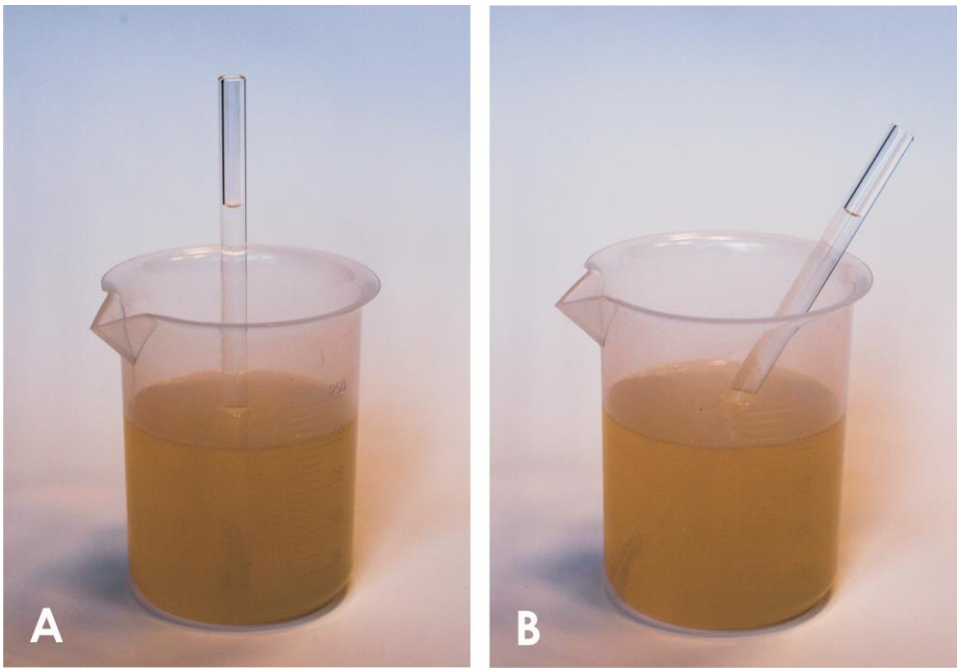

Slika 2. Fantom za vrednotenje metode razgradnje jetrnih žil iz MRI slik. A. Steklena cevka v navpičnem položaju. B. Steklena cevka v nagnjenem položaju.

Vrednotenje na realnih primerih je bilo narejeno na slikah šestih pacientov, ki so bili pred tem zdravljeni z elektrokemoterapijo kot del klinične študije zdravljenja jetrnih metastaz raka debelega črevesa (Edhemovic et al. 2014). Zlati standard so v navedenih slikah predstavljale konture, ki jih je ročno vrisala radiologinja.

ŠTUDIJA VPLIVA ŽILNIH STRUKTUR IN NAPAK RAZGRADNJE NA PORAZDELITEV ELEKTRIČNEGA POLJA V TUMORJU

Za namene določanja vpliva bližine žilnih struktur na porazdelitev električnega polja v tumorju sem izvedla numerično analizo na osnovi preprostega modela tumorja in žil, različnih velikosti in relativnih položajev glede na tumor, ki je bil sestavljen iz krogle in valja. V modelu sem spreminjala velikosti krogle (tumorja) in valja (žile) ter tudi razdaljo med tumorjem in žilo ter položaj valja v odnosu na elektrode (navpično ali paralelno). Za vse možne kombinacije sem izračunala optimalne vrednosti parametrov za uspešno pokritje celotnega tumorja z dovolj močnim električnim poljem v primeru, ko model ne vključuje žile. Potem sem tako dobljene parametre uporabila na modelu, ki žilo vključuje, in določevala spremembe v porazdelitvi električnega polja. Grafični prikaz modela z različnim položajem žil v odnosu na elektrode je prikazan na Sliki 3.

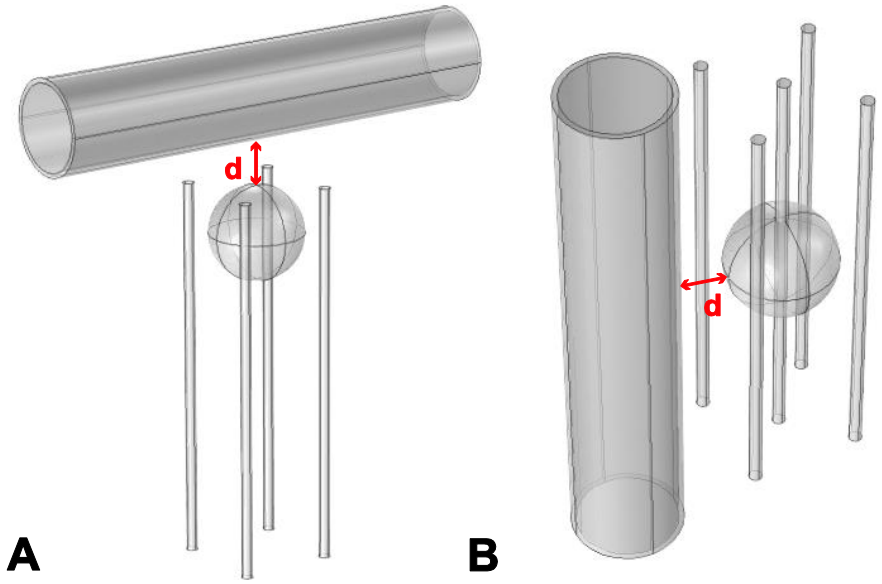

Slika 3. Teoretični model žile v bližini tumorja. A. Različica z žilo, ki je položena navpično v odnosu na elektrode. B. Različica z žilo paralelno z elektrodami.

Za namene določanja vpliva napak avtomatske razgradnje jetrnih žil na porazdelitev električnega polja med zdravljenjem jetrnih tumorjev s terapijami, ki temeljijo na elektroporaciji, sem opravila analizo dveh modelov pridobljenih iz medicinskih slik resničnih bolnikov. V navedene modele sem uvedla različice napak metode za avtomatsko razgradnjo žil ter opazovala vpliv na porazdelitev električnega polja.

POSTOPEK VREDNOTENJA IN POPRAVLJANJA REZULTATOV RAZGRADNJE MEDICINSKIH SLIK Z ROČNIM POPRAVLJANJEM OBRISOV

Rezultati avtomatske razgradnje medicinskih slik so znotraj spletnega orodja za načrtovanje terapij, ki temeljijo na elektroporaciji, prikazani kot 2D obrisi, ki so izrisani na originalnih rezinah. Za potrebe vrednotenja in popravljanja teh rezultatov sem ustvarila metodo, ki uporabniku omogoča preprosto spreminjanje prikazane konture. Sam obris je za ta namen poenostavljen in prikazan na zaslonu kot množica povezanih točk, katerim lahko uporabnik z uporabo računalniške miške spreminja položaj. Število točk je na začetku nastavljeno na 20% prvotnega števila točk obrisa. Zmanjšanje števila točk obrisa temelji na meri vpliva določene točke, ki se izračuna na podlagi kota in dolžine med sosednjimi robovi obrisa (Latecki & Lakämper 1999). Dodatno pa lahko tudi sam uporabnik spreminja 'gostoto' obrisa, ki je izražena kot odstotek začetnega števila točk, in sicer lahko to naredi na ravni vsake

posamezne rezine. V primeru, da se uporabnik odloči spremeniti gostoto obrisa potem ko je nekaterim točkam že spremenil lokacijo, se spremenjeni del obrisa rekonstruira s pomočjo prileganja kubične interpolacijske krivulje. Na ta način rekonstruirani odsek postane del celotnega obrisa, na podlagi katerega se lahko znova naredi redčenje točk.

POSTOPEK ZA UPORABO PREDZNANJ IZ BAZE OVREDNOTENIH REZULTATOV RAZGRADENJ ZA IZBOLJŠAVO NOVIH PRIMEROV RAZGRADENJ

Ker v primeru algoritma za razgradnjo jetrnih žil iz MRI slik, ki sem ga razvila v prvem delu svojega doktorata, ni bilo nobenih parametrov, ki bi jih lahko optimizirali na podlagi baze ovrednotenih rezultatov, sem dodatno implementirala še algoritem za razgradnjo prostate, prav tako iz MRI slik. Implementirani algoritem temelji na poravnavi že obstoječih razgrajenih slik z neznano sliko in zlitju poravnanih oznak v enotno razgradnjo (Litjens et al. 2012). Pri opisani metodi ima velik vpliv na končni rezultat in čas izvajanja razgradnje izbira podmnožice že razgrajenih primerov, ki bodo uporabljeni za razgradnjo neznanega primera. V svojem delu sem predlagala nov način izbire navedene podmnožice, ki temelji na parametrih zajetih slik, ki so zapisani v DICOM datoteki MRI slike, ter na osnovi variabilnosti ocenjevalca, ki je ovrednotil že razgrajeni primer. Predlagano metodo sem preizkušala tudi na javno dostopni bazi razgrajenih prostat iz štirih različnih inštitucij (Litjens et al. 2014).

REZULTATI IN RAZPRAVA

Rezultati dela opravljenega v sklopu tega doktorata kažejo, da so razviti postopki avtomatske razgradnje medicinskih slik v kombinaciji z uporabniku prijaznim načinom vrednotenja in popravljanja dovolj natančni in robustni, da se lahko uporabljajo tudi v kliniki.

Na osnovi vrednotenja avtomatske metode za razgradnjo jetrnih žil iz MRI slik na podlagi fantomov in realnih primerov sem ocenila, da lahko metoda v povprečju povzroči napako v velikosti 0,89 mm, medtem ko je ta napaka v najslabšem primeru lahko 4,04 mm.

V kontekstu zdravljenja globlje ležečih tumorjev, kot so jetrni tumorji, s terapijami, ki temeljijo na elektroporaciji, dobi ta ocenjena vrednost napake smisel le, če se opazuje njen vpliv na morebitne napake pri samem načrtovanju zdravljenja. Ker vpliv žil na porazdelitev električnega polja v področju tumorja še nikoli ni bil določen, sem najprej na podlagi enostavnega teoretičnega modela ocenila kako velike žile in pri kakšni razdalji od tumorja

lahko negativno vplivajo na rezultat zdravljenja z elektroporacijo. Rezultati teh modelov kažejo, da imajo lahko negativen vpliv na pokritost tumorja z dovolj močnim električnim poljem že žile s premerom 3 mm in več, ki so od tumorja oddaljene manj kot 5 mm. Čeprav je morebiten negativen vpliv odvisen še od števila elektrod in položaja žile glede na elektrode, je potrebno žile premera 3 mm in več kljub vsemu upoštevati že v modelih za načrtovanje zdravljenja z elektroporacijo. Glede vrednotenja vpliva napake metode za avtomatsko razgradnjo jetrnih žil rezultati kažejo, da je metoda dovolj robustna, da ne povzroča negativnega vpliva na pokritost tumorja z električnim poljem, vendarle samo, če konfiguracija elektrod pri izvajanju terapije vključuje tudi elektrodo, ki je vstavljena v sredino tumorja.

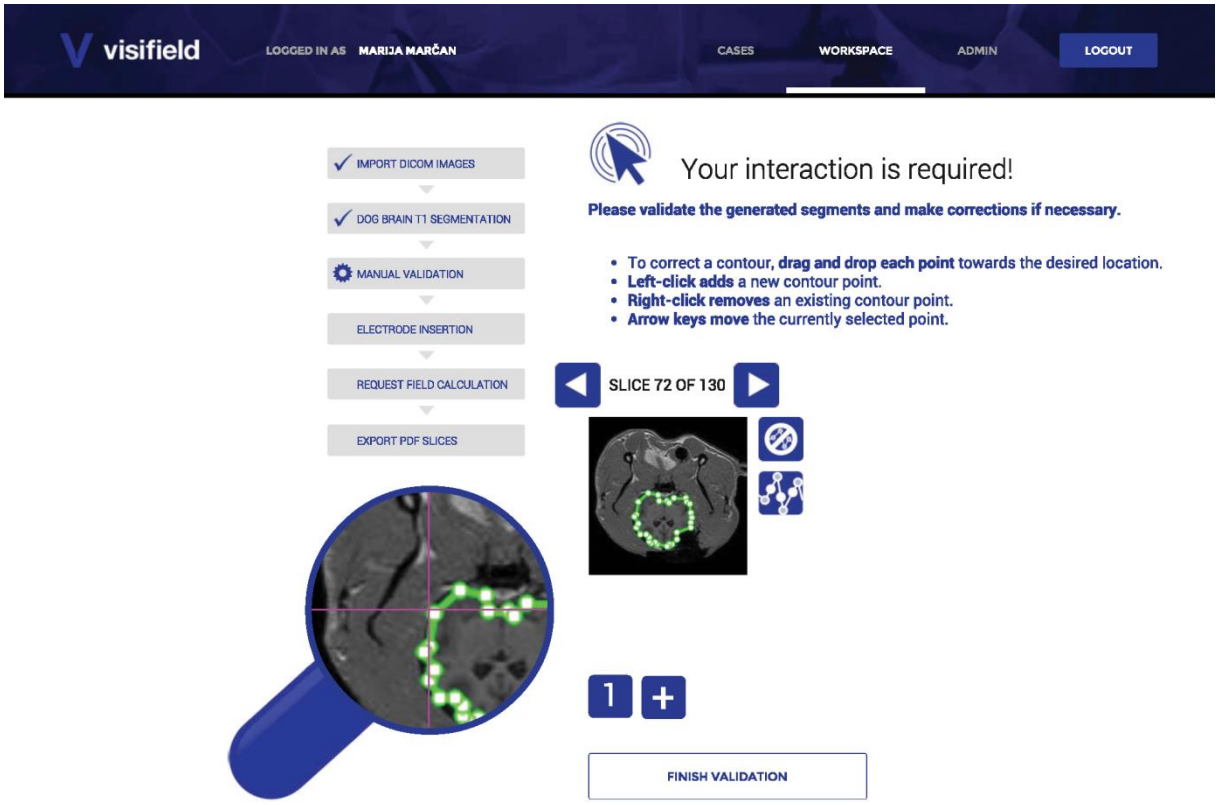

Slika 4. Modul za vrednotenje in popravljanje rezultatov avtomatske razgradnje medicinskih slik.

Tudi v primeru, da algoritem za avtomatsko razgradnjo jetrnih žil povzroči napako, ki je večja od ocenjene povprečene napake, ima uporabnik še zmeraj možnost tako napako popraviti znotraj spletnega orodja za načrtovanje. Modul, ki omogoča vrednotenje in popravljanje rezultatov segmentacije je prikazan na Sliki 4. Navedeni modul, skupaj s celotnim orodjem za načrtovanje, je že bil ocenjen s strani treh klinikov in dveh strokovnjakov s področja

načrtovanja zdravljenja iz štirih različnih inštitucij. Tako mnenja uporabnikov kot merjenje časa, ki so ga porabili za vrednotenje rezultatov razgradnje s predlaganim orodjem, kažejo, da je metoda popravljanja dovolj prilagodljiva in hkrati enostavna za uporabo s strani klinikov.

Obetavne rezultate smo bili dobili tudi pri vrednotenju predlaganega postopka izbire najbolj primernih predhodno razgrajenih slik za razgradnjo novih. Če se predlagani postopek uporabi v algoritmu za avtomatsko razgradnjo prostate, je končna povprečna vrednost mere podobnosti (ie »Dice koeficient«) za 2% večja, kot če bi uporabili vse dostopne predhodno razgrajene primere. Poleg tega je čas same razgradnje zmanjšan za vsaj 50%. V primerjavi z že obstoječimi postopki izbire obstoječih primerov je končni rezultat pridobljen s predlagano metodo le nekoliko boljši (0.5%), vendar je statistično značilno boljši. Dejstvo pa je, da je vrednotenje izvedeno na podlagi le petdesetih primerov, medtem ko je predlagana metoda namenjena večjim bazam že obstoječih primerov.

ZAKLJUČKI

Glavni namen predstavljene disertacije je bil raziskati zmožnost uporabe postopkov za avtomatsko razgradnjo medicinskih slik v postopku načrtovanja zdravljenja globlje ležečih čvrstih tumorjev s terapijami, ki temeljijo na elektroporaciji. Ker je osnovna hipoteza bila, da noben avtomatski algoritem za razgradnjo ne more biti dovolj zanesljiv, da bi lahko popolnoma odpravil potrebo po človeškem mnenju, so avtomatske metode razgradnje dopolnjene še z ergonomsko metodo za enostavno vrednotenje in popravljanje morebitnih napak pri razgradnji.

Vključitev razvitih metod razgradnje in vrednotenja v enotno orodje, kot je spletno orodje za načrtovanje terapij, ki temeljijo na elektroporaciji, ima za posledico kopičenje strokovno ovrednotenih primerov. Takšno bazo primerov je možno uporabiti za izboljšavo razgradnje novih primerov, kar je tudi uspešno implementirano in ovrednoteno v tej disertaciji.

Ne nazadnje je uporaba postopkov za avtomatsko razgradnjo medicinskih slik v kombinaciji z mehanizmom vrednotenja in popravljanja, ki zagotavlja pravilnost geometrijskega modela pacienta, zelo pomemben pogoj za avtomatizacijo celotnega postopka načrtovanja zdravljenja. Nujnost uporabe specifičnega inženirskega znanja o elektroporaciji in predvsem

porazdelitvi električnega polja je, kljub obetavnim rezultatom, eden izmed glavnih razlogov, zakaj je širjenje zdravljenja globlje ležečih tumorjev z elektroporacijo v klinično rabo danes počasen proces. S končno avtomatiziranim celotnim procesom načrtovanja zdravljenja upamo, da bo zdravljenje, ki temelji na elektroporaciji, postalo dostopno tudi kot standardna terapija bolnikom z globlje ležečimi tumorji in ne bo ostalo le del znanstvenih raziskav.

IZVIRNI PRISPEVKI K ZNANOSTI

POSTOPEK RAZGRADNJE MEDICINSKIH SLIK ZA NAČRTOVANJE ZDRAVLJENJA GLOBLJE LEŽEČIH ČVRSTIH TUMORJEV S TERAPIJAMI NA OSNOVI ELEKTROPORACIJE

Algoritem za razgradnjo kritičnih struktur (cevastih struktur, kot so na primer velike žile v jetrih) zagotavlja natančen, bolniku prilagojen geometrijski model za numerično modeliranje postopkov zdravljenja, ki temeljijo na elektroporaciji, in posledično pripravi bolniku prilagojen načrt zdravljenja. Načrti zdravljenja, ki so prilagojeni bolniku, so nujni predpogoj zdravljenja globlje-ležečih čvrstih tumorjev s terapijami, ki temeljijo na elektroporaciji. Algoritmi razgradnje z minimalno zahtevano interakcijo uporabnika bistveno zmanjšujejo čas, ki je potreben za izdelavo posameznega načrta zdravljenja z elektroporacijo. Poenostavitev procesa načrtovanja zdravljenja z vidika klinikov hkrati ustvarja spodbudnejše okolje za uporabo terapij, ki temeljijo na elektroporaciji, za zdravljenje globlje ležečih čvrstih tumorjev v novih področjih človeškega telesa. V svojem delu sem razvila nov algoritem za avtomatsko razgradnjo jetrnih žil iz magnetnoresonačnih (MRI) slik. Delovanje razvitega algoritma sem ovrednotila na podlagi primerov, ki jih je ročno razgradila radiologinja.

ŠTUDIJA VPLIVA ŽILNIH STRUKTUR IN NAPAK RAZGRADNJE NA PORAZDELITEV ELEKTRIČNEGA POLJA V TUMORJU

Izločanje geometrijskega modela anatomije bolnika neizogibno proizvaja tudi napake. Da bi zagotovili robustnost načrtovanja zdravljenja, je potrebno oceniti potencialni vpliv takšnih napak na porazdelitev električnega polja. V drugem delu svojega doktorata sem se zato osredotočila na določanje vpliva napak avtomatske razgradnje jetrnih žil na porazdelitev električnega polja med zdravljenjem jetrnih tumorjev s terapijami, ki temeljijo na elektroporaciji. Najprej sem izvedla numerično analizo na osnovi preprostega modela tumorja

in žil različnih velikosti in relativnih položajev, ki je bil sestavljen iz krogle in valja. Potem sem opravila analizo dveh modelov, ki so bili pridobljeni iz medicinskih slik resničnih bolnikov, v katere sem uvedla različice napak metode za avtomatsko razgradnjo žil.

POSTOPEK VREDNOTENJA IN POPRAVLJANJA REZULTATOV RAZGRADNJE MEDICINSKIH SLIK Z ROČNIM POPRAVLJANJEM OBRISOV

Desetletja razvoja na področju razgradnje medicinskih slik so pokazala, da še vedno ni mogoče v celoti odpraviti človeškega faktorja iz postopka razgradnje. Glede na visoko stopnjo zahtev za robustnost metod za razgradnjo medicinskih slik, kot so zastavljene za postopke načrtovanja terapij, je očitno, da je človeško mnenje nujno za zagotovitev veljavnih 3D modelov. Človeško mnenje se lahko uporabi po začetnem postopku razgradnje kot določena oblika mehanizma potrjevanja z namenom zagotavljanja potrebne ravni zanesljivosti. Da bi olajšala ta postopek potrjevanja, sem razvila metodo, ki zahteva interakcijo uporabnika, pri kateri se čas in napor potreben za opravljanje vrednotenja bistveno zmanjša. Takšen mehanizem potrjevanja razgradnje ne le pomaga zagotoviti veljavnost načrtov zdravljenja, ampak ponuja tudi dragocene povratne informacije o uspešnosti algoritma za razgradnjo.

POSTOPEK ZA UPORABO PREDZNANJ IZ BAZE OVREDNOTENIH REZULTATOV RAZGRADENJ ZA IZBOLJŠAVO NOVIH PRIMEROV RAZGRADENJ

Zbiranje povratnih informacij preko vrednotenja in popravljanja razgradnje s strani uporabnikov povzroči oblikovanje podatkovne baze razgrajenih primerov. Takšna baza se lahko uporabi tako kot vir za pridobivanje globljega vpogleda v uspešnost algoritmov kot tudi za izboljšavo samega algoritma. Medtem ko se razgradnja medicinskih slik s strani strokovnjakov še zmeraj obravnava kot zlati standard in postopek, ki je bolj zanesljiv kot računalniško podprta razgradnja, ostaja dejstvo, da je tudi človeška razgradnja podvržena napakam. Različne mere, kot so recimo variabilnost med različnimi ocenjevalci in variabilnost posameznega ocenjevalca, se pogosto uporabljajo za kvantitativno določevanje kakovosti človeške razgradnje. V svojem delu sem razvila pristop za sistematično vključitev znanja o variabilnosti ocenjevalcev ter znanja o parametrih pridobljenih medicinskih slik v obstoječe algoritme za avtomatsko razgradnjo medicinskih slik z namenom izboljšanja rezultatov

razgradnje novih primerov. Navedeno znanje je mogoče pridobiti iz obstoječih, že razgrajenih primerov, ki so shranjeni v bazi podatkov.

INTRODUCTION

BASIC PRINCIPLES OF ELECTROPORATION

Exposing a biological cell to a sufficiently high electric field causes increased permeability of the cell membrane. This increased permeability of the membrane allows transfer of molecules which normally lack membrane transport mechanisms. The described effect of the electric field on the cell is called electroporation (Neumann et al. 1982; Kotnik et al. 2012). Electroporation can be classified as either reversible or irreversible. The reversible/irreversible nature of electroporation is in strong correlation with pulse amplitude, duration and number of pulses. In reversible electroporation, the cell membrane eventually returns to its normal state. Irreversible electroporation however leads to cell death because the cell membrane is permanently disrupted or due to the extensive loss of the intracellular components (Davalos et al. 2005; Sano et al. 2010).

APPLICATIONS OF ELECTROPORATION IN MEDICINE

There are many applications of electroporation which are being successfully introduced into clinical practice (Yarmush et al. 2014) such as electrochemotherapy (ECT) (Marty et al. 2006; Miklavčič et al. 2012), electroporation based gene transfer for gene therapy (Heller & Heller 2010), DNA vaccination (Zhang et al. 2004) and non-thermal irreversible electroporation ablation (N-TIRE) (Rubinsky et al. 2007; Garcia et al. 2011). Of the above mentioned applications only ECT and IRE are being used to treat deep-seated tumors.

ELECTROCHEMOTHERAPY (ECT)

An idea of combining reversible electroporation with poorly permeant chemotherapeutic drugs (such as cysplatin and bleomycin) in order to increase their cytotoxicity was born in

the end of 1980s (Orlowski et al. 1988). In the 1990s this method was termed electrochemotherapy (Mir et al. 1991) and started its progress from mice experiments (Serša et al. 1995) through establishment of standard operating procedures for locally treating cutaneous and subcutaneous tumors in humans (Mir et al. 2006) to applications on deep-seated tumors (Miklavcic et al. 2010; Edhemovic et al. 2014).

An ECT treatment starts by first injecting the chemotherapeutic drug either intravenously into the patient or directly into the tumor. After that a specifically designed pulse generator and electrodes are used to deliver the electric pulses to the tumor area (Miklavčič et al. 2014; Reberšek et al. 2014). In the case of cutaneous tumors and subcutaneous tumors the electrodes used have a fixed geometry and are usually either plate electrodes or an array of small needle electrodes, depending on the tumor type. While there are cases when needle electrodes with fixed geometry can be used also on deep-seated tumors, the position and size of deep-seated tumors is usually such that it requires application of several individual, long needle electrodes. If long needle electrodes are used their position varies with respect to individual patient and tumor geometry.

IRREVERSIBLE ELECTROPORATION (IRE)

The possibility of inducing targeted cell death using irreversible electroporation has found its use in medicine as a tissue ablation technique (Rubinsky et al. 2007). The specific appeal of irreversible electroporation is the fact that it does not introduce significant thermal effects (Davalos et al. 2005), unlike some other forms of focal therapies such as radiofrequency ablation and cryoablation. Also, it was shown that irreversible electroporation preserves the extracellular matrix, major vascular and other sensitive structures (Al-Sakere et al. 2007; Jiang et al. 2015).

The principle of an IRE treatment is similar to ECT, except for the lack of chemotherapeutic drugs. Since IRE is usually performed in deep-seated tumors and internal organs it is performed using long individual needle probe electrodes. As is the case with ECT the positioning of the electrodes varies with patient geometry.

PARAMETERS FOR EFFECTIVE ELECTROPORATION OF TISSUES

The key condition that needs to be satisfied in order for electroporation to occur is to establish an electric field of sufficient strength (Miklavcic et al. 1998; Miklavcic et al. 2006). When talking about electroporation in practice the sufficient electric field strength is defined regarding two thresholds: the reversible electroporation threshold and the irreversible electroporation threshold. Intuitively, in order to achieve reversible electroporation the electric field must be above the reversible electroporation threshold, but lower than the irreversible electroporation threshold. Consequently, in the case of irreversible electroporation it suffices that the electric field be above the irreversible electroporation threshold.

The success of electroporation on general level depends on several factors. Primary factors are the parameters of the delivered electric pulses: their number, amplitude, duration and repetition frequency (Pucihar et al. 2011). In the case of tissue electroporation, namely ECT and IRE these parameters are today somewhat standardized in order to achieve optimal results. Another factor which is very important in electroporation of tissues is the electric field distribution, which in turn depends on electric properties of the tissue, the distance between the electrodes and pulse parameters, especially their amplitude and number (Miklavcic et al. 1998; Garcia et al. 2014). Also, it was established that the electric properties of the tissues, namely the electric conductivity, increase due to electroporation and this change then consequently affects the electric field distribution (Šel et al. 2005; Pavselj et al. 2005; Cukjati et al. 2007; Ivorra & Rubinsky 2007; Neal et al. 2012; Corovic et al. 2013).

When one takes all of the above mentioned factors and puts them into context of treating deep-seated tumors with electroporation-based treatments the question of successful treatment becomes very complicated to grasp. With each patient having different tumor geometry and variety of other different, sometimes even critical tissues surrounding the tumor, the parameters which would ensure the coverage of the whole tumor by an electric field of sufficient strength cannot be defined through standard operating procedure. The solution to this problem can however be found in the form of patient-specific treatment planning.

TREATMENT PLANNING FOR ELECTROPORATION OF DEEP-SEATED TUMORS

Treatment planning has already been established as an important process in several different technologies for cancer treatment such as radiotherapy (Lecchi et al. 2008), cryotherapy (Butz et al. 2000), laser-induced interstitial thermotherapy (Schwarzmaier et al. 1998), radiofrequency ablation (Chen et al. 2009) and others. In the case of these technologies treatment planning not only enables routine performance of the treatment but is also key to performing the treatment successfully. The common characteristic of treatment planning for all of the above mentioned procedures is that they rely on patient-specific geometry which is extracted from medical images after which a model is generated to find the optimal treatment parameters.

The first steps towards applying similar principles to plan electroporation-based treatments were done through development of numerical models of electroporation (Pavselj et al. 2005) and tissue conductivity changes (Šel et al. 2005). These models were based on simple geometric forms and took into account only the properties of the target tissue. Afterwards the models have evolved to include optimization algorithms (Županič et al. 2008; Corovic et al. 2008) which calculate the necessary voltage applied per different electrode pairs in order to achieve complete coverage of the tumor with a sufficiently high electric field. Finally a 3D model of other tissues and structures which surround the tumor was also included so that the optimization procedure can take into account minimization of irreversible electroporation in non-tumor tissues (Županič & Miklavčič 2010; Kos et al. 2010a; Miklavcic et al. 2010). In order to be able to include an accurate 3D geometry of the patient into the model methods of medical image segmentation had to be applied (Pavliha et al. 2012).

WEB-BASED TOOL FOR TREATMENT PLANNING

The treatment planning for electroporation-based treatments of deep-seated tumors as it is performed today is a process where both medical image segmentation and numerical modeling play an equally important role (Zupanic et al. 2012). This unified treatment-planning procedure was first evaluated on a clinical study of ECT of colorectal liver metastases (Edhemovic et al. 2011; Edhemovic et al. 2014). For the purpose of supporting this study specific algorithms for automatic segmentation of liver and hepatic vessels were created and evaluated (Pavliha, Mušič, et al. 2013; Marcan et al. 2014). Although the

application of treatment planning in the mentioned clinical study was a success (Edhemovic et al. 2014) several key steps still need to be performed in order to translate the treatment planning procedure into routine clinical use. The main challenge that has to be solved in order to achieve this is to embed highly specific engineering knowledge in procedures which can be run with as least user interaction as possible while ensuring the necessary level of accuracy and robustness.

The first steps towards adapting the treatment planning procedure for everyday use by clinicians were done through an idea and first implementation of a treatment planning tool that could be run through an Internet browser (Pavliha, Mušič, et al. 2013). Such web-based tool consists of two main components: server and client. The server side contains the database and runs all the underlying algorithms that encapsulate the engineering knowledge. The client side serves merely as a graphical user interface through which the user can upload patient images, select the treatment planning process with respect to the organ of interest and receive the results of the planning.

The workflow of the treatment planning process of the proposed web-based tool was modeled after the workflow for radiotherapy treatment planning. Therefore, automatic segmentation and numerical modeling modules were joined by a new module which would ensure robustness and accuracy - the module for segmentation validation. The idea of this module is to present the user with the results of the automatic segmentation algorithm and give the possibility to adjust the results if necessary and finally confirm their validity. In case some organ or structure of interest cannot be automatically segmented with sufficient accuracy (such is the case with tumors) or the algorithm for automatic segmentation is not yet available the user is given the option to delineate the structure manually.

Finally, the 3D model generated by segmentation requires one more feature that needs to be specified by the user before numerical modeling can proceed, and that is the electrodes. Given the variability of available electrodes and different possible entry paths of the electrodes the tool relies on the user knowledge which is better suited to specify these parameters than any system could do automatically. Schematic of the final version of the web-based electroporation treatment-planning workflow with all the components is shown in Figure 1.

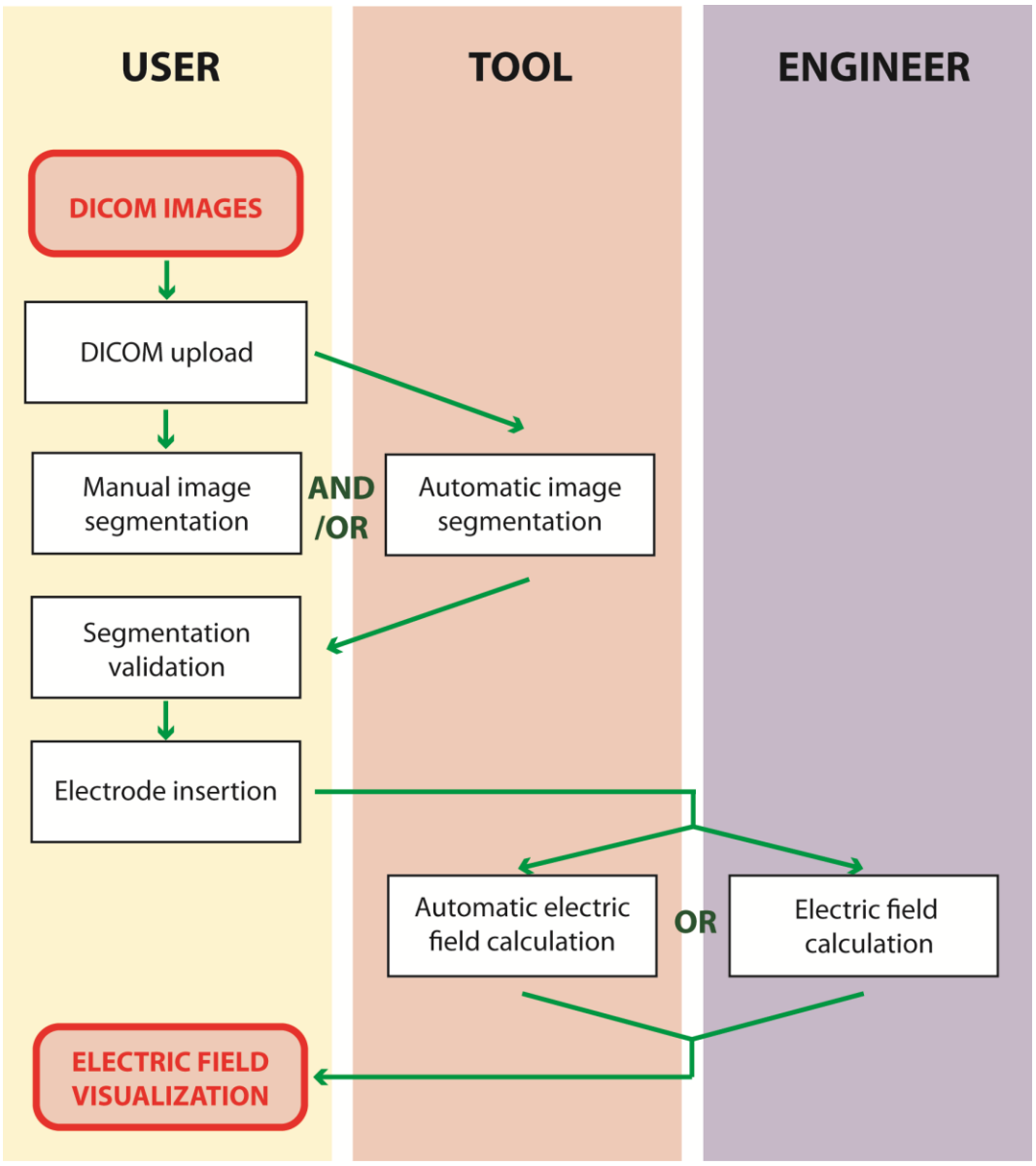

Figure 1. Workflow of the web-based tool for treatment planning of electroporation-based treatments

SEGMENTATION OF MEDICAL IMAGES

Segmentation of medical images implies delineation of different organs or objects of interest, whether manually or by applying some computer algorithm. In a broader sense and specifically in the case of computer-assisted segmentation it has also grown to include various methods of image preprocessing, post processing and localization of the target object (Wong 2005; Withey & Koles 2008).

Regarding its applicability, segmentation of medical images is undoubtedly a crucial part of many clinical tasks which are today performed routinely. These tasks include not only

diagnostics but also more complex activities such as intraoperative navigation and treatment planning. Although manual segmentation performed by an expert radiologist is today still considered to be the gold standard it is also a tedious and time-consuming task. This not only complicates the implementation of the whole treatment-planning process in the clinic but also introduces the problem of intra- and inter-rater variability (Warfield et al. 2004). Algorithms for automatic segmentation of medical images have proven to be effective in alleviating the rater variability and performance time problem (Klein et al. 2008).

Although the field of medical image segmentation has evolved to the extent that it today counts numerous different categories based on some common algorithm characteristics with even more algorithms appearing recently that combine approaches from several categories, the task of accurate medical image segmentation remains an open problem. There is no single algorithm that could be successfully applied on all targets of interest. Even with specialization of algorithms based on the segmentation target there are still large differences in imaging modalities which cause even further specialization. These specializations have motivated organization of special 'grand challenges' for segmentation of a specific target from a specific modality (Deng & Du 2008; Litjens et al. 2014). Such events consist of publicly available datasets of training and test data and a carefully formulated evaluation framework which enables direct comparison of different segmentation algorithms. The results of each segmentation algorithm are published online and usually a summary scientific paper is published with description of all the algorithms that participated in the challenge and systematic comparison of their performance. The role of these challenges in better structuring the medical image segmentation research and stimulating faster convergence towards better algorithms is indispensable.

Though the medical image segmentation community is producing new, better automatic algorithms faster than ever, the stakes of directly using the results of automatic segmentation in the clinic are high. It would therefore be wise, perhaps even mandatory, to use some kind of mechanism of segmentation validation and correcting by an expert clinician (Warfield et al. 2004; Saad et al. 2010; Deeley et al. 2013) in order to ensure the validity of the segmentation results. Additionally, if such validation mechanism is joined with the automatic segmentation algorithm into an integral solution it enables building a database of expert-validated segmentations which can then be used in improving the automatic segmentation algorithm.

One such integrated tool is for instance the web-based tool for treatment planning of electroporation-based treatments.

AIMS OF THE DOCTORAL THESIS

The focus of this doctoral thesis was application of medical image segmentation in pre-treatment planning for electroporation-based treatments of deep-seated solid tumors. Building a pre-treatment plan for an electroporation-based treatment of deep-seated solid tumors requires a patient-specific geometry model for accurate calculations of treatment parameters. The methods developed in this thesis facilitate generation of patient geometry for medical images from various sources (clinical centers), thus contributing to the robustness of the pre-treatment planning process. The accuracy of the developed algorithms was assessed with respect to recent advances in medical image segmentation validation and having in mind the purpose of the segmentation. A part of the validation process included a sensitivity study to assess the impact of segmentation accuracy on treatment outcome and define the level of accuracy needed to ensure reliable pre-treatment planning for electroporation-based treatments.

The goal of this thesis was also to complement the segmentation by introducing the process of its validation and improvement, thus creating a segmentation cycle. The segmentation cycle consists of three phases: segmentation, validation and evolution. The validation phase utilizes user feedback regarding the correctness of the segmentation. The users need to be able to validate and correct the segmentation results through an ergonomic user interface. The user interface should implement methods to minimize required user actions in an intelligent way.

The process of user validation results in increased level of segmentation and treatment planning reliability and also provides a valuable database of new segmented and validated cases. The knowledge gathered in the database of segmented cases was incorporated in the

existing segmentation algorithm workflow in order to improve the algorithm performance, thus closing the segment-validate-evolve cycle.

RESEARCH PAPERS

SEGMENTATION OF HEPATIC VESSELS FROM MRI IMAGES FOR PLANNING OF ELECTROPORATION-BASED TREATMENTS IN THE LIVER

MARCAN Marija, PAVLIHA Denis, MAROLT MUSIC Maja, FUCKAN Igor, MAGJAREVIC Ratko, MIKLAVCIC Damijan

Radiology and Oncology 48(3): 267-281, 2014.

EFFECT OF BLOOD VESSEL SEGMENTATION ON THE OUTCOME OF ELECTROPORATION-BASED TREATMENTS OF LIVER TUMORS

MARČAN Marija, KOS Bor, MIKLAVČIČ Damijan

PLoS ONE: 10(5): e0125591, 2015.

WEB-BASED TOOL FOR VISUALIZATION OF ELECTRIC FIELD DISTRIBUTION IN DEEP-SEATED BODY STRUCTURES AND FOR PLANNING ELECTROPORATION-BASED TREATMENTS

MARČAN Marija, PAVLIHA Denis, KOS Bor, FORJANIČ Tadeja, MIKLAVČIČ Damijan

Biomedical Engineering Online: in press, 2015.

MULTI-ATLAS SEGMENTATION OF MRI IMAGES ENHANCED WITH ATLAS SELECTION BASED ON IMAGING PROPERTIES AND RATER VARIABILITY

MARČAN Marija, MIKLAVČIČ Damijan

IEEE Transactions on Medical Imaging: submitted, 2015.

PAPER 1

Title: Segmentation of hepatic vessels from MRI images for planning of electroporation-based treatments in the liver

Authors: MARCAN Marija, PAVLIHA Denis, MAROLT MUSIC Maja, FUCKAN Igor, MAGJAREVIC Ratko, MIKLAVCIC Damijan

Publication: Radiology and Oncology

DOI: 10.2478/raon-2014-0022

Year: 2014

Volume: 48

Number: 3

Pages: 267 - 281

Impact factor: 1.667

Ranking:

Category name	Total journals in category	Journal rank in category	Quartile in category
oncology	203	155	Q4

research article

Segmentation of hepatic vessels from MRI images for planning of electroporation-based treatments in the liver

Marija Marcan[1], Denis Pavliha[1], Maja Marolt Music[2], Igor Fuckan[3], Ratko Magjarevic[4], Damijan Miklavcic[1]

[1] University of Ljubljana, Faculty of Electrical Engineering, Ljubljana, Slovenia
[2] Institute of Oncology Ljubljana, Ljubljana, Slovenia
[3] Clinical Department for Diagnostic and Interventional Radiology, Clinical Hospital "Dubrava", Zagreb, Croatia
[4] University of Zagreb, Faculty of Electrical Engineering and Computing, Zagreb, Croatia

Radiol Oncol 2014

Received 9 January 2014
Accepted 10 April 2014

Correspondence to: Prof. Damijan Miklavčič, Ph.D., Faculty of Electrical Engineering, University of Ljubljana, Tržaška 25, 1000 Ljubljana, Slovenia. E-mail: damijan.miklavcic@fe.uni-lj.si

Disclosure: No potential conflicts of interest were disclosed.

Introduction. Electroporation-based treatments rely on increasing the permeability of the cell membrane by high voltage electric pulses delivered to tissue via electrodes. To ensure that the whole tumor is covered by the sufficiently high electric field, accurate numerical models are built based on individual patient geometry. For the purpose of reconstruction of hepatic vessels from MRI images we searched for an optimal segmentation method that would meet the following initial criteria: identify major hepatic vessels, be robust and work with minimal user input.

Materials and methods. We tested the approaches based on vessel enhancement filtering, thresholding, and their combination in local thresholding. The methods were evaluated on a phantom and clinical data.

Results. Results show that thresholding based on variance minimization provides less error than the one based on entropy maximization. Best results were achieved by performing local thresholding of the original de-biased image in the regions of interest which were determined through previous vessel-enhancement filtering. In evaluation on clinical cases the proposed method scored in average *sensitivity* of 93.68%, *average symmetric surface distance* of 0.89 mm and *Hausdorff distance* of 4.04 mm.

Conclusions. The proposed method to segment hepatic vessels from MRI images based on local thresholding meets all the initial criteria set at the beginning of the study and necessary to be used in treatment planning of electroporation-based treatments: it identifies the major vessels, provides results with consistent accuracy and works completely automatically. Whether the achieved accuracy is acceptable or not for treatment planning models remains to be verified through numerical modeling of effects of the segmentation error on the distribution of the electric field.

Key words: electrochemotherapy; non-thermal irreversible electroporation; treatment planning; hepatic vessel segmentation; non-invasive tumor treatments; MRI of liver

Introduction

Exposing a biological cell to a sufficiently high electric field causes increased permeability of the cell membrane. This increased permeability of the membrane allows transfer of molecules which normally lack membrane transport mechanism into the cell. The described effect of the electric field on the cell is called *electroporation*.[1,2] Electroporation can be classified as either reversible or irreversible. The reversible/irreversible nature of electroporation is in strong correlation with pulse amplitude, duration and number of pulses. In reversible electroporation, the cell membrane eventually returns to its normal state. Irreversible electroporation however leads to cell death because the cell

 doi:10.2478/raon-2014-0022

membrane is permanently disrupted or due to the extensive loss of the intracellular components. Combination of reversible electroporation with traditional methods of chemotherapy has resulted in a new method for tumor treatment named *electrochemotherapy* (ECT).[3–5] Irreversible electroporation (IRE) has found its application in tumor treatment as a tissue ablation procedure, its main advantage being the fact that, if controlled properly, it does not thermally damage the tissue.[6–8]

Tumor treatments based on electroporation like ECT and IRE include placement of the electrodes in the tissue and delivery of the electric pulses. In order for the treatment to be successful the whole tumor must be covered by a sufficiently high electric field. The magnitude and distribution of the electric field depends on the number and the position of the electrodes, the amplitudes of pulses applied per electrode pair and the electric properties of the tissue, especially conductivity.[9,10]

Prediction of parameters needed for successful treatment is easier for surface tumors which is why the ECT was first performed on skin tumors.[4] Ensuring the complete tumor coverage with a sufficiently high electric field is however more challenging in the case of deep-seated solid tumors as well as large tumors.[11] This was well demonstrated in a case where a patient with a deep-seated tumor in the thigh was treated with ECT.[12] The post-treatment evaluation showed that 6% of the tumor volume was not covered by a sufficiently high electric field, which caused the tumor to regrow. The reasons which reduce predictability of the electric field distribution in deep-seated tumors are the tumor position, high diversity in tumor size and shape, and presence of the surrounding tissues with different electric conductivities. Predictability of an adequate distribution of the electric field can be best achieved by calculating a patient-specific treatment plan as a part of an electroporation-based treatment procedure.[13] A patient-specific treatment plan for electroporation-based treatment of deep-seated solid tumors takes into account patient geometry and tissue properties to generate an optimal set of treatment parameters.[14,15]

Correctness of a treatment plan is ensured by an accurate model of the patient which includes the tumor with critical surrounding tissues and structures. The patient model is built by segmenting the medical images and then used to perform numerical calculations of the electric field distribution. A proof-of-concept was provided in a clinical study in which colorectal metastases in the liver were treated by means of ECT.[16] For the purpose of the mentioned clinical study, an algorithm for automatic segmentation of the liver from MRI images was developed.[17] Similar treatment planning process is well-established in radiotherapy where it has been in use for decades.[18] Generation of models from medical images for subsequent numerical calculations has also been used as a part of treatment planning for radiofrequency ablation (RFA) of liver tumors.[19,20]

Other than liver and tumor tissue, critical structures that need to be included in the model for both RFA and electroporation-based treatments of the liver are hepatic vessels. For the purpose of radiofrequency ablation, vessels which measure more than 3 mm in diameter size have been described as critical because of their influence on heat propagation.[21] In case of electroporation-based treatment of the liver the hepatic vessels are important for other reasons. Firstly, the electric conductivity of the vessels is different than that of the liver tissue and tumors, which can have an impact on the electric field distribution, especially in cases when a tumor is situated close to large vessels.[22] Secondly, during an electroporation-based treatment the surgeons insert needle electrodes into the liver tissue and these should not damage larger hepatic vessels. The hepatic vessels which were identified by surgeons as critical are vena cava and vena porta with branches up to second order, left, middle and right hepatic vein, and larger hepatic arteries. These vessels will thus be the ones we will most certainly want to include in our model. Lastly, the model of vessels built from medical images can be used for intra-operative visualization to help surgeons navigate during the insertion of the electrodes.

The problem of segmentation of vessels in general[23] and hepatic vessels in particular has been an area of interest for several decades. The interest in segmentation of hepatic vessels resulted in exploring several different approaches. First attempts were based solely on thresholding[24] and region growing.[25,26] The evolution of highly popular methods for enhancement of tubular structures[27–29] resulted in their combinations with thresholding[30] and region growing.[20,31–33] Other than tube-enhancing filtering the traditional methods of segmentation were enhanced through use of Gaussian mixture models[34,35] and by utilizing morphology of the vascular tree through centerline extraction.[20,31] More advanced methods for segmentation of hepatic vessels include those based on graph-cuts[36,37], active contours[38] and morphological properties embedded in context-based voting system.[39]

All these methods for vessel segmentation have however been designed for and applied to CT images. To our knowledge, no method so far was tested on MRI images. Although CT images have been considered superior for hepatic vessels, the vessels are also visible in MRI images, especially when a contrast agent is applied. With respect to the colorectal metastases of the liver, multiple studies have shown that MRI is superior to CT in sensitivity and accuracy of detecting tumor lesions.[40–45] If MRI is a modality of choice for detecting the tumors, using the same modality to segment the hepatic vessels would avoid the need for registration and errors that inevitably come with it. Another reason why MRI is a method of choice for planning of electroporation-based treatments is possibility to directly observe the distribution of the electric field using the magnetic resonance electric impedance tomography (MREIT), which was described in the work of Kranjc *et al*.[46,47] and is being actively explored.

Given all of the mentioned advantages of MRI over CT in treatment of colorectal metastases in the liver with electroporation-based treatments, we directed our research towards segmentation and validation of segmentation of hepatic vessels from MRI images. The segmentation method used for hepatic vessels has to be robust and include minimal or no user interaction. These prerequisites are necessary for using the procedure for hepatic vessel segmentation as a module in the process of treatment planning.[48] Having this in mind, the segmentation methods we tested were built upon already established and robust approaches based on filtering, vessel enhancement, automatic thresholding and region growing. Data used in validation consisted of two sources: a phantom and clinical cases. The phantom was used to optimize the segmentation parameters and analyze the performance of methods in detail. Images of clinical cases were then used to validate the performance of segmentation methods under realistic conditions.

Materials and methods

Segmentation of hepatic vessels

In order to segment the hepatic vessels from MRI images we tested several simple approaches, alone and their combinations. The main approaches include vessel enhancement filtering, thresholding, region growing, connected component analysis and morphological operations.

To determine the optimal method for our purpose we tested two different thresholding methods on different input: on original de-biased images and on the results of vessel enhancement filtering. The thresholding of that input was performed on the slice level and is referred to as *global* thresholding. The thresholding method that performed best on phantoms was also tested *locally* on smaller regions of original de-biased images determined by vessel enhancement filtering.

Pre-processing phase

Prior to running any of the methods on the original images we performed de-biasing in order to remove the inhomogeneity of image intensity. The intensity inhomogeneity is a product of the magnetic field inhomogeneity in the MRI device.[49] The applied de-biasing method is publicly available and based on the work of Zheng *et al*.[50] After de-biasing the images were masked with the results of liver segmentation.[17]

Vessel enhancement filtering

The filter we used is based on the work of Frangi *et al*.[28] The filter differentiates line-like from blob-like and plate-like structures by observing the relationships between eigenvalues of the Hessian matrix in each voxel of the image. Before applying the filter, the image is scaled by filtering with Gaussian kernels of different size σ. The value of σ is set to a value that equals the size of the diameter of the vessels we wish to enhance.

For each scale σ the probability of a voxel belonging to a line, i.e. *vesselness* is calculated as:

$$v(\sigma)=\begin{cases} 0 & \text{if} \quad \lambda_2>0 \| \lambda_3>0 \\ (1-\exp(-\frac{R_a^2}{2\alpha^2}))\exp(-\frac{R_b^2}{2\beta^2})(1-\exp(-\frac{S^2}{c})) & \text{else} \end{cases} \quad (1)$$

where $|\lambda_1| \le |\lambda_2| \le |\lambda_3|$ are eigenvalues of the Hessian matrix in three dimensions, $R_a=\frac{|\lambda_2|}{|\lambda_3|}$ and $R_b=\frac{|\lambda_1|}{\sqrt{|\lambda_2\lambda_3|}}$ are parameters which discriminate line-like structures from plate-like and blob-like structures, and $S=\|H_\sigma\|_F=\sqrt{\sum_j \lambda_j^2}$ is the Frobenius norm of the Hessian matrix. Values of parameters α and β were chosen through optimization on phantoms and were selected as 0.3 and 0.7, respectively. Value of parameter c is calculated for each case and for each value of scale σ according to the following equation:

$$c = \frac{1}{2}\|H_\sigma\|_F = \frac{1}{2}\sqrt{\sum_j \lambda_j^2} \quad (2)$$

The parameter c is used in the expression for vesselness as is, without squaring and multiplying by 2 as it is done in the original work of Frangi *et al*.[28] The reason for this is better enhancement of vessel structures. The final vesselness filtered image is obtained by calculating the maximum of vesselness values at different scales for each voxel of the image.

Thresholding

Out of many thresholding methods developed until today we chose to implement two of the most successful as reported by Sankur *et al*.[51] The first method is based on minimizing intra-class variance.[52] The second method is based on maximization of image entropy.[53] Both methods are completely automatic and were implemented to determine the threshold on slice level on an image histogram with values in the 16-bit range.

We assessed the performance of the two thresholding methods globally on de-biased original images and vesselness filtered images of both phantoms and clinical cases. Additionally we assessed the method that performed better globally on smaller regions of interest. The details of local thresholding are described in the section *Proposed method*.

Proposed method

Through analysis of the results of previously described methods applied on both phantom and clinical data, we derived a method comprised of the best aspects of vessel enhancement filtering and thresholding. Vessel enhancement filtering is excellent for locating the position of the vessels but unable to determine their exact borders. Thresholding of the de-biased original image can detect vessel borders but not with consistent accuracy throughout the whole image. The proposed method is therefore based on *local* thresholding of smaller regions of interest (ROI), rather than deriving a single threshold for the whole slice. The ROIs for local thresholding are determined based on the output of vessel enhancement filtering. Detailed steps of the proposed method with all the input, output, parameters and dimension in which the step is performed are provided in Table 1.

First, we performed sinc interpolation to obtain isotropic voxels (O2) so that we could perform vesselness filtering.[54] After that we applied the vesselness filtering on the interpolated, de-biased, masked original images (O3). The filtered image (O4) was interpolated once again to obtain the original voxel size (O5). In the end of the filtering section the result of vesselness filtering has to be once again masked with the original liver mask to suppress the high response which appears in the area where background borders with the liver (O6).

The output of the vesselness filtering has high values for voxels with high probability of belonging to a vessel and is very low for very small vessels. The voxels with small vesselness values might also be a result of image noise. For this reason we have chosen a small threshold of 0.05 of the maximum vesselness value. All of the voxels with a vesselness value higher than this threshold are isolated into a basic vessel model (O7). A basic vessel model thus consists of voxels with high certainty of belonging to a vessel. The same small threshold for output of Frangi's vessel enhancing filter was already successfully used in the work of Dongen *et al*. to prevent false positives in the algorithm for extraction of pulmonary vasculature.[55]

To eliminate the smallest vessels which are not of interest for electroporation-based treatments we morphologically open the results to remove all objects with a diameter smaller than 3 mm. We need to keep only larger objects (O8) because the smallest hepatic vessels from the list of those that should not be damaged during the electrode insertion are the main hepatic arteries, and they measure around 3 mm in diameter and more.[56]

After we have extracted and morphologically opened the basic vessel model (O8) we proceed with local thresholding to determine the exact vessel borders. To extract the ROIs we first perform the connected component analysis on the slice level to break the basic vessel model into smaller 2D objects (O9). These objects are then morphologically dilated with a structuring element in the shape of a disc with a radius of 5 pixel. The dilation gives us the ROIs (O10) within which we perform the local thresholding (O12). The threshold for each ROI is calculated based on variance minimization.

The final steps in the proposed method are meant to refine the results by adding possibly missed nearby voxels and removing small objects. For this purpose we perform region growing with results of local thresholding (O12) as seed points. Region growing is performed on de-biased original images in 3D by searching the 27-neighborhood of each seed voxel. A threshold for adding new voxels is determined on a slice level as a median value of intensities of voxels already marked as vessels. The thresholds are re-calculated after each series of newly found voxels. The region growing stops once there are no new voxels that could be added.

TABLE 1. Sequential list of all the steps performed within the proposed optimal method, along with inputs, outputs and parameters of each step and the dimension (2D or 3D) in which the step is performed. *(Ox)* denotes an output from a previous step where x is the step number.

No	Step	Input	Output	Parameters	Dimension
1	Bias removal	Original unmasked image	De-biased image (O1)	/	2D
2	Sinc interpolation to obtain isotropic voxels	De-biased image (O1) Liver mask	Interpolated de-biased image (O2') Interpolated liver mask (O2'')	/	3D
3	Masking	Interpolated de-biased image (O2') Interpolated liver mask (O2'')	Interpolated masked de-biased image (O3)	/	2D
4	Frangi filtering	Interpolated masked de-biased image (O3)	Interpolated vesselness filtered image (O4)	Gaussian kernel σ=[1,12] with a step of 0.5 α=0.3 β=0.7 c= half of Frobenius norm	3D
5	Interpolation to original voxel size	Interpolated vesselness filtered image (O4)	Vesselness filtered image (O5)	/	3D
6	Masking	Vesselness filtered image (O5) Liver mask	Masked vesselness filtered image (O6)	/	2D
7	Thresholding with a low threshold	Masked vesselness filtered image (O6)	Basic vessel model (O7)	Threshold = 0.05 * max(vesselness)	3D
8	Removal of small objects	Basic vessel model (O7)	Basic vessel model with objects with diameter > 3 mm (O8)	Size of small object = number of pixel of a circle with 3 mm diameter	2D
9	Connected component analysis	Basic vessel model with objects with diameter > 3 mm (O8)	Basic objects (O9)	/	2D
10	Dilation	Basic object (O9)	ROI of object (O10)	Structuring element: disc with radius = 5	2D, per object
11	Masking	De-biased image (O1) Liver mask	Masked de-biased image (O11)	/	2D
12	Local thresholding	ROI of object (O10) Masked de-biased image (O11)	Locally thresholded image (O12)	Threshold determined for each ROI through variance minimization	2D, per object
13	Region growing	Locally thresholded image (O12) Masked de-biased image (O11)	Region grown image (O13)	Threshold = median of locally thresholded image, per slice 27-neighborhood	2D/3D
14	Erosion	Liver mask	Eroded mask (O14)	Structuring element: disc with radius = 6	2D
15	Masking	Region grown image (O13) Eroded mask (O14)	Segmented image (O15)	/	2D
16	Removal of small objects	Segmented image (O15)	Segmented image with objects with diameter > 3 mm (O16)	Size of small object = number of pixel of a circle with 3 mm diameter	2D

After region growing we mask the results (O13) with an eroded liver mask (O14) to eliminate boundary outliers. This step is in general unnecessary if the provided liver masks are completely accurate and contain only liver voxels. Otherwise the results of the vessel segmentation will also include a small strip around the liver which in original images is of similar intensity as vessels. The final step in the proposed method includes once again morphologically opening the results (O15) to remove all objects with a diameter smaller than 3 mm.

In order to give better insight into the proposed method we provide output of all the relevant steps in Figure 1. The outputs are the result of applying the proposed method on a clinical case. For all of the presented steps we provide a one slice output and for some steps also the complete 3D model, if relevant.

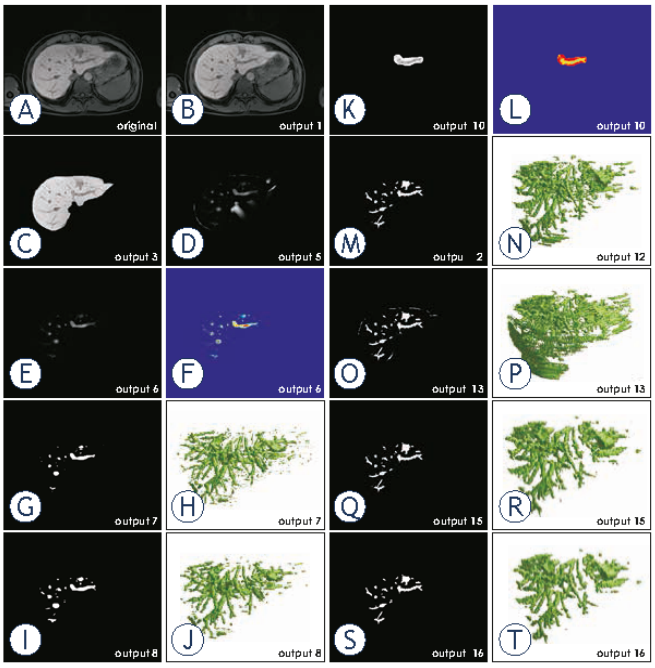

FIGURE 1. Output of the proposed method applied on a clinical case. **(A)** Original image. **(B)** De-biased original image. **(C)** Masked de-biased original image. **(D)** Vesselness filtered image. **(E)** Masked vesselness filtered image. **(F)** The same output as in E. presented in colored scale. **(G)** Basic vessel model with small objects. **(H)** Basic vessel model with small objects shown in 3D. **(I)** Basic vessel model without small objects. **(J)** Basic vessel model without small objects shown in 3D. **(K)** Basic object with ROI. **(L)** Basic object with ROI in colored scale. **(M)** Result of local thresholding. **(N)** Result of local thresholding shown in 3D. **(O)** Result of region growing. **(P)** Result of region growing shown in 3D. **(Q)** Result of masking with an eroded mask. **(R)** Result of masking with an eroded mask shown in 3D. **(S)** Final result after the removal of small objects. **(T)** Final result after the removal of small objects shown in 3D.

Most of the parameters that are used in the proposed method are calculated automatically based on the image. These parameters include the two most critical parameters: the value of c used in the vessel enhancing filter that influences the filter output most[57] and thresholds in the local thresholding step. Values of two of the remaining parameters of the vessel enhancing filter, α and β, were chosen based on validation on phantoms. The rest of the parameters that had to be set do not directly influence the accuracy of the results but rather determine the region of interest in which the main parameters operate. These less-sensitive parameters are namely a threshold in step 7 and a structuring element in step 9 (Table 1). We would, however, not suggest setting these parameters to more than ±25% of the values used in this paper. There is one parameter remaining that strongly influences the

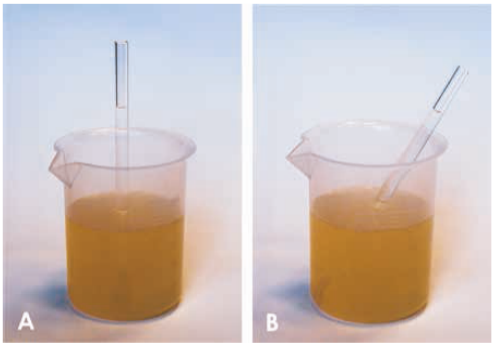

FIGURE 2. A simple phantom constructed for validation of hepatic vessel segmentation from MRI images. The phantom is made of agarose gel and a glass tube filled with physiological solution inserted in: **(A)** perpendicular position. **(B)** tilted position.

output of the vessel enhancement filter, and that is the value of σ in the Gaussian kernel. This parameter needs to be set only once and according to the size of the vessels one wishes to extract, as is stated in the work of Frangi *et al.*[28]

Phantom design

Our primary concern in hepatic vessel segmentation was the accuracy of segmentation rather than the segmentation sensitivity to the depth of the vessel tree. For this reason we created a phantom which enabled detailed observation of whether a certain method over- or undersegments. The phantom was composed of a cup filled with agarose gel and a tube filled with physiological solution inserted into that gel, similar to the work of Merkx *et al.*[58] and Jiang *et al.*[59] The gel was prepared as a 0.5% solution of agarose in 100 ml distilled water, doped with 0.17 mM MnCl2 to enhance MRI signal properties.[60] Three glass tubes with outer diameters of 4, 6 and 8 mm were filled with physiological solution in order to model the vessels. Each tube was inserted into its own cup filled with agarose gel perpendicularly to the cup bottom. Another set of tubes, also with 4, 6 and 8 mm outer diameters were inserted into another three cups filled with agarose gel, but this time in a tilted position. In total, we had six cups containing tubes. An example demonstrating different positions of the tube inside the cup is shown in Figure 2. All six cups were placed in a Siemens Avanto 1.5T MRI device and imaged at the same time in order to ensure the same imaging conditions for all six phantoms. Imaging parameters were set as in the standard protocol for imaging of the abdomen: T1-weighted, VIBE breath-hold, coronal plane with body coil. We im-

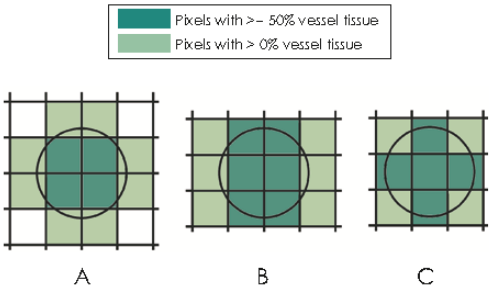

FIGURE 3. Theoretical model of reference vessel area with all possible positions of the object relative to the sampling grid. An example for the 2.56 pixel/diameter resolution. **(A)** vessel with a center in the pixel point, **(B)** vessel with the center on the middle of one of the pixels' edges, **(C)** vessel with a center position right in the middle of one of the pixels. The pixels with >= 50% vessel tissue are a subset of pixels with >0% vessel tissue.

aged in two intra-slice resolutions: 1.56 mm by 1.56 mm and 1.04 mm by 1.04 mm. The slice thickness in both cases was 2 mm.

In order to be able to directly compare different vessel diameters imaged with different resolutions, we expressed the vessel diameters in *number of pixel/diameter* instead of in mm. The same approach was already used in papers which also evaluated accuracy of determining vessel area from MR angiography data.[58,59] When expressed in pixel/diameter, the value of different resolutions we observed were 2.56 pix, 3.84 pix, 5.12 pix, 5.76 pix and 7.69 pix per diameter.

Clinical data

For validation on clinical data we obtained MRI images of six patients that were a part of Phase I/II clinical study "Treatment of Liver Metastases with Electrochemotherapy (ECTJ)" (EudraCT number 2008- 008290-54; ClinicalTrials.gov (NCT01264952)).[16] The study was conducted at the Institute of Oncology Ljubljana, Ljubljana, Slovenia. Regulatory approvals from the Institutional board, as well as from the National Medical Ethics Committee were obtained. Written consents of the patients were obtained. The series on which we performed the segmentation were the ones on which the colorectal metastases are most visible. The segmentation of the liver was also performed on the same image series by a method described by Pavliha *et al.*[17] The reason for choosing the series where the liver, hepatic vessels and colorectal metastases are all visible was to avoid the need for subsequent registration. The chosen series were T1-weighted, VIBE breath-hold, transversal plane, with body coil and imaged 20 minutes after injection of the Primovist® (Bayer Group, Germany) contrast agent. Images were acquired with a Siemens AVANTO 1.5T MRI device at the Institute of Oncology in Ljubljana. In three cases the inter-slice resolution was 0.684 mm by 0.684 mm with a slice thickness of 2.75 mm. In the other three cases the inter-slice resolution was 1.188 mm by 1.188 mm with a slice thickness of 3 mm.

Accuracy assessment metrics

Phantom data

Once the images have been segmented, we counted the number of pixel characterized as 'vessel' in each slice, thus obtaining the *segmented vessel area*. For *reference vessel area* we created a theoretical model which observes different ways in which a perfect circle can be positioned relative to the sampling grid of certain size, depending on the circle size and the grid size. The illustration of our theoretical model for the case of 2.56 pixel/diameter is presented in Figure 3.

The need for such theoretical model is caused by *partial volume effect*, i.e. an artifact in medical imaging where the value of a border pixel between different tissue types is influenced by the amount of tissues it is composed of. After segmentation, the pixel can be characterized as belonging to only one tissue type. Which type will it be depends on the amount in which a certain type is present in the pixel, but also on the segmentation method. Some segmentation methods, for instance, would characterize every pixel that contains any amount of vessel as a vessel pixel.[59] We have therefore defined three reference area values in our theoretical considerations. The first value, the *optimal vessel area* is the number of all pixels which contain at least half of the vessel tissue (pixels marked darker in Figure 3). The second reference value, the *maximum vessel area* is the number of all pixels that contain any amount of the vessel tissue (all colored pixels in Figure 3). The third reference value is *calculated vessel area* which is the mathematically calculated area of the perfect circle, expressed in number of pixels. The three reference area values (optimal, maximum and calculated) are calculated for each resolution and each of the three positions of object illustrated in Figure 3. The final *optimal vessel area* for a certain resolution is the smallest of the optimal vessel area calculated for three positions (in Figure 3 that would be 4 pixels in case A).The final *maximum vessel area* for a certain resolution is the largest of the maximum vessel area calculated for

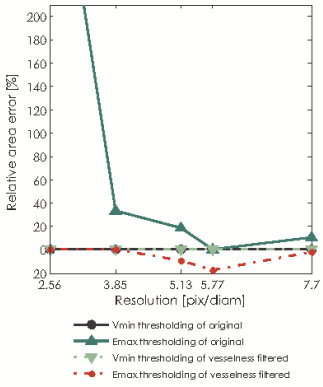

FIGURE 4. Median accuracy of segmented area of phantom in perpendicular position as a function of resolution for different segmentation methods: variance minimization thresholding of the original image, entropy maximization thresholding of the original image, vesselness filtered image thresholded by variance minimization thresholding, and vesselness filtered image thresholded by entropy maximization thresholding.

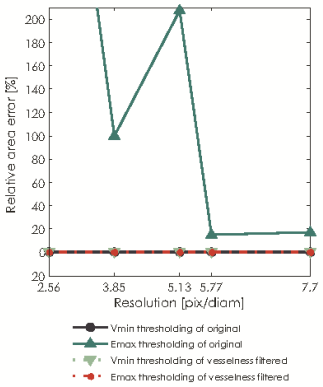

FIGURE 5. Median accuracy of segmented area of phantom in tilted position as a function of resolution for different segmentation methods: variance minimization thresholding of the original image, entropy maximization thresholding of the original image, vesselness filtered image thresholded by variance minimization thresholding, and vesselness filtered image thresholded by entropy maximization thresholding.

three positions (in Figure 3 that would be 12 pixels in cases A and B).

If the number of pixel contained in segmented vessel area falls in the range between *optimal vessel area* and *maximum vessel area*, we consider the segmentation valid. Otherwise, we count the number of pixels outside this range as *pixels missed*. The segmentation error is expressed as *relative area error*, in percent:

$$\text{relative area error } [\%] = \frac{\text{number of pixels missed}}{\text{calculated vessel area}} * 100\% \quad (3)$$

Clinical data

The gold standard for the evaluation of segmentation of clinical data is a segmentation performed by manually determining an optimal threshold for each slice and manually drawing possibly missed contours. The segmentation result was additionally validated by one of the authors (MMM) who is an experienced radiologist and who manually adjusted the segmentation where necessary. The evaluation of the segmentation of clinical data was performed on the level of objects detected in individual slices.

Metrics used for validation included a hit rate, i.e. a ratio of the number of detected objects against the number of all objects in the image, sensitivity (SEN = true positives / (true positives + false negatives)), average symmetric surface distance (ASSD)[34,61] and Hausdorff distance. ASSD provides a measure of the average mutual distance between edges of the two surfaces, while Hausdorff distance is in fact the maximum symmetric surface distance. ASSD and Hausdorff distance were calculated according to equations (4) and (5), respectively:

$$ASSD = \frac{\sum_{a \in A} \min_{b \in B} \|a-b\| + \sum_{b \in B} \min_{a \in A} \|a-b\|}{N_A + N_B} \quad (4)$$

$$H(A,B) = \max\left\{ \max_{a \in A}(\min_{b \in B} \|a-b\|), \max_{b \in B}(\min_{a \in A} \|a-b\|) \right\} \quad (5)$$

where A and B denote the borders of segmented and reference objects, a and b are points on A and B respectively. $\|a-b\|$ denotes the distance between a and b. N_A and N_B are the number of points on A and B.

We have chosen to use ASSD and Hausdorff distance to describe the segmentation specificity rather than a measure of specificity itself (SPEC=true negatives / (false positives + true negatives)) since a high number of true negatives (background) would always yield a high value of specificity. The values of sensitivity, ASSD and Hausdorff distance for the whole image were obtained by calculating a median of those values for all objects. We calculated the median instead of the mean since the data did not conform to Normal distribution.

Additional to previously described metrics we also used the receiver operating characteristics (ROC) curve analysis to objectively compare results of image filtering with original and de-biased images.[62–64] The ROC curves used were constructed with threshold as a parameter.

Results

The first part of this section shows the results of segmenting phantom images. There we assess the performance of thresholding algorithms based on variance minimization and entropy maximization on original and vesselness filtered images. The second part shows the results of segmenting images obtained from clinical cases. In this part we present the comparison of methods that performed best on phantoms and the method based on local thresholding, i.e. the proposed method.

Images of phantoms

For the validation on phantom data, Figure 4 shows relative area error of different segmentation meth-

ods for segmentation of tube phantom in perpendicular position under different image resolutions. The thresholding method based on variance minimization produces 0% error on both original images and vesselness filtered images. The thresholding method based on entropy maximization undersegments the vesselness filtered images and highly oversegments the original images. As could be expected, an absolute value of error drops with increasing resolution.

Figure 5 also shows the same error as Figure 4, only for the phantom in tilted position. The thresholding method based on variance minimization again produces 0% error on both original images and vesselness filtered images. The thresholding method based on entropy maximization produces an error only in the case of original images, which as expected drops with increasing resolution. Notably, an absolute error of the method based on entropy maximization applied on original images is higher for the phantom with tube in tilted position than for the phantom in perpendicular position. An error for the same thresholding method applied on vesselness filtered images in the case of tilted phantom is 0%.

In conclusion, thresholding based on variance minimization outperformed the thresholding based on entropy maximization on both original and vesselness filtered images.

Images of clinical cases

In this section the thresholding method that performed best on images of phantoms, which is thresholding based on variance minimization, was also applied to images of clinical cases. The thresholding was first applied globally on de-biased original images and on vesselness filtered images. After that we applied our proposed method which is based on local thresholding.

Based on visual inspection only it was possible to determine that direct global slice-by-slice thresholding of vesselness filtered images results in large undersegmentation of the vessels. The segmentation inaccuracy is shown in Figure 6, where Figure A shows one slice of the original data while Figure B shows the result of the segmentation of the same slice using thresholding of the result of the vesselness filter. Figure 6.C shows the result of global thresholding of the de-biased original slice based on minimization of variance. Although more accurate than thresholding of the vesselness filtered image, this approach detects many false positives on the liver border. In Figure 6.D we can observe that false positives from Figure 6.C can be avoided by our proposed method which also provides the highest level of accuracy. Figure 6.E shows the gold standard – the radiologist segmentation. Figure 6.F is a 3D representation of the segmentation by the proposed method.

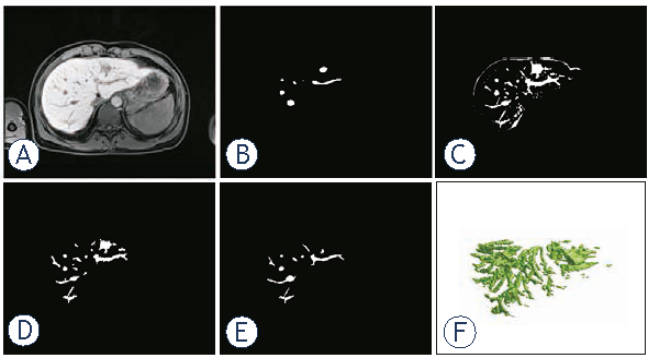

FIGURE 6. Visual comparison of performance of global thresholding and our proposed method. **(A)** Original image slice. **(B)** Results of variance minimization based global thresholding of the vesselnes filtered image. **(C)** Results of variance minimization based global thresholding of the de-biased original image **D.** Results of our proposed method. **(E)** Gold standard – a radiologist segmentation. **(F)** 3D result of the segmentation by the method in **(D).**

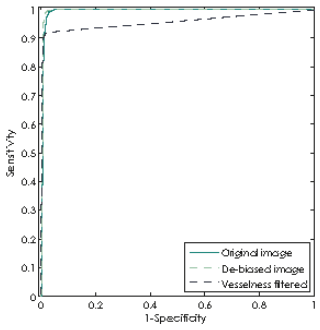

FIGURE 7. Demonstration of performance of simple binary classifier (thresholding) on original image, original image with removed bias and vesselness filtered image using ROC curves.

To additionally explore the potential of differently filtered images at providing an accurate segmentation, we observed the ROC curves of original images, de-biased images and vesselness filtered images. As shown in Figure 7, optimal thresholding of the de-biased images can provide highly accurate segmentations, while slightly outperforming thresholding of the original images and more significantly of the vesselness filtered images. Regardless of the choice of the threshold, direct thresholding of vesselness filtered images can barely reach the sensitivity above 90%.

Final comparison of methods that performed best on phantoms (global thresholding of original de-biased images and vesselness filtered images

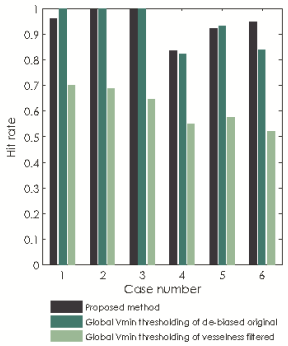

FIGURE 8. Comparison of hit rates for all six clinical cases segmented with three methods: the proposed method, global variance minimization thresholding of the original de-biased image and global variance minimization thresholding of the vesselness filtered image.

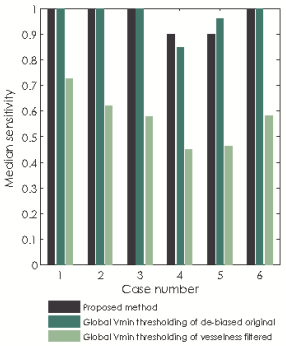

FIGURE 9. Comparison of median sensitivity for all six clinical cases segmented with three methods: the proposed method, global variance minimization thresholding of the original de-biased image and global variance minimization thresholding of the vesselness filtered image.

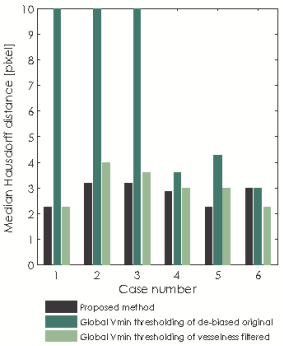

FIGURE 10. Comparison of median Hausdorff distance for all six clinical cases segmented with three methods: the proposed method, global variance minimization thresholding of the original de-biased image and global variance minimization thresholding of the vesselness filtered image.

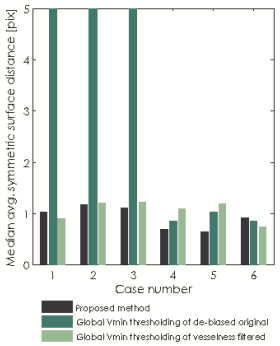

FIGURE 11. Comparison of median average symmetric surface distance (ASSD) for all six clinical cases segmented with three methods: the proposed method, global variance minimization thresholding of the original de-biased image and global variance minimization thresholding of the vesselness filtered image.

based on variance minimization) and the proposed method based on local thresholding is given by observing hit rate, median sensitivity, median Hausdorff distance and median average symmetric surface distance (ASSD) per clinical case. In Figure 8 we can observe that methods based on global thresholding of the original de-biased images have a hit rate around or above 90%, while results of global thresholding of vesselness filtered images identify less than 70% of all objects. Similar results are observed for median sensitivity in Figure 9. The values of median sensitivity are again around or above 90% for global thresholding of original de-biased images and below 70% for global thresholding of vesselness filtered images.

The differences between the proposed method and methods based on global thresholding can be observed through median Hausdorff distance and median ASSD in Figures 10 and 11, respectively. Values of median Hausdorff distance for the proposed method are for all cases in the range of around 2.2 pixels to 3.2 pixels. Values of median Hausdorff distance for global thresholding of original cases are in five out of six cases higher than those for the proposed method, in three cases even extremely high (above 10 pixel), indicating overestimation of the threshold on the global level. Values of median Hausdorff distance for thresholding of vesselness filtered images are mostly higher than those observed for the proposed method, ranging between 2.2 pixels and 4 pixels. As for median ASSD, values for all methods are in almost all cases below 1.2 pixels, except for an extreme for global thresholding in the same three cases which also provided extremes for the median Hausdorff distance.

Final quantitative results of our proposed segmentation method are given in Tables 2 and 3. In Table 2 we provide results of validating the segmentation of all vessels that are critical for electroporation-based treatments of liver metastases as indicated previously in the paper. The mean hit rate for these vessels is high: 96.7% of objects that build up main vessels were detected. The mean value of median sensitivity of the detected objects is 93.7%. The mean error measured through ASSD is 1 pixel, while maximum error in specificity expressed through mean Hausdorff distance reaches 4.26 pixels.

The statistics in Table 3 includes all the vessels that were marked by the radiologist. Median sensitivity nearly equals the one of main vessels with 96.65%. Mean value of median ASSD which equals 0.92 pixel and mean value of median Hausdorff distance which equals 2.77 pixels indicate smaller level of error in specificity for smaller, more regularly shaped vessels.

Discussion

The main aim of the study described in this paper was to find a method which would successfully

TABLE 2. Results of segmentation of major hepatic vessels only from six clinical cases. Segmentation was performed by the method based on local thresholding. Results show hit rate of all objects in all slices, median sensitivity (SEN), median average symmetric surface distance and median Hausdorff distance.

CASE	Number of objects	Pixel resolution [mm]	Hit rate [%]	Median SEN	Median ASSD [pix]	Median ASSD [mm]	Median Hausdorff distance [pix]	Median Hausdorff distance [mm]
1	43	0.684	92.9	98.0	1.3	0.9	4.4	3.0
2	69	0.684	98.4	96.4	1.1	0.7	3.6	2.5
3	38	0.684	100.0	100.0	1.1	0.7	4.1	2.8
4	31	1.188	96.4	85.3	0.7	0.8	2.2	2.7
5	31	1.188	92.3	84.2	1.3	1.5	8.1	9.6
6	25	1.188	100.0	98.2	0.6	0.7	3.2	3.8
OVERALL (mean)			**96.7**	**93.7**	**1.0**	**0.9**	**4.3**	**4.1**

TABLE 3. Results of segmentation of all hepatic vessels from six clinical cases. Segmentation was performed by the method based on local thresholding. Results show median sensitivity (SEN), median average symmetric surface distance and median Hausdorff distance.

CASE	Number of objects	Pixel resolution [mm]	Median SEN	Median ASSD [pix]	Median ASSD [mm]	Median Hausdorff distance [pix]	Median Hausdorff distance [mm]
1	305	0.684	100.0	1.0	0.7	2.2	1.5
2	347	0.684	100.0	1.2	0.8	3.2	2.2
3	328	0.684	100.0	1.1	0.8	3.2	2.2
4	327	1.188	89.9	0.7	0.8	2.8	3.4
5	400	1.188	90.0	0.6	0.8	2.2	2.7
6	454	1.188	100.0	0.9	1.1	3.0	3.6
OVERALL (mean)			**96.7**	**0.9**	**0.8**	**2.8**	**2.6**

segment hepatic vessels from MRI images for the purpose of generating a patient-specific treatment plan for electroporation-based treatment like electrochemotherapy and non-thermal irreversible electroporation. The purpose for which the segmentation will be used has resulted in specific criteria the segmentation method must meet. Firstly, the segmentation method must detect all hepatic vessels that are considered critical in electroporation-based treatments of the liver, which are basically all major hepatic vessels with branches up to second order. Secondly, the method has to be robust. Thirdly, the method has to perform segmentation with minimal or no user interaction required. As for accuracy of the segmentation method, there were no limits posed prior to the beginning of the study. Having in mind that no segmentation method provides absolutely accurate results we rather aimed at finding the best method that would meet the set criteria and assess what is the maximum inaccuracy that method produces. Only after the maximum inaccuracy has been quantified we can conclude if segmenting hepatic vessels from MRI images for electroporation-based treatments is feasible or not.

The first step in finding a method that could segment hepatic vessels from MRI images while satisfying all the mentioned criteria was using the established methods already used on CT images. Since we intended to test several methods we needed means of evaluation that would enable objective comparison of segmentation results. We decided to start with a simple phantom model of a single vessel for detailed observation of methods' behaviors and continue assessing robustness of methods on clinical data.

Our first choice of segmentation methods were the most widely used approaches of identifying vessels with vessel-enhancing filters and automatic thresholding. Regarding automatic thresholding, we have tested two different methods: thresholding based on intra-variance minimization and thresholding based on entropy maximization. Both thresholding methods were applied on both original de-biased and vesselness filtered images, thus resulting in in four different combinations. All four segmentation procedure combinations were run on both phantom data and clinical data. The results of evaluation on phantom data showed that intra-variance minimization thresholding applied on both original and vesselness filtered images of phantoms provides segmentation without errors. An entropy-maximizing thresholding applied on phantom data was not successful and showed tendency to over-estimate the optimal threshold, both for original and vesselness-filtered images.

Application of variance-minimization thresholding alone and in combination with vessel enhancement on clinical data did not provide satisfying results. Although variance-minimization thresholding on the level of the whole slice had a high hit-rate and sensitivity (as seen in Figures 8 and 9, respectively) it resulted in large oversegmentation error in half of clinical cases (seen in Figures 10 and 11). Namely, the large oversegmentation error appeared in clinical cases with larger image resolution. The reason for this is the fact that the difference between the size (expressed in number of pixels) of foreground (vessels) and the size of background (liver) is larger in images with higher resolution. Additionally, larger difference between foreground and background size also means larger difference between their variance, which was shown to cause oversegmentation of foreground objects when the intra-variance minimization thresholding method is applied.[65–67] The other issue of variance-minimization thresholding applied on original images was that it detected not only vessels but also the liver border which had intensity values similar to vessels (Figure 6.C). Vessel enhancement on the other hand was not sensitive enough. The reason for such low sensitivity is primarily large slice thickness of the clinical data. With a gap of 3 mm between neighboring slices the changes in vessel forms are not smooth enough. Most cases where vessel enhancement was used so far had much smaller slice thickness, with sometimes even isotropic voxels.[20,30,32,33,36] Also, hepatic vessels as seen in medical images, especially major vessels, do not have a shape of a perfect tube. These shape irregularities result in smaller values of vesselness for large vessels which can then not be detected by automatic thresholding.

The complementing weaknesses of vessel enhancement and thresholding on a global level resulted in a segmentation method that would combine these two approaches in a different way. The proposed segmentation method utilizes vessel enhancement thresholded with a low threshold to determine the existence of a vessel. The automatic thresholding method then performs the thresholding in a small region of interest just around the location of a vessel detected in the first step. Regarding the dimension in which each step of the proposed method was performed, we have utilized 3D information only to determine the basic vessel model. For determining the accurate vessel borders we relied on the original 2D information in order to avoid interpolation necessary to obtain isotropic voxels.

The evaluation of the proposed method on clinical data resulted in no large over-segmentations (Figures 10 and 11) with high values of hit-rate (Figure 8) and sensitivity (Figure 9) for both major vessels and all vessels together (tables 2 and 3, respectively). Value of average symmetric surface distance indicates that an error in segmentation of any vessel, major or small is mostly likely to be smaller than 1 pixel. Value of the median Hausdorff distance indicates that, if a larger segmentation error, i.e. an *outlier* appears, it is most likely to be 4.3 pixel for major vessels and 2.8 pixel in general, as seen in Tables 2 and 3, respectively.

A comparison with results of previously developed methods for segmentation of hepatic vessels from CT images was difficult. The general obstacle for such comparison is lack of a publicly available database that all methods would be tested on as well as the lack of unified, standard criteria for validation. Some attempts to standardize validation that would enable direct comparison were made through MICCAI grand challenges which were already organized for segmentation of liver and liver tumors from CT images.[61,68] A similar grand challenge yet remains to be organized for segmentation of hepatic vessels from images of any modality. The main obstacle to performing any kind of comparison of our results was the fact that there are not many results to be compared with. We have searched the Web of Science directory for all papers on the topic of hepatic/liver vessel segmentation from CT images, along with referenced and referencing papers of matches. The search yielded only 19 matches in the past 20 years. Out of 19 papers, 17 of them were tested on clinical data while the remaining 2 were tested only on phantom data. Out of the mentioned 17 papers only 1 paper[39] included a detailed evaluation similar to ours in which the authors assessed the method accuracy and error in the form of average distance as we have. The results from that paper report an average distance of 0.9 mm to 4.4 mm, which is comparable to our findings. The authors also state that »the misclassified vessels do not deviate from the ground truth far away«.[39] In the majority of the remaining 16 papers the evaluation was qualitative based on visual inspection of "goodness" of the segmentation.

Although no definite conclusions can be made about the validity of our method based on direct comparison with other methods, positive conclusions can be drawn with respect to the criteria set at the beginning of our research. Firstly, the method we propose is able to detect all vessels critical for electroporation-based treatments of liver with

above 93% sensitivity. The errors that are produced in segmentation of critical vessels appear in amount which is sufficiently low to enable a fast correction by an expert radiologist. Namely, manual validation by an expert radiologist is a step that should still be mandatory in the process of treatment planning and would also provide valuable feedback for improvement of the segmentation method.

Secondly, the proposed segmentation method is robust to variations in image resolution, imaging devices and protocols. We have shown that the method consistently provided results of high sensitivity when validated on images of different intra-slice resolution. Regarding the slice thickness the results could only be improved using smaller thickness while we would not suggest using images with slices thicker than 3 mm because of high complexity of hepatic vasculature. Given the fact that main method parameters (namely thresholds and parameter c that regulates response of the vesselness filter to high contrast) are automatically calculated from the image, the method is expected to perform well regardless of the imaging device. In order to be used on image series imaged with different protocols only one change should be made. Should the vessels in such case appear brighter instead of darker against the background a minus sign should be added in front of the equation for the vesselness filter.

Thirdly, the method is performed completely automatically with no user input, assuming that the liver is segmented automatically.[17]

Finally, the evaluation of the proposed method resulted in a quantitative estimation of a segmentation error which is most likely to appear in the worst case of segmentation – 2.8 pixels. Assuming the lowest image resolution of our test images, which was 1.188 mm per pixel, the above mentioned segmentation error would translate to 3.3 mm. For comparison, a study on registering CT with MRI images of the liver performed in 2005 reports a mean registration error of 14.0-18.9 mm,[69] while a newer study from 2010 reports a mean error of 3.3 mm.[70] If a segmentation of hepatic vessels was performed on CT images and then registered with MRI images for colorectal metastases segmentation the total error of vessel model would be even higher due to the error of segmentation on CT images itself. It is thus indeed more feasible to perform the hepatic vessel segmentation with our proposed method directly on MRI images. Still, in order to give a final decision if the proposed method of segmentation of hepatic vessels from MRI images can be used in treatment planning of liver tumors with electroporation-based treatments an additional assessment is needed. The additional assessment would be based on introducing the estimated value of the segmentation error – 2.8 pixels – into treatment plan calculations and observe its influence on the distribution of the electric field.

Acknowledgements

This work was supported by the Slovenian Research Agency. Research was conducted in the scope of the Electroporation in Biology and Medicine, European Associated Laboratory. The first author would like to thank Uroš Mitrović for constructive discussion on image segmentation and Dr. Barbara Mali for discussion on statistical methods, both from University of Ljubljana, Faculty of Electrical Engineering. This manuscript is a result of the networking efforts of the COST Action TD1104 (http://www.electroporation.net).

References

1 Neumann E, Schaefer-Ridder M, Wang Y, Hofschneider PH. Gene transfer into mouse lyoma cells by electroporation in high electric fields. *EMBO J* 1982; **1:** 841-5.

2 Kotnik T, Kramar P, Pucihar G, Miklavcic D, Tarek M. Cell membrane electroporation- Part 1: The phenomenon. *IEEE Electr Insul Mag* 2012; **28:** 14-23.

3 Mir LM, Orlowski S, Belehradek J, Paoletti C. Electrochemotherapy potentiation of antitumour effect of bleomycin by local electric pulses. *Eur J Cancer* 1991; **27:** 68-72.

4 Sersa G, Miklavcic D, Cemazar M, Rudolf Z, Pucihar G, Snoj M. Electrochemotherapy in treatment of tumours. *Eur J Surg Oncol* 2008; **34:** 232-40.

5 Mali B, Jarm T, Snoj M, Sersa G, Miklavcic D. Antitumor effectiveness of electrochemotherapy: a systematic review and meta-analysis. *Eur J Surg Oncol* 2013; **39:** 4-16.

6 Lacković I, Magjarević R, Miklavčič D. Three-dimensional finite-element analysis of joule heating in electrochemotherapy and in vivo gene electrotransfer. *IEEE Trans Dielectr Electr Insul* 2009; **16:** 1338-47.

7 Davalos R V., Mir LM, Rubinsky B. Tissue Ablation with Irreversible Electroporation. *Ann Biomed Eng* 2005; **33:** 223-31.

8 Chu KF, Dupuy DE. Thermal ablation of tumours: biological mechanisms and advances in therapy. *Nat Rev Cancer* 2014; **14:** 199-208.

9 Kos B, Zupanic A, Kotnik T, Snoj M, Sersa G, Miklavcic D. Robustness of treatment planning for electrochemotherapy of deep-seated tumors. *J Membr Biol* 2010; **236:** 147-53.

10 Miklavcic D, Beravs K, Semrov D, Cemazar M, Demsar F, Sersa G. The importance of electric field distribution for effective in vivo electroporation of tissues. *Biophys J* 1998; **74:** 2152-8.

11 Mali B, Miklavcic D, Campana LG, Cemazar M, Sersa G, Snoj M, et al. Tumor size and effectiveness of electrochemotherapy. *Radiol Oncol* 2013; **47:** 32-41.

12 Miklavcic D, Snoj M, Zupanic A, Kos B, Cemazar M, Kropivnik M, et al. Towards treatment planning and treatment of deep-seated solid tumors by electrochemotherapy. *Biomed Eng Online* 2010; **9:** 10.

13 Pavliha D, Kos B, Zupanič A, Marčan M, Serša G, Miklavčič D. Patient-specific treatment planning of electrochemotherapy: Procedure design and possible pitfalls. *Bioelectrochemistry* 2012; **87:** 265-73.

14 Kos B, Zupanic A, Kotnik T, Snoj M, Sersa G, Miklavcic D. Robustness of treatment planning for electrochemotherapy of deep-seated tumors. *J Membr Biol* 2010; **236:** 147-53.

15 Županič A, Čorović S, Miklavčič D. Optimization of electrode position and electric pulse amplitude in electrochemotherapy. *Radiol Oncol* 2008; **42:** 93-101.

16 Edhemovic I, Gadzijev EM, Brecelj E, Miklavcic D, Kos B, Zupanic A, et al. Electrochemotherapy: a new technological approach in treatment of metastases in the liver. *Technol Cancer Res Treat* 2011; **10:** 475-85.

17 Pavliha D, Mušič MM, Serša G, Miklavčič D. Electroporation-based treatment planning for deep-seated tumors based on automatic liver segmentation of MRI images. *PLoS One* 2013; **8:** e69068.

18 Fraass B, Doppke K, Hunt M, Kutcher G, Starkschall G, Stern R, et al. American Association of Physicists in Medicine Radiation Therapy Committee Task Group 53: quality assurance for clinical radiotherapy treatment planning. *Med Phys* 1998; **25:** 1773-829.

19 Payne S, Flanagan R, Pollari M, Alhonnoro T, Bost C, O'Neill D, et al. Image-based multi-scale modelling and validation of radio-frequency ablation in liver tumours. *Philos Trans A Math Phys Eng Sci* 2011; **369:** 4233-54.

20 Alhonnoro T, Pollari M, Lilja M, Flanagan R, Kainz B, Muehl J, et al. Vessel Segmentation for Ablation Treatment Planning and Simulation. In: Jiang T, Navab N, Pluim JPW, et al., editors. *Medical image computing and computer-assisted intervention : MICCAI International Conference on Medical Image Computing and Computer-Assisted Intervention*. Volume 6361. Springer Berlin Heidelberg; 2010. pp. 45-52.

21 Hansen PD, Rogers S, Corless CL, Swanstrom LL, Siperstien a E. Radiofrequency ablation lesions in a pig liver model. *J Surg Res* 1999; **87:** 114-21.

22 Sersa G, Jarm T, Kotnik T, Coer A, Podkrajsek M, Sentjurc M, et al. Vascular disrupting action of electroporation and electrochemotherapy with bleomycin in murine sarcoma. *Br J Cancer* 2008; **98:** 388-98.

23 Lesage D, Angelini ED, Bloch I, Funka-Lea G. A review of 3D vessel lumen segmentation techniques: models, features and extraction schemes. *Med Image Anal* 2009; **13:** 819-45.

24 Glombitza G, Lamade W, Demiris a M, Gopfert M, Mayer a, Bahner ML, et al. Virtual planning of liver resections: image processing, visualization and volumetric evaluation. *Int J Med Inform* 1999; **53:** 225-37.

25 Zahlten C, Jürgens H, Evertsz CJG, Leppek R, Peitgen H-O, Klose KJ. Portal vein reconstruction based on topology. *Eur J Radiol* 1995; **19:** 96-100.

26 Selle D, Preim B, Schenk A, Peitgen H-O. Analysis of vasculature for liver surgical planning. *IEEE Trans Med Imaging* 2002; **21:** 1344-57.

27 Sato Y, Nakajima S, Shiraga N, Atsumi H, Yoshida S, Koller T, et al. Three-dimensional multi-scale line filter for segmentation and visualization of curvilinear structures in medical images. *Med Image Anal* 1998; **2:** 143-68.

28 Frangi AF, Niessen WJ, Vincken KL, Viergever MA. Multiscale vessel enhancement filtering. In: Wells WM, Colchester A, Delp S, editors. *Medical Image Computing and Computer-Assisted Intervention - MICCAI '98 (1998)*. Springer Berlin Heidelberg; 1998. pp. 130-7.

29 Krissian K, Malandain G, Ayache N, Vaillant R, Trousset Y. Model-Based Detection of Tubular Structures in 3D Images. *Comput Vis Image Underst* 2000; **80:** 130-71.

30 Conversano F, Franchini R, Demitri C, Massoptier L, Montagna F, Maffezzoli A, et al. Hepatic vessel segmentation for 3D planning of liver surgery experimental evaluation of a new fully automatic algorithm. *Acad Radiol* 2011; **18:** 461-70.

31 Bauer C, Pock T, Sorantin E, Bischof H, Beichel R. Segmentation of interwoven 3d tubular tree structures utilizing shape priors and graph cuts. *Med Image Anal* 2010; **14:** 172-84.

32 Shang Q, Clements L, Galloway RL, Chapman WC, Dawant BM. Adaptive directional region growing segmentation of the hepatic vasculature. In: Reinhardt JM, Pluim JPW, editors. *Proceedings of SPIE*. Volume 6914. SPIE; 2008. p. 69141F-10.

33 Beichel R, Pock T, Janko C, Zotter RB, Reitinger B, Bornik A, et al. Liver segment approximation in CT data for surgical resection planning. In: Fitzpatrick JM, Sonka M, editors. *Proceedings of SPIE*. SPIE; 2004. pp. 1435-46.

34 Wang G, Zhang S, Li F, Gu L. A new segmentation framework based on sparse shape composition in liver surgery planning system. *Med Phys* 2013; **40:** 051913.

35 Soler L, Delingette H, Malandain G, Montagnat J, Ayache N, Koehl C, et al. Fully automatic anatomical, pathological, and functional segmentation from CT scans for hepatic surgery. *Comput aided Surg Off J Int Soc Comput Aided Surg* 2001; **6:** 131-42.

36 Pamulapati V, Wood BJ, Linguraru MG. Intra-hepatic vessel segmentation and classification in multi-phase CT using optimized graph cuts. In: Yoshida H, Sakas G, Linguraru MG, editors. *2011 IEEE International Symposium on Biomedical Imaging: From Nano to Macro*. Volume 7029. IEEE; 2011. pp. 1982-5.

37 Esneault S, Lafon C, Dillenseger J-L. Liver vessels segmentation using a hybrid geometrical moments/graph cuts method. *IEEE Trans Biomed Eng* 2010; **57:** 276-83.

38 Shang Y, Deklerck R, Nyssen E, Markova A, de Mey J, Yang X, et al. Vascular active contour for vessel tree segmentation. *IEEE Trans Biomed Eng* 2011; **58:** 1023-32.

39 Chi Y, Liu J, Venkatesh SK, Huang S, Zhou J, Tian Q, et al. Segmentation of liver vasculature from contrast enhanced CT images using context-based voting. *IEEE Trans Biomed Eng* 2011; **58:** 2144-53.

40 Bipat S, van Leeuwen MS, Comans EFI, Pijl MEJ, Bossuyt PMM, Zwinderman AH, et al. Colorectal liver metastases: CT, MR imaging, and PET for diagnosis--meta-analysis. *Radiology* 2005; **237:** 123-31.

41 Chan VO, Das JP, Gerstenmaier JF, Geoghegan J, Gibney RG, Collins CD, et al. Diagnostic performance of MDCT, PET/CT and gadoxetic acid (Primovist®)-enhanced MRI in patients with colorectal liver metastases being considered for hepatic resection: initial experience in a single centre. *Ir J Med Sci* 2012; **181:** 499-509.

42 Floriani I, Torri V, Rulli E, Garavaglia D, Compagnoni A, Salvolini L, et al. Performance of imaging modalities in diagnosis of liver metastases from colorectal cancer: a systematic review and meta-analysis. *J Magn Reson Imaging* 2010; **31:** 19-31.

43 Fowler KJ, Linehan DC, Menias CO. Colorectal liver metastases: state of the art imaging. *Ann Surg Oncol* 2013; **20:** 1185-93.

44 Mainenti PP, Mancini M, Mainolfi C, Camera L, Maurea S, Manchia A, et al. Detection of colo-rectal liver metastases: prospective comparison of contrast enhanced US, multidetector CT, PET/CT, and 1.5 Tesla MR with extracellular and reticulo-endothelial cell specific contrast agents. *Abdom Imaging* 2010; **35:** 511-21.

45 Muhi A, Ichikawa T, Motosugi U, Sou H, Nakajima H, Sano K, et al. Diagnosis of colorectal hepatic metastases: comparison of contrast-enhanced CT, contrast-enhanced US, superparamagnetic iron oxide-enhanced MRI, and gadoxetic acid-enhanced MRI. *J Magn Reson Imaging* 2011; **34:** 326-35.

46 Kranjc M, Bajd F, Serša I, Miklavčič D. Magnetic resonance electrical impedance tomography for monitoring electric field distribution during tissue electroporation. *IEEE Trans Med Imaging* 2011; **30:** 1771-8.

47 Kranjc M, Bajd F, Sersa I, Woo EJ, Miklavcic D. Ex vivo and in silico feasibility study of monitoring electric field distribution in tissue during electroporation-based treatments. *PLoS One* 2012; **7:** e45737.

48 Pavliha D, Kos B, Marčan M, Zupanič A, Serša G, Miklavčič D. Planning of electroporation-based treatments using Web-based treatment planning software. *J Membr Biol* 2013; **246:** 833-42.

49 Vovk U, Pernus F, Likar B. A review of methods for correction of intensity inhomogeneity in MRI. *IEEE Trans Med Imaging* 2007; **26:** 405-21.

50 Zheng Y, Grossman M, Awate SP, Gee JC. Automatic correction of intensity nonuniformity from sparseness of gradient distribution in medical images. *Med Image Comput Comput Assist Interv* 2009; **12:** 852-9.

51 Sankur B. Survey over image thresholding techniques and quantitative performance evaluation. *J Electron Imaging* 2004; **13:** 146.

52 Otsu N. A Threshold Selection Method from Gray-Level Histograms. *IEEE Trans Syst Man Cybern* 1979; **9:** 62-6.

53 Kapur JN, Sahoo PK, Wong AKC. A new method for gray-level picture thresholding using the entropy of the histogram. *Comput Vision, Graph Image Process* 1985; **29:** 273-85.

54 Yaroslavsky LP. Efficient algorithm for discrete sinc interpolation. *Appl Opt* 1997; **36:** 460-3.

55 Van Dongen E, van Ginneken B. Automatic segmentation of pulmonary vasculature in thoracic CT scans with local thresholding and airway wall removal. In: *2010 IEEE International Symposium on Biomedical Imaging: From Nano to Macro*. IEEE; 2010. pp. 668-71.

56 Augusto L, Braga F, Silveira C, Paula V, Fazan S. Arterial diameter of the celiac trunk and its branches . Anatomical study 1 Diâmetro arterial do tronco celíaco e seus ramos . *Estudo Anatômico* 2009; **24:** 43-7.

57 Olabarriaga S., Breeuwer M, Niessen W. Evaluation of Hessian-based filters to enhance the axis of coronary arteries in CT images. *Int Congr Ser* 2003; **1256:** 1191-6.

58 Merkx M a G, Bescós JO, Geerts L, Bosboom EMH, van de Vosse FN, Breeuwer M. Accuracy and precision of vessel area assessment: manual versus automatic lumen delineation based on full-width at half-maximum. *J Magn Reson Imaging* 2012; **36:** 1186-93.

59 Jiang J, Haacke EM, Dong M. Dependence of vessel area accuracy and precision as a function of MR imaging parameters and boundary detection algorithm. *J Magn Reson Imaging* 2007; **25:** 1226-34.

60 Virtanen JM, Komu ME, Parkkola RK. Quantitative liver iron measurement by magnetic resonance imaging: in vitro and in vivo assessment of the liver to muscle signal intensity and the R2* methods. *Magn Reson Imaging* 2008; **26:** 1175-82.

61 Deng X, Du G. Editorial: 3D segmentation in the clinic: A grand challenge II-liver tumor segmentation. In: *International Conference on Medical Image Computing and Computer Assisted Intervention*. 2008. pp. 1-12.

62 Van Erkel a R, Pattynama PM. Receiver operating characteristic (ROC) analysis: basic principles and applications in radiology. *Eur J Radiol* 1998; **27:** 88-94.

63 Obuchowski NA. Receiver operating characteristic curves and their use in radiology. *Radiology* 2003; **229:** 3-8.

64 Wagner RF, Metz CE, Campbell G. Assessment of medical imaging systems and computer aids: a tutorial review. *Acad Radiol* 2007; **14:** 723-48.

65 Hou Z, Hu Q, Nowinski WL. On minimum variance thresholding. *Pattern Recognit Lett* 2006; **27:** 1732-43.

66 Medina-Carnicer R, Madrid-Cuevas FJ. Unimodal thresholding for edge detection. *Pattern Recognit* 2008; **41:** 2337-46.

67 Xu X, Xu S, Jin L, Song E. Characteristic analysis of Otsu threshold and its applications. *Pattern Recognit Lett* 2011; **32:** 956-61.

68 Heimann T, Van Ginneken B, Styner MA, Arzhaeva Y, Aurich V, Bauer C, et al. Comparison and evaluation of methods for liver segmentation from CT datasets. *IEEE Trans Med Imaging* 2009; **28:** 1251-65.

69 Christina Lee W-C, Tublin ME, Chapman BE. Registration of MR and CT images of the liver: comparison of voxel similarity and surface based registration algorithms. *Comput Methods Programs Biomed* 2005; **78:** 101-14.

70 Elhawary H, Oguro S, Tuncali K, Morrison PR, Tatli S, Shyn PB, et al. Multimodality non-rigid image registration for planning, targeting and monitoring during CT-guided percutaneous liver tumor cryoablation. *Acad Radiol* 2010; **17:** 1334-44.

PAPER 2

Title: Effect of blood vessel segmentation on the outcome of electroporation-based treatments of liver tumors

Authors: MARČAN Marija, KOS Bor, MIKLAVČIČ Damijan

Publication: PLoS ONE

DOI: 10.1371/journal.pone.0125591

Year: 2015

Volume: 10

Number: 5

Pages: e0125591

Impact factor: 3.534

Ranking:

Category name	Total journals in category	Journal rank in category	Quartile in category
multidisciplinary sciences	55	8	Q1

PLOS | ONE

RESEARCH ARTICLE

Effect of Blood Vessel Segmentation on the Outcome of Electroporation-Based Treatments of Liver Tumors

Marija Marčan, Bor Kos, Damijan Miklavčič*

University of Ljubljana, Faculty of Electrical Engineering, Ljubljana, Slovenia

* damijan.miklavcic@fe.uni-lj.si

CrossMark

OPEN ACCESS

Citation: Marčan M, Kos B, Miklavčič D (2015) Effect of Blood Vessel Segmentation on the Outcome of Electroporation-Based Treatments of Liver Tumors. PLoS ONE 10(5): e0125591. doi:10.1371/journal.pone.0125591

Academic Editor: Qinghui Zhang, University of Nebraska Medical Center, UNITED STATES

Received: November 17, 2014

Accepted: March 14, 2015

Published: May 5, 2015

Copyright: © 2015 Marčan et al. This is an open access article distributed under the terms of the Creative Commons Attribution License, which permits unrestricted use, distribution, and reproduction in any medium, provided the original author and source are credited.

Data Availability Statement: Medical images that were used to create real-patient models in this study are third-party data from the "Treatment of Liver Metastases with Electrochemotherapy (ECTJ)" (EudraCt no. 2008-008290- 54, registered at Clinicaltrials.gov no. NCT01264952). Interested researchers may wish to request access to these images by contacting the authors of the clinical study: Prof. Gregor Sersa (GSersa@onko-i.si) and Ibrahim Edhemovic MD, PhD (ibrahim.edhemovic@mf.uni-lj.si). COMSOL models from the rest of the study are publicly available on the COMSOL Model Exchange

Abstract

Electroporation-based treatments rely on increasing the permeability of the cell membrane by high voltage electric pulses applied to tissue via electrodes. To ensure that the whole tumor is covered with sufficiently high electric field, accurate numerical models are built based on individual patient anatomy. Extraction of patient's anatomy through segmentation of medical images inevitably produces some errors. In order to ensure the robustness of treatment planning, it is necessary to evaluate the potential effect of such errors on the electric field distribution. In this work we focus on determining the effect of errors in automatic segmentation of hepatic vessels on the electric field distribution in electroporation-based treatments in the liver. First, a numerical analysis was performed on a simple 'sphere and cylinder' model for tumors and vessels of different sizes and relative positions. Second, an analysis of two models extracted from medical images of real patients in which we introduced variations of an error of the automatic vessel segmentation method was performed. The results obtained from a simple model indicate that ignoring the vessels when calculating the electric field distribution can cause insufficient coverage of the tumor with electric fields. Results of this study indicate that this effect happens for small (10 mm) and medium-sized (30 mm) tumors, especially in the absence of a central electrode inserted in the tumor. The results obtained from the real-case models also show higher negative impact of automatic vessel segmentation errors on the electric field distribution when the central electrode is absent. However, the average error of the automatic vessel segmentation did not have an impact on the electric field distribution if the central electrode was present. This suggests the algorithm is robust enough to be used in creating a model for treatment parameter optimization, but with a central electrode.

Introduction

Exposing a biological cell to a sufficiently high electric field causes increased permeability of the cell membrane. This increased permeability of the membrane allows transfer of molecules which normally lack membrane transport mechanisms into the cell. The described effect of the

repository: http://www.comsol.com/community/exchange/261/.

Funding: This work was supported by the Slovenian Research Agency (ARRS). Research was conducted in the scope of the Electroporation in Biology and Medicine (EBAM) European Associated Laboratory (LEA). The funders had no role in study design, data collection and analysis, decision to publish, or preparation of the manuscript.

Competing Interests: The authors have declared that no competing interests exist.

electric field on the cell is called electroporation [1, 2]. Electroporation can be either reversible or irreversible. The reversible/irreversible nature of electroporation is strongly dependent on pulse amplitude, duration, and number of pulses [3]. In reversible electroporation, the cell membrane eventually returns to its normal state. Irreversible electroporation however leads to cell death because the cell membrane is permanently disrupted or due to the extensive loss of the intracellular components [4]. Combination of reversible electroporation with traditional methods of chemotherapy has resulted in a technology for tumor treatment named electrochemotherapy (ECT) [5, 6]. Irreversible electroporation (IRE) has found its application in tumor treatment as a tissue ablation procedure, its main advantage being the fact that it does not rely on thermal effects to achieve tissue ablation [7, 8].

In order for the tumor treatments based on electroporation to be successful the whole tumor must be covered by a sufficiently high electric field [9]. The magnitude and distribution of the electric field depends on the number and the position of the electrodes, the amplitudes of pulses applied per electrode pair and the electric properties of the tissue, especially conductivity [10, 11]. Ensuring the complete tumor coverage with a sufficiently high electric field is challenging in the case of deep-seated solid tumors as well as large tumors [12–14]. Predictability of an adequate distribution of the electric field can be best achieved by calculating a patient-specific treatment plan as a part of an electroporation-based treatment procedure [15–17].

A patient-specific treatment plan for electroporation-based treatment of deep-seated solid tumors takes into account patient geometry and tissue properties to generate an optimal set of treatment parameters [18, 19]. The patient model is built by segmenting the medical images and then used to perform numerical calculations of the electric field distribution. First use of the treatment planning procedure was done in a patient with a metastasis in the thigh [15], then the procedure was upgraded in a clinical study of liver metastases [20]. For the purpose of treating the colorectal metastases by ECT, an algorithm for automatic segmentation of the liver from MRI images was developed [21], as well as an algorithm for segmentation of hepatic vessels reported in our previous work [22].

Segmentation of medical images is susceptible to errors, which must be taken into account when analyzing robustness of the treatment plan. In order to evaluate the effect of errors in segmentation of hepatic vessels we performed studies consisting of numerical modeling of the electric field distribution in ECT and IRE of a simplified model of tumor and vessel, and ECT of two models obtained from two real patients. The first part of the studies focused on determining in what measure the vessels of different sizes influence the distribution of the electric field in an already optimized model. Through these experiments we aimed to establish if ignoring the vessels in the numerical calculations could potentially have negative effects on the tumor coverage with a sufficiently high electric field. The second part of the studies observed the effect of known errors of the vessel segmentation method reported in our previous work [22] on possible over- or underestimation of the electric field distribution which leads to over- or under-treatment.

Materials and Methods

Simplified model

The simplified model consisted of a sphere and a cylinder, where the sphere represented the tumor and the cylinder represented the vessel. We used three different sphere diameters: 10 mm, 30 mm and 50 mm. Such choice of sphere size was made because colorectal metastases in the liver that are most often treated with ECT have a diameter 10–30 mm [20], while primary tumors in the liver can be as large as 50 mm. The vessel that was included in the model varied in size and position relative to the tumor. The diameters of the vessel were 1 mm, 3 mm, 5 mm,

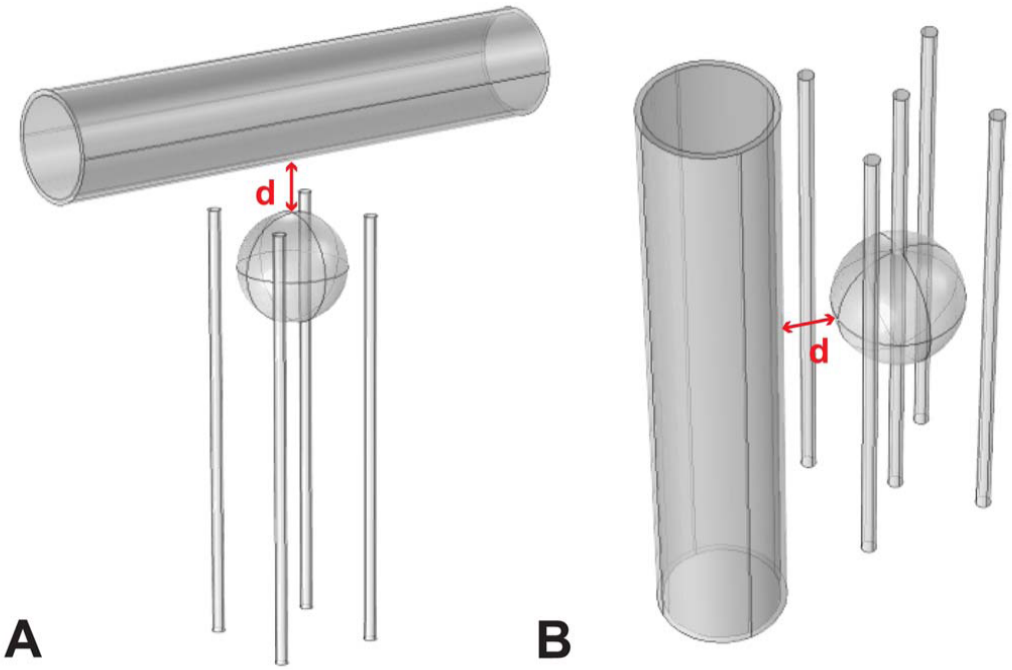

Fig 1. Two different electrode configurations and two different positions of the vessel. A: 4 electrodes with vessel perpendicular to them. B: 5 electrodes with vessel parallel to them. "d" denotes distance from vessel to tumor.

doi:10.1371/journal.pone.0125591.g001

10 mm and 15 mm, which are all actual sizes of hepatic vessels. The vessel was positioned in two different orientations, as shown in Fig 1: perpendicular (A) and parallel to the electrodes (B). Additionally, we varied the distance of the vessel from the tumor, setting it to 0 mm, 1 mm, 3 mm, 5 mm and 10 mm. These variations in vessel size and position were applied on all combinations of tumor size and treatment type as indicated in Table 1. The vessel was modeled as a combination of blood tissue and vessel wall tissue which had a thickness of 10% of the vessel diameter. Such vessel structure is observed in veins, which make up the majority of large hepatic vessels (vena porta, vena cava and main hepatic veins) [23].

For all three tumor sizes we used electrodes of 1.2 mm diameter with an active tip of 40 mm length. The number and the position of the electrodes varied depending on the tumor size and the type of the electroporation-based treatment (ECT or IRE). The information about number and the position of the electrodes per combination of tumor size and treatment is presented in Table 1. Generally, the depth of the electrode relative to tumor was such that the tumor was positioned in the middle of the active part of the electrodes. The only exceptions to this rule were made in cases of a 10 mm tumor and large vessels (10 mm and 15 mm diameter) perpendicular to the electrodes, where the depth was adjusted in order to avoid electrodes penetrating the vessels. In such cases, the depth of the electrodes was set to 1 or 5 mm further than the edge of the tumor that is near the vessel. Complete geometry was transformed into a mesh of free

Table 1. Electrode number and position per tumor size and treatment type.

Tumor diameter size [mm]	Treatment	Electrode number	Electrode position
10	ECT	4	4 in a box around the tumor, 2 mm away from the tumor edge
10	ECT	5	4 in a box around the tumor, 2 mm away from the tumor edge + 1 in the center
30	ECT	5	4 in a box around the tumor, 2 mm away from the tumor edge + 1 in the center
50	ECT	7	6 in a hexagon around the tumor, 2 mm away from the tumor edge + 1 in the center
10	IRE	4	4 in a box around the tumor, 2 mm away from the tumor edge
10	IRE	5	4 in a box around the tumor, 2 mm away from the tumor edge + 1 in the center
30	IRE	7	6 in a hexagon inside the tumor, 7 mm away from the tumor center + 1 in the center

doi:10.1371/journal.pone.0125591.t001

tetrahedral elements using the user-controlled meshing sequence of COMSOL Multiphysics (COMSOL, Stockholm, Sweden) with element size set to 'Fine' according to COMSOL properties and values of all other properties left default. The number of elements ranged from 50000 to 70000, based on the specific geometry.

All models included a dynamic change in the conductivity of all tissues that occurs due to electroporation [19, 24, 25]. The conductivity change was modeled as a smoothed Heaviside function of the electric field in the range between the threshold of reversible electroporation, E_0 and the irreversible threshold, E_1 [24, 25]. Values of the above mentioned thresholds for liver and tumor tissue were taken from literature [26], while for the vessel wall and the blood they were estimated based on the experiments performed on similar tissue [27, 28]. We have also used different initial and final conductivities, σ_0 and σ_1 for each of the tissues [26–31]. The values of E_0 and E_1 along with initial and final conductivities σ_0 and σ_1 for each tissue are given in Table 2. It should be noted that while the conductivity increase for liver and tumor tissues was already determined by measurements [28, 29], for vessel wall and blood tissue we had to extrapolate the data from measurements on similar tissue. Therefore, for vessel walls we have chosen the conductivity increase factor of 3 based on experiments made with muscle tissue [28]. For blood we first made the assumption that it is in fact a suspension of red blood cells in a high conductive medium (plasma), with a normal cell volume fraction of 0.46. We then referred to the previous work of Pavlin et al. on cell suspension electroporation [27, 32] and determined that factor of conductivity for blood with given assumptions is around 0.5.

For all the models we calculated the electric field distribution using finite element analysis in COMSOL Multiphysics (COMSOL, Stockholm, Sweden). From the resulting electric field distribution we extracted the percentage of tumor volume covered with the electric field higher than the target field, which is 400 V/cm for ECT and 600 V/cm for IRE. The values of target fields are determined based on the definition that a successful electroporation-based treatment

Table 2. Values of electroporation thresholds and conductivities for different tissues with corresponding sources.

Tissue	E_0 [V/cm]	E_1 [V/cm]	σ_0 [S/m]	σ_1 [S/m]
Liver	350 [28]	700 [28]	0.04 [29]	0.12 [26, 28, 29]
Tumor	400 [26]	800 [26]	0.2 [30]	0.7 [26, 28, 30]
Vessel wall	400 [28]	800 [28]	0.26 [31]	0.78 [25, 26, 28, 31]
Blood	400 [27]	1100 [27]	0.7 [31]	1.05 [27, 31, 32]

doi:10.1371/journal.pone.0125591.t002

achieves above 99.9% cell kill. The statistical model of cell kill due to electroporation was previously described in the work of Golberg et al. [33] and states that cell kill depends not only on the electric field but also on number of pulses and pulse duration. Depending on number of pulses used the target field that is necessary to achieve 99.9% cell kill can thus be lower than E_1. In our case the target field values are set with respect to the number of pulses typically used for different electroporation-based treatment, which is 8 for ECT and 90 for IRE.

The workflow of the numerical calculations was divided in two parts. Firstly, we observed only the model of the tumor without the vessel, on which we employed the optimization algorithm described in the work of Zupanic et al [19]. The optimization was performed with respect to the voltages between neighboring (outer) pairs of electrodes and between the electrodes in diagonal direction. The geometry of the model, along with the electrode positions, was kept constant. The optimization criterion was to achieve 100% coverage of the tumor with a sufficiently high electric field (400 V/cm for ECT or 600 V/cm for IRE), while minimizing the amount of liver tissue covered by the electric field above the IRE threshold for liver (400 V/cm) [33, 34]. Secondly, we included the vessel into the model and performed the calculation of the electric field distribution with the same values of voltages that were optimal for the model without the vessel. We then determined the percent of the tumor that was covered with a sufficiently high electric field. In this way, the difference between a model that does not take vessels into account and the one that does was obtained. The above described workflow was performed for all combinations of tumor size and treatment type indicated in Table 1. and for all variations in vessel size and position.

Real patient model

Two models used in the second part of the studies were obtained from patients that were treated with ECT for a colorectal liver metastasis. The first patient was also reported in the work of Edhemovic et al. [16, 20]. Five years after the ECT that patient is alive and disease-free.

Specificity of these particular cases is that the tumor was located in the close vicinity of major hepatic vessels: vena cava and the second branches of the hepatic vein. One MRI slice along with the reconstructed 3D model for each case are shown in Fig 2. The sizes of the tumors, as determined by the radiologist, were 35 mm × 20 mm for the first tumor and 15 mm × 11 mm for the second tumor.

The 3D models of the tumors and the nearby vessels were obtained based on the segmentation of the MRI images by an expert radiologist. The number of the electrodes used in the two cases varied due to different tumor sizes. For the first case, the actual treatment was performed using six individual electrodes: two inside the tumor and four outside. We kept the same electrode configuration in our model. For the second case, the actual treatment was performed using five individual electrodes: one inside the tumor and four outside. In our model we used the same five electrode configuration and additionally created a model with only four outer electrodes (without the central electrode in the tumor). Therefore, we had three models in total: one model for the first case and two for the second case.

In all three models we varied the size and the position of the vessels in order to include the error of the automatic vessel segmentation algorithm. The mentioned algorithm for automatic segmentation of hepatic vessels from MRI images was described and validated in our previous work [22]. The results of the validation report an average error of the algorithm to be 0.9 pixel, while the maximum error is 2.8 pixels. These values of the error were introduced in the model through six transformations: enlarging, shrinking, shift left, shift right, shift up and shift down. The values used in the transformations were rounded from 0.9 and 2.8 to 1 and 3, respectively, in order to use integers.

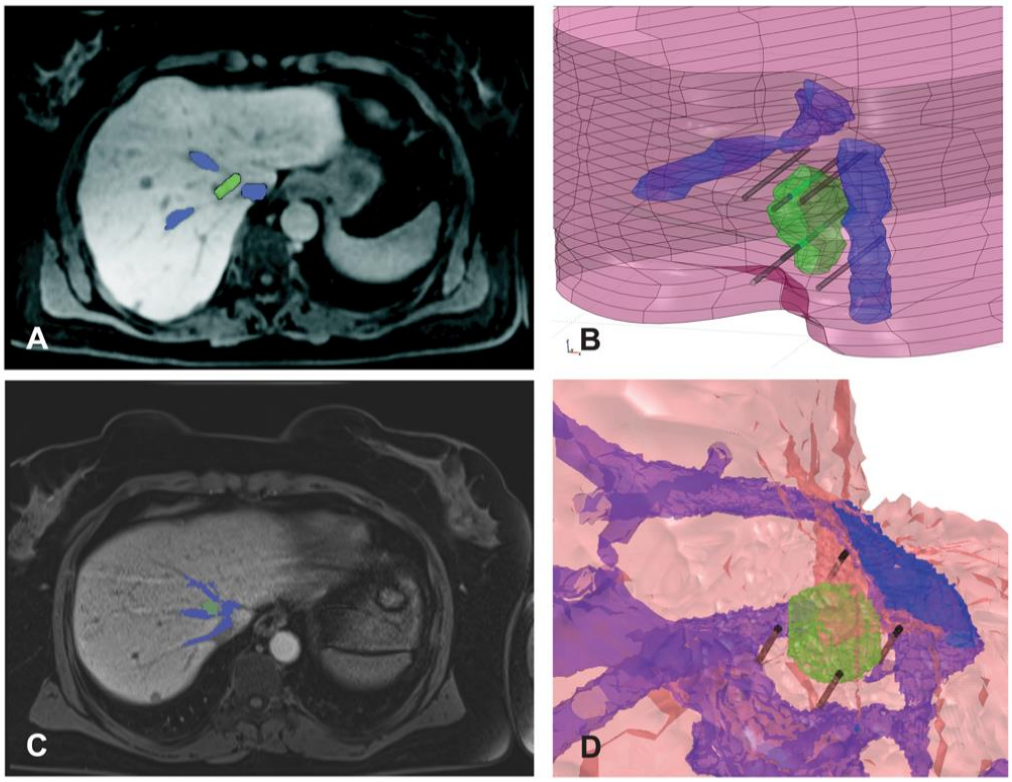

Fig 2. Real patient cases used in our study. A: MRI of the liver for first patient case. B: Reconstructed 3D model of the first case with inserted electrodes. C: MRI of the liver for second patient case. D: Reconstructed 3D model of the second case with inserted electrodes. In all images the structure colored green is the tumor, while the nearby major vessels are colored blue.

doi:10.1371/journal.pone.0125591.g002

The electrodes were initially positioned at the coordinates used in the actual treatments. However, in the models with modified vessel size and position it could happen that the initial electrode trajectory would go through the vessel, which should be avoided when possible, since it can cause failure of pulse delivery due to excessive currents. Namely, the currently available ECT and IRE pulse generator have a 50 A maximum current limit. The high conductivity of blood can cause currents to rise above that limit, which causes the generator to abort pulse delivery to that particular electrode pair. We have therefore visually inspected images of all models with modified vessels and minimally adjusted the electrode positions to avoid having an electrode go through the vessel.

The workflow of the numerical calculations in this part of the study was reversed in respect to the workflow of the simplified model. Here we first introduced the error in vessel geometry, after which we ran the optimization of the treatment, resulting in optimal values of voltages per electrode pair. Again, only the voltages were optimized, while the positions of the electrodes

were kept constant, as they were set in the original treatment of the patient. The obtained values of optimal voltages were then used in numerical calculations on an original model with correct vessel geometry. Based on the results of these calculations we then calculated the coverage of the tumor with a sufficiently high electric field and observed if there was any insufficient coverage of the tumor that could have happened due to errors in vessel segmentation. On the real patient geometries we performed only the calculations for ECT treatment.

Additionally, we also calculated the differences in the coverage of tumors from real patient models between correct vessel geometry and not taking the vessels into account at all. The workflow for these calculations was the same as described above, with the difference that in the first step instead of introducing an error in vessel geometry the vessels were simply excluded from the model.

Ethics statement

The two patients whose medical images were used in the experiments were a part of a clinical study "Treatment of Liver Metastases with Electrochemotherapy (ECTJ)" (EudraCt no. 2008-008290- 54, registered at Clinicaltrials.gov no. NCT01264952). The study was prospective, phase I/II, conducted at the Institute of Oncology Ljubljana, Ljubljana, Slovenia. Regulatory approvals from the Institutional board, as well as from the Medical Ethics Committee of the Republic of Slovenia were obtained, under following document numbers: KME 45/09/08, 108/10/12, and 46/12/13. Written consents of the patients were obtained. The patients included in the clinical study were treated according to the principles expressed in the Declaration of Helsinki.

Results

Simplified model

The first step of the studies performed on the simplified model, optimization of the model without the vessels, gave optimal values of voltages. The positions of the electrodes were not optimized. The obtained voltages are presented in Table 3 for each individual combination of tumor size, treatment type and electrode number.

The values of voltages obtained from optimization as well as position of the electrodes were kept constant after including the vessels in the model. In Figs 3–6 we present results of the studies performed on a simplified model with both tumor and vessel. In all of the figures the coverage of the tumor volume by a sufficiently high electric field is plotted against the distance of the vessel from the tumor, grouped by different sizes of the vessel. The red line in all of the figures indicates a threshold of the tumor coverage required for a successful treatment, which is set to 99.9%. The choice of threshold being 99.9% was made for better readability of the figures and is otherwise in no way different than if we had chosen to set it to 100%. Each of the Figs 3–6 presents a different combination of tumor size, treatment type and electrode number. The figures are divided into an A. and B. part, where A. shows a case with vessel perpendicular to the electrodes while B. shows the case with vessel parallel to the electrodes. In cases of ECT of 50 mm tumor, IRE of 10 mm tumor with 5 electrodes and IRE of 30 mm tumor, the vessels have no negative effect on the tumor volume coverage at all. Therefore results of these cases are not graphically shown in this manuscript.

Based on results presented in Figs 3–6 neglecting vessels in model of the electric field distribution causes the tumor not to be entirely covered by sufficiently high electric field. The percentage of the tumor that is not covered with sufficiently high electric field leads to incomplete treatment, i.e. treatment failure. The extent of the negative effect of neglecting vessels depends on tumor size, vessel diameter, distance to tumor and orientation regarding the electrodes. For tumors with 10 mm diameter, the negative effect is observed for vessels with diameter 3–10

Table 3. Optimal voltages for a model without the vessel, per tumor size, treatment type and electrode number.

Tumor diameter size [mm]	Treatment	Electrode number	Voltage between outer electrodes [V]	Diagonal voltage [V]
10	ECT	4	600	1000
10	ECT	5	800	500
30	ECT	5	2300	1500
50	ECT	7	1000	3000
10	IRE	4	3000	900
10	IRE	5	1100	2500
30	IRE	7	2900	2700

Diagonal voltage stands for voltage between the center electrode and surrounding electrodes. In the case of a configuration with 4 electrodes diagonal voltage is the voltage between non-neighbor electrodes.

doi:10.1371/journal.pone.0125591.t003

mm that are less than 3 mm away from the tumor, and vessels 10 mm or larger that are less than 5 mm away from the tumor. This observation was made for the worst case, which is ECT with 4 electrodes (Fig 3). For tumors with 30 mm diameter the worst case of the negative effect is again ECT, where the critical vessels have a diameter 7 mm and more and are within 5 mm distance to the tumor. In general, the negative influence of the vessels is directly proportional to vessel size and inversely proportional to vessel distance from the tumor. The only anomaly to this rule is observed for ECT and IRE of a 10 mm tumor performed with 4 electrodes, where the electrode depths (and subsequently optimal voltages) had to be changed for 10 mm and 15 mm vessels in order to avoid having all 4 electrodes go through the vessel, as described in the Materials and methods section. In the case of IRE of 10 mm tumor the breach of the vessel was inevitable up to 3 mm away from the tumor, which resulted in higher tumor coverage for 10 mm and 15 mm vessels than logically anticipated.

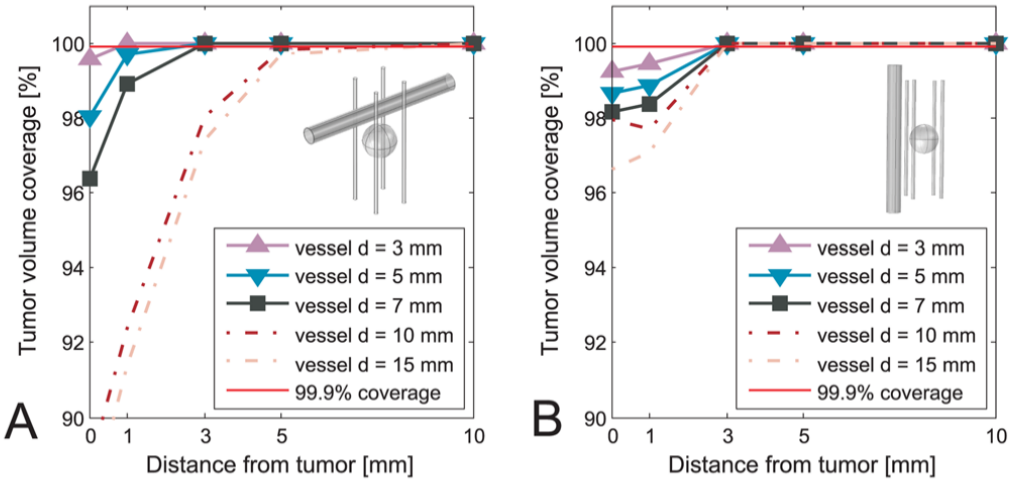

Fig 3. Tumor coverage for ECT of simplified model of 10 mm tumor with 4 electrodes. The coverage is plotted against different distances between vessel and tumor, and with respect to different vessel positions and sizes. A: Vessel perpendicular to the electrodes. B: Vessel parallel to the electrodes.

doi:10.1371/journal.pone.0125591.g003

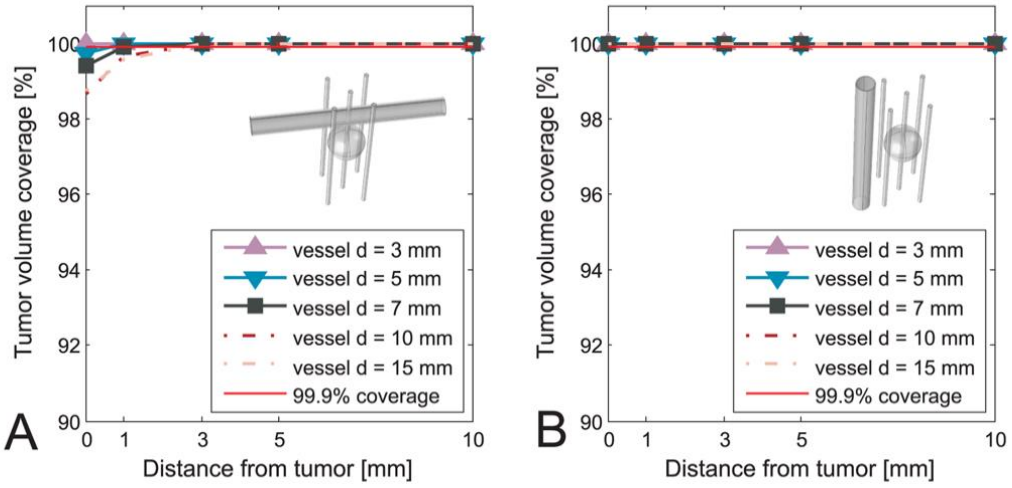

Fig 4. Tumor coverage for ECT of simplified model of 10 mm tumor with 5 electrodes. The coverage is plotted against different distances between vessel and tumor, and with respect to different vessel positions and sizes. A: Vessel perpendicular to the electrodes. B: Vessel parallel to the electrodes.

doi:10.1371/journal.pone.0125591.g004

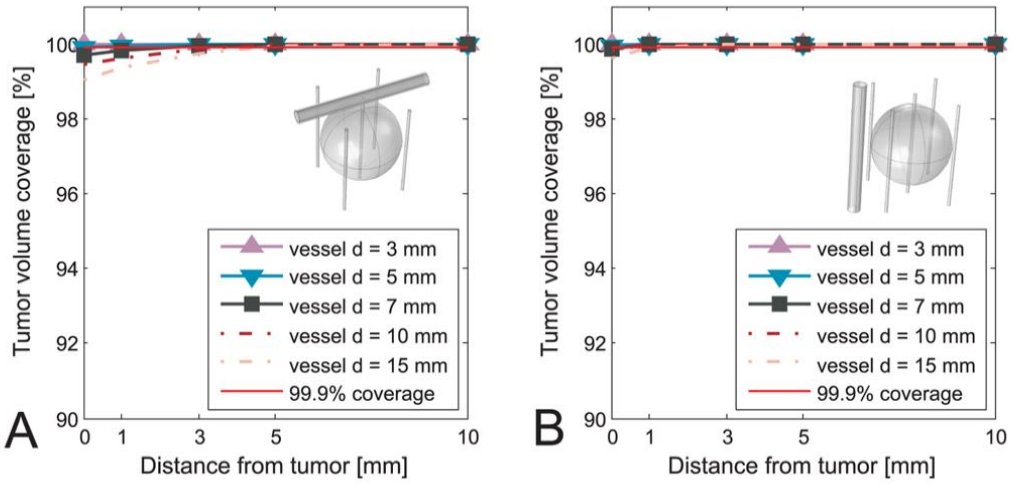

Fig 5. Tumor coverage for ECT of simplified model of 30 mm tumor. The coverage is plotted against different distances between vessel and tumor, and with respect to different vessel positions and sizes. A: Vessel perpendicular to the electrodes. B: Vessel parallel to the electrodes.

doi:10.1371/journal.pone.0125591.g005

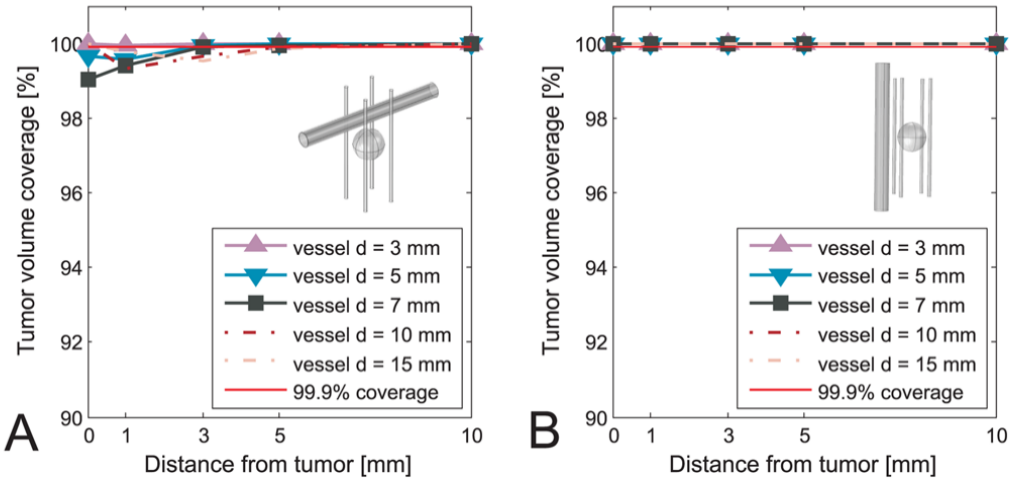

Fig 6. Tumor coverage for IRE of simplified model of 10 mm tumor with 4 electrodes. The coverage is plotted against different distances between vessel and tumor, and with respect to different vessel positions and sizes. A: Vessel perpendicular to the electrodes. B: Vessel parallel to the electrodes.

doi:10.1371/journal.pone.0125591.g006

The negative effect is observed in both ECT and IRE, although in IRE to a smaller extent, as is seen by comparing Figs 3 and 6. It is also significantly more pronounced in cases where all the electrodes are outside the tumor, and not so much if central electrode was present (Figs 3 vs. 4). Another interesting point to note by comparing the A and the B sides of all the Figs 3–6 is that the negative effect of the vessel on tumor coverage is higher when a vessel is perpendicular to the electrodes than when it is parallel to them. We also included a 2D color map of several slices for one of the simplified models in order to provide the visual insight at exactly how is the electric field distribution in tumor deformed due to presence of a vessel. The model in question is the one where the significant difference in tumor coverage was observed, namely it is the model of ECT of the 10 mm tumor with 4 electrode configuration and with a 7 mm vessel positioned at 0 mm away from the tumor. Fig 7 shows both the case where vessel is perpendicular to the electrodes (Fig 7A), and the case where vessel is parallel to the electrodes (Fig 7B). For better comparison of the impact of the vessel position with respect to the electrodes the planes in both Fig 7A and 7B are oriented parallel to the vessel. The relative position of the planes along the third axis (the one which the plane does not span) is the same in both cases and fixed at -4 mm, 0 mm, and 4 mm away from the tumor center.

Real patient model

Results for the model of the first patient (larger tumor with six electrodes) did not show any negative effect on the coverage of the tumor volume for all possible types of segmentation errors that were observed in this study.

Results for the two models of the second patient are shown in Fig 8. The figure shows the coverage of the tumor by a sufficiently high electric field against different types of

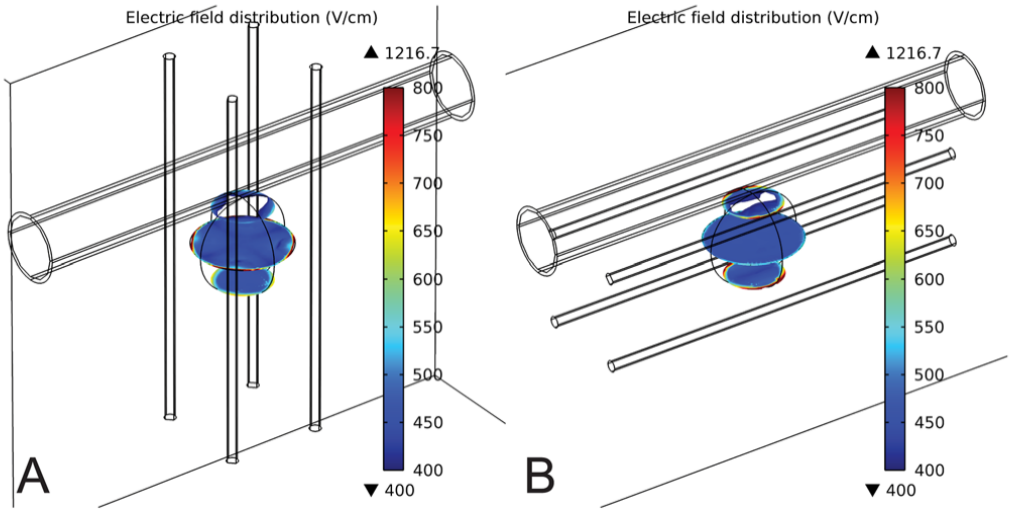

Fig 7. 2D sliced color map of the electric field distribution for a case where a significant difference in tumor coverage is observed as a result of the presence of the blood vessel. The color map is presented for a simplified model of ECT of a 10 mm tumor with a 4 electrode configuration and in the presence of a 7 mm vessel which is 0 mm away from the tumor. The color maps are shown for two vessel positions: A: Vessel perpendicular to the electrodes. B: Vessel parallel to the electrodes. The slices for which the color map is shown span the plane parallel to the vessel. The relative position of the planes along the third axis (the one which the plane does not span) is the same in both cases and fixed at -4 mm, 0 mm, and 4 mm away from the tumor center.

doi:10.1371/journal.pone.0125591.g007

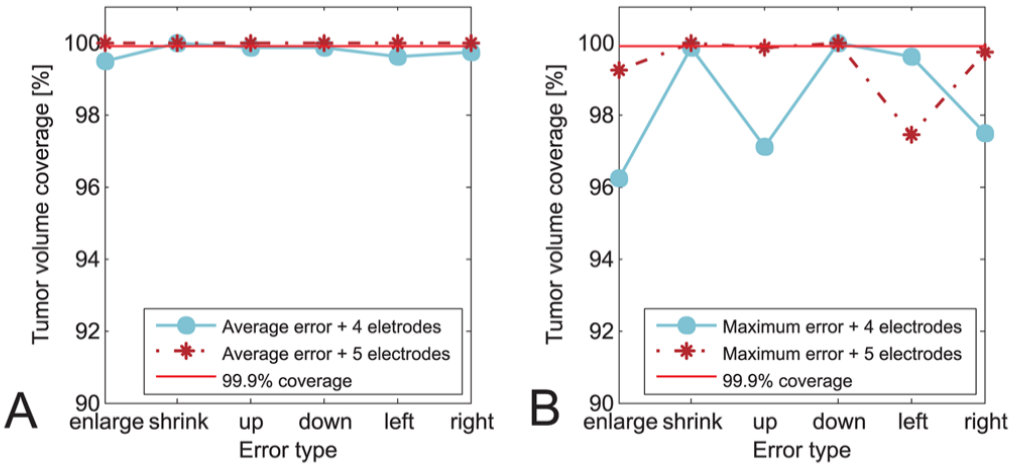

Fig 8. Tumor coverage for ECT of real case second patient with 15 mm × 11 mm tumor. The coverage is plotted against different types of transformations used to induce an error in vessel geometry and with respect to different sizes of the error. A: Configuration with four electrodes. B: Configuration with five electrodes.

doi:10.1371/journal.pone.0125591.g008

transformations used to induce an error in vessel model that was used for optimization of treatment parameters. Fig 8A shows the results of the model where an average segmentation error (1 pixel) was introduced. Fig 8B shows the results of the model where the maximum segmentation error (3 pixels) was introduced. In both Fig 8A and 8B the results are grouped per two models: the model with four electrodes (no central electrode) and the model with five electrodes (with central electrode). It can be observed that the negative effect of the vessels is higher for maximum segmentation error than for average segmentation error, as would be expected. It is interesting to note that the negative effect of the maximum error is significantly larger in the case where no central electrode is present. Similar difference in the electrode configuration is also noted for average segmentation error. The difference for the average error is that the negative effect is minimal for the case of no central electrode and completely non-existent when the central electrode is present.

The results of comparing the real patient models with correct vessel geometry to real patient models where vessels were not taken into account differed between the two observed patients. For the first patient there was no difference in tumor coverage with a sufficiently high electric field if the vessels were not taken into account during the numerical optimizations of the voltages. For the second patient, if the vessels are not taken into account during optimizations the resulting coverage of the tumor would be 97.22% for the model with four electrodes and 99.87% for the case with five electrodes.

Discussion

In this paper we constructed and analyzed various situations of electric field distribution in the tumor with nearby vessels of different size, orientation and position with respect to tumor tissue and the electrodes. The first aim was to determine in what measure vessels influence the distribution of the electric field, or more precisely, what error occurs in the model of electroporation-based treatments if the vessels are ignored and the consequence of that error on tumor treatment. The second aim was to determine if the automatic segmentation method of hepatic vessels developed in our previous work [22] is robust enough to be used as a part of an automatic treatment planning procedure. In other words, we examined if the known and estimated error of the automatic segmentation method would negatively affect the coverage of the tumor with a sufficiently high electric field.

The results of the first part of the study show that ignoring the presence of a hepatic vessel near a tumor indeed can influence the electric field distribution in such a way that the coverage of the tumor with a sufficiently high electric field decreases. These findings are in accordance with a recent publication by Golberg et al. [35] which studied the effect of nearby blood vessels on cell survival during IRE ablation and found that the presence of vessels near target tissue causes so-called "electric field sinks". Moreover, we have found that whether the tumor will or will not be sufficiently covered (above 99.9%) directly depends on the tumor size, vessel size and distance between tumor and the vessel. According to the results of this study, for ECT of small tumors (10 mm diameter) the vessels that will have a negative effect are all vessels larger than 3 mm in diameter and less than 3 mm away from the tumor. For ECT of medium-sized tumors (30 mm diameter), all vessels larger than 7 mm in diameter and less than 5 mm away from the tumor will have a negative effect. Vessels are not expected to have any negative effect on the ECT of large tumors (50 mm in diameter).

In the case of IRE, the negative effect of vessels is observed only for IRE of small tumors (10 mm diameter) performed with four electrodes outside the tumor, i.e. without any central electrodes. Observing both IRE and ECT with and without the central electrode unanimously

confirms that an electrode configuration with one electrode in the center is more robust and should be the preferred choice in electroporation-based treatments in organs with a high contrast between the conductivity of normal and tumor tissue. It should however be noted that insertion of the central electrode has been raising certain concerns in the medical community, namely regarding the added risk of blood vessel puncture and potential to seed tumor cells along the electrode track upon removal. Regarding the risk of blood vessel puncture, based on the reports of the surgeons that have performed the ECT on the liver one electrode that partially punctures the vessel does not have a critical effect on the vessel structure. Such electrode configuration which would include an electrode that completely punctures the vessel or several electrodes partially puncturing it is something that can be avoided through careful treatment planning. As for the potential of tumor cell seeding upon electrode removal, given the fact that the electric field has the highest values in the close vicinity of the electrodes [34] it would seem theoretically unlikely that any tumor cells would survive in the area near electrodes. However, since we have received reports from several clinicians performing electroporation-based treatments about noticing tumor reseeding along the track of removal of the central electrode (personal communication) it would be wise to perform further investigations of the matter.

The results of the second part of the study confirm what was already shown in the first part: ignoring the vessels while optimizing the treatment can result in tumor under-treatment. Another conclusion the results of studies performed on real patient models confirm is that a large vessel close to tumor without any central electrodes represents a risk of not covering a tumor with a sufficiently high electric field, leading potentially to under-treatment. According to our results, using a central electrode compensates the negative effects that the average anticipated error of the automatic vessel segmentation method (which is 1 pixel) can have on tumor coverage. It is however still possible for the algorithm to produce an error up to 3 pixels, which can negatively affect the tumor coverage even if the central electrode is present. An error of such magnitude is rare and when it does appear it is of smaller scope than we modeled in our experiments, i.e. it is present on usually one side of the object while we introduced it on the whole object edge. Nevertheless, a mechanism to remove this error should be ensured by presenting the results of the automatic vessel segmentation to the clinician or a radiologist for validation before the start of the calculations of the electric field distribution. In case such large error appears the user should be able to spot it relatively easy and can then correct it.

In general, this paper was motivated by the aim to observe the relationship between tumor size, vessel size, and vessel distance between the tumor and the vessel. We aimed at determining the effect of the combinations of these three parameters on the distribution of the electric field and consequently, on the coverage of the tumor with a sufficiently high electric field. We expected that the negative effect of the vessel will be larger for smaller tumors. We also expected that the negative effect of the vessels will be proportional to vessel size and inversely proportional to distance between tumor and vessel. These expectations were confirmed by the results, but not completely. Some anomalies were noted in the cases where the vessels were larger than the tumors and the electrodes were going through the vessels, namely for tumors of 10 mm diameter. The observed anomalies were such that they could negatively affect the success of the electroporation-based treatment, indicating the treatment planning procedure should also be mindful of the mutual position of the electrodes and vessels, not only electrodes and the tumor. This observation increases the level of complexity of an already extremely complex model. With such complexity, the best approach for a successful electroporation-based treatment should necessarily include a treatment planning procedure performed on the whole three-dimensional model.

Acknowledgments

This work was supported by the Slovenian Research Agency. The authors would like to thank Dr. Matej Kranjc of the University of Ljubljana, Faculty of Electrical Engineering for an extensive discussion regarding electrode configurations.

Author Contributions

Conceived and designed the experiments: MM DM. Performed the experiments: MM BK. Analyzed the data: MM. Contributed reagents/materials/analysis tools: MM BK. Wrote the paper: MM. Designed the software used in analysis: BK.

References

1. Neumann E, Schaefer-Ridder M, Wang Y, Hofschneider PH. Gene transfer into mouse lyoma cells by electroporation in high electric fields. The EMBO journal. 1982; 1(7):841–5. PMID: 6329708
2. Kotnik T, Kramar P, Pucihar G, Miklavcic D, Tarek M. Cell membrane electroporation- Part 1: The phenomenon. IEEE Electrical Insulation Magazine. 2012; 28(5):14–23. doi: 10.1109/MEI.2012.6268438
3. Pucihar G, Krmelj J, Reberšek M, Napotnik TB, Miklavčič D. Equivalent pulse parameters for electroporation. IEEE transactions on bio-medical engineering. 2011; 58(11):3279–88. doi: 10.1109/TBME.2011.2167232 PMID: 21900067
4. Golberg A, Yarmush ML. Nonthermal irreversible electroporation: fundamentals, applications, and challenges. IEEE transactions on bio-medical engineering. 2013; 60(3):707–14. doi: 10.1109/TBME.2013.2238672 PMID: 23314769
5. Mir LM, Orlowski S, Belehradek J, Paoletti C. Electrochemotherapy potentiation of antitumour effect of bleomycin by local electric pulses. European journal of cancer (Oxford, England: 1990). 1991; 27 (1):68–72. doi: 10.1016/0277-5379(91)90064-K
6. Miklavčič D, Mali B, Kos B, Heller R, Serša G. Electrochemotherapy: from the drawing board into medical practice. Biomedical engineering online. 2014; 13(1):29. doi: 10.1186/1475-925X-13-29 PMID: 24621079
7. Davalos RV, Mir LM, Rubinsky B. Tissue Ablation with Irreversible Electroporation. Annals of Biomedical Engineering. 2005; 33(2):223–231. doi: 10.1007/s10439-005-8981-8 PMID: 15771276
8. Martin RCG, McFarland K, Ellis S, Velanovich V. Irreversible electroporation in locally advanced pancreatic cancer: potential improved overall survival. Annals of surgical oncology. 2013; 20 Suppl 3(August):S443–9. doi: 10.1245/s10434-012-2736-1 PMID: 23128941
9. Miklavcic D, Corovic S, Pucihar G, Pavselj N. Importance of tumour coverage by sufficiently high local electric field for effective electrochemotherapy. European Journal of Cancer Supplements. 2006; 4 (11):45–51. doi: 10.1016/j.ejcsup.2006.08.006
10. Miklavcic D, Beravs K, Semrov D, Cemazar M, Demsar F, Sersa G. The importance of electric field distribution for effective in vivo electroporation of tissues. Biophysical journal. 1998; 74(5):2152–8. doi: 10.1016/S0006-3495(98)77924-X PMID: 9591642
11. Kos B, Zupanic A, Kotnik T, Snoj M, Sersa G, Miklavcic D. Robustness of treatment planning for electrochemotherapy of deep-seated tumors. The Journal of membrane biology. 2010; 236(1):147–53. doi: 10.1007/s00232-010-9274-1 PMID: 20596859
12. Mali B, Miklavcic D, Campana LG, Cemazar M, Sersa G, Snoj M, et al. Tumor size and effectiveness of electrochemotherapy. Radiology and oncology. 2013; 47(1):32–41. doi: 10.2478/raon-2013-0002 PMID: 23450195
13. Yarmush ML, Golberg A, Serša G, Kotnik T, Miklavčič D. Electroporation-based technologies for medicine: principles, applications, and challenges. Annual review of biomedical engineering. 2014; 16:295–320. doi: 10.1146/annurev-bioeng-071813-104622 PMID: 24905876
14. Scheffer HJ, Nielsen K, de Jong MC, van Tilborg AaJM, Vieveen JM, Bouwman ARa, et al. Irreversible electroporation for nonthermal tumor ablation in the clinical setting: a systematic review of safety and efficacy. Journal of vascular and interventional radiology: JVIR. 2014; 25(7):997–1011. doi: 10.1016/j.jvir.2014.01.028 PMID: 24656178
15. Miklavcic D, Snoj M, Zupanic A, Kos B, Cemazar M, Kropivnik M, et al. Towards treatment planning and treatment of deep-seated solid tumors by electrochemotherapy. BioMedical Engineering Online. 2010; 9:10. doi: 10.1186/1475-925X-9-10 PMID: 20178589

16. Edhemovic I, Gadzijev EM, Brecelj E, Miklavcic D, Kos B, Zupanic A, et al. Electrochemotherapy: a new technological approach in treatment of metastases in the liver. Technology in cancer research & treatment. 2011; 10(5):475–85.

17. Pavliha D, Kos B, Županič A, Marčan M, Serša G, Miklavčič D. Patient-specific treatment planning of electrochemotherapy: procedure design and possible pitfalls. Bioelectrochemistry (Amsterdam, Netherlands). 2012; 87:265–73. doi: 10.1016/j.bioelechem.2012.01.007

18. Neal RE, Rossmeisl JH, Garcia PA, Lanz OI, Henao-Guerrero N, Davalos RV. Successful treatment of a large soft tissue sarcoma with irreversible electroporation. Journal of clinical oncology: official journal of the American Society of Clinical Oncology. 2011; 29(13):e372–7. doi: 10.1200/JCO.2010.33.0902

19. Zupanic A, Kos B, Miklavcic D. Treatment planning of electroporation-based medical interventions: electrochemotherapy, gene electrotransfer and irreversible electroporation. Physics in medicine and biology. 2012; 57(17):5425–40. doi: 10.1088/0031-9155/57/17/5425 PMID: 22864181

20. Edhemovic I, Brecelj E, Gasljevic G, Marolt Music M, Gorjup V, Mali B, et al. Intraoperative electrochemotherapy of colorectal liver metastases. Journal of surgical oncology. 2014; 110(3):320–7. doi: 10.1002/jso.23625 PMID: 24782355

21. Pavliha D, Mušič MM, Sersa G, Miklavčič D. Electroporation-based treatment planning for deep-seated tumors based on automatic liver segmentation of MRI images. PloS one. 2013; 8(8):e69068. doi: 10.1371/journal.pone.0069068 PMID: 23936315

22. Marcan M, Pavliha D, Music MM, Fuckan I, Magjarevic R, Miklavcic D. Segmentation of hepatic vessels from MRI images for planning of electroporation-based treatments in the liver. Radiology and Oncology. 2014; 48(3):267–281. doi: 10.2478/raon-2014-0022 PMID: 25177241

23. Marieb EN, Hoehn K. Human Anatomy & Physiology. My A and P Series. Pearson Benjamin Cummings; 2007.

24. Sel D, Cukjati D, Batiuskaite D, Slivnik T, Mir LM, Miklavcic D. Sequential finite element model of tissue electropermeabilization. IEEE transactions on bio-medical engineering. 2005; 52(5):816–27. doi: 10.1109/TBME.2005.845212 PMID: 15887531

25. Corovic S, Lackovic I, Sustaric P, Sustar T, Rodic T, Miklavcic D. Modeling of electric field distribution in tissues during electroporation. Biomedical engineering online. 2013; 12:16. doi: 10.1186/1475-925X-12-16 PMID: 23433433

26. Pavliha D, Kos B, Marcan M, Zupanic A, Sersa G, Miklavcic D. Planning of electroporation-based treatments using Web-based treatment-planning software. The Journal of membrane biology. 2013; 246 (11):833–42. doi: 10.1007/s00232-013-9567-2 PMID: 23780414

27. Pavlin M, Kanduser M, Rebersek M, Pucihar G, Hart FX, Magjarevic R, et al. Effect of cell electroporation on the conductivity of a cell suspension. Biophysical journal. 2005; 88(6):4378–90. doi: 10.1529/biophysj.104.048975 PMID: 15792975

28. Cukjati D, Batiuskaite D, André F, Miklavcic D, Mir LM. Real time electroporation control for accurate and safe in vivo non-viral gene therapy. Bioelectrochemistry (Amsterdam, Netherlands). 2007; 70 (2):501–7. doi: 10.1016/j.bioelechem.2006.11.001

29. Gabriel S, Lau RW, Gabriel C. The dielectric properties of biological tissues: II. Measurements in the frequency range 10 Hz to 20 GHz. Physics in Medicine and Biology. 1996; 41(11):2251–2269. doi: 10.1088/0031-9155/41/11/002 PMID: 8938025

30. Haemmerich D, Schutt DJ, Wright AW, Webster JG, Mahvi DM. Electrical conductivity measurement of excised human metastatic liver tumours before and after thermal ablation. Physiological measurement. 2009; 30(5):459–66. doi: 10.1088/0967-3334/30/5/003 PMID: 19349647

31. Foundation I. Pluim JPW, Dawant BM, editors. Frequency-dependent dielectric properties IT'IS Foundation;. Available from: http://www.itis.ethz.ch/itis-for-health/tissue-properties/database/dielectric-properties/.

32. Pavlin M, Miklavcic D. Effective Conductivity of a Suspension of Permeabilized Cells: A Theoretical Analysis. Biophysical journal. 2003; 85(2):719–729. doi: 10.1016/S0006-3495(03)74515-9 PMID: 12885623

33. Golberg A, Rubinsky B. A statistical model for multidimensional irreversible electroporation cell death in tissue. Biomedical engineering online. 2010; 9:13. doi: 10.1186/1475-925X-9-13 PMID: 20187951

34. Garcia Pa, Davalos RV, Miklavcic D. A numerical investigation of the electric and thermal cell kill distributions in electroporation-based therapies in tissue. PloS one. 2014; 9(8):e103083. doi: 10.1371/journal.pone.0103083 PMID: 25115970

35. Golberg A, Bruinsma BG, Uygun BE, Yarmush ML. Tissue heterogeneity in structure and conductivity contribute to cell survival during irreversible electroporation ablation by "electric field sinks". Scientific Reports. 2015; 5:8485. doi: 10.1038/srep08485 PMID: 25684630

PAPER 3

Title: Web-based tool for visualization of electric field distribution in deep-seated body structures and for planning electroporation-based treatments

Authors: MARČAN Marija, PAVLIHA Denis, KOS Bor, FORJANIČ Tadeja, MIKLAVČIČ Damijan

Publication: Biomedical Engineering Online[1]

DOI: /

Year: 2015

Volume: /

Number: /

Pages: /

Impact factor: 1.75

Ranking:

Category name	Total journals in category	Journal rank in category	Quartile in category
engineering, biomedical	76	35	Q2

[1] At the time of writting, the manuscript has been in press.

RESEARCH

Web-based tool for visualization of electric field distribution in deep-seated body structures and planning of electroporation-based treatments

Marija Marčan, Denis Pavliha, Bor Kos, Tadeja Forjanič and Damijan Miklavčič*

*Correspondence:
damijan.miklavcic@fe.uni-lj.si
University of Ljubljana, Faculty of Electrical Engineering, Trzaska 25, SI-1000 Ljubljana, Slovenia
Full list of author information is available at the end of the article

Abstract

Background: Treatments based on electroporation are a new and promising approach to treating tumors, especially non-resectable ones. The success of the treatment is, however, heavily dependent on coverage of the entire tumor volume with a sufficiently high electric field. Ensuring complete coverage in the case of deep-seated tumors is not trivial and can in best way be ensured by patient-specific treatment planning. The basis of the treatment planning process consists of two complex tasks: medical image segmentation, and numerical modeling and optimization.

Methods: In addition to previously developed segmentation algorithms for several tissues (human liver, hepatic vessels, bone tissue and canine brain) and the algorithms for numerical modeling and optimization of treatment parameters, we developed a web-based tool to facilitate the translation of the algorithms and their application in the clinic. The developed web-based tool automatically builds a 3D model of the target tissue from the medical images uploaded by the user and then uses this 3D model to optimize treatment parameters. The tool enables the user to validate the results of the automatic segmentation and make corrections if necessary before delivering the final treatment plan.

Results: Evaluation of the tool was performed by five independent experts from four different institutions. During the evaluation, we gathered data concerning user experience and measured performance times for different components of the tool. Both user reports and performance times show significant reduction in treatment-planning complexity and time-consumption from 1-2 days to a few hours.

Conclusions: The presented web-based tool is intended to facilitate the treatment planning process and reduce the time needed for it. It is crucial for facilitating expansion of electroporation-based treatments in the clinic and ensuring reliable treatment for the patients. The additional value of the tool is the possibility of easy upgrade and integration of modules with new functionalities as they are developed.

Keywords: electroporation; electrochemotherapy; irreversible electroporation; electric field distribution; treatment planning; numerical modeling; web-based

Background

Exposing a biological cell to an electric field results in structural changes in the cell plasma membrane. If the electric field is sufficiently high, the changes in the trans-membrane voltage cause the membrane to become permeable to molecules

which otherwise cannot cross it. The described phenomenon is termed electroporation [1] and can be either reversible or irreversible. If the electric field at given pulse characteristics exceeds the reversible electroporation threshold, the cell eventually returns to its normal state and survives; this is called reversible electroporation. However, if the electric field exceeds the threshold of irreversible electroporation or the cell is exposed to the electric field too long, the changes in the membrane lead to irreversible electroporation (IRE) characterized by cell death.

Both reversible and irreversible electroporation have found their use in treatment of tumors [2]. Combination of reversible electroporation and cytotoxic drugs used in chemotherapy produces an increased drug uptake in the tumor cells and a more efficient therapy. Such treatment has been termed electrochemotherapy (ECT) [3–5]. On the other hand, the permanent damage to cells caused by irreversible electroporation can be used to ablate the tumor cells directly. Since ablation with irreversible electroporation, for most part, does not employ a thermal mechanism of cell death, as opposed to e.g. radiofrequency ablation, IRE has also been termed non thermal irreversible electroporation (NTIRE) [6–8]. The basis of both therapies is the application of electric pulses with adequate amplitude, duration and pulse repetition frequency using specially designed pulse generators and electrodes [9].

While the ECT for skin tumors has already been accepted into several clinical guidelines, the application of ECT and IRE on deep-seated tumors is still in an earlier clinical phase of testing [5, 10–14]. In the case of deep seated tumors, it is challenging to ensure the complete target volume coverage with a sufficiently high electric field, which is the main prerequisite for successful tumor treatment [15–17]. Positions and the trajectory of electrode insertion have to be precisely determined along with optimal pulse parameters. Taking into account the additional problem of patient and tumor anatomical variability, the best way to ensure that the target tissue is exposed to sufficiently high electric fields is by performing patient-specific treatment planning [18, 19].

In order to improve the prediction of treatment outcome, we have developed a web-based tool for visualization of electric field distribution on geometric model of patient anatomy acquired through segmentation of medical images. As an inspiration for our workflow, we have used the radiotherapy and radiofrequency ablation treatment planning (TP) procedures, which consist of several steps [19]: medical imaging of the patient, image processing and extraction of model geometry, and numerical modeling with determination of the optimal treatment parameters. All these steps have been adjusted for electroporation-based treatment planning.

Our aim was to create a tool which the clinicians could easily use without the help of engineers or without deep technical knowledge. Such a tool should relieve the user from performing unnecessary steps from the engineering domain while keeping the necessary level of robustness and reliability. In this way the tool aids the spread of use of ECT and IRE to clinics with no or minimal specific engineering support. The final product is a web-based tool for visualization of electric field distribution and planning of electroporation-based treatments which is described in detail in following sections.

Methods

The developed workflow for electric field visualization consists of several steps. The user first uploads medical images in DICOM format or selects such images from a previously-uploaded case. After uploading, there is an option for immediate and permanent anonymization of the data. Medical images can, then, be segmented manually or automatically by selecting the desired segmentation target (e.g. liver on MRI images, or bone tissue on CT images, etc.). It is important to note that, in case of tumor segmentation, it can currently be done only using the manual segmentation module.

After automatic segmentation, the user is given the possibility to inspect and correct the obtained segmentation results and validate them. Finally, the user specifies the trajectory vector of the inserted electrodes and either decides to execute automatic electric field modeling or to send the segmented case to an experienced engineer from our team to evaluate and model the case. In either case, the final output that is given to the user is a 'Treatment report' in the form of a pdf file. This file contains all the information regarding electrode positioning, the optimal pulses that should be applied per each electrode pair, volumes of reversibly and irreversibly treated areas of all tissues and 2D illustrations of the electric field distribution. The diagram of the workflow of our tool is shown in Figure 1, while an example treatment plan is shown in Figure 2.

Medical image segmentation

The process of image segmentation depends on the target organ. So far, we have implemented algorithms for liver and bone tissue segmentation of human patients and brain tissue segmentation of canine patients, therefore making the tool available also for veterinary medicine [20–24].

Automatic liver segmentation using our tool can be performed on MRI or CT images. Methods for liver extraction using MRI data are based on region growing, adaptive thresholding and active contours according to the work of Pavliha et al. [25]. A different, two-stage method is used for CT liver extraction: rough estimation of liver region by identifying the largest connected component on Euclidean distance maps is followed by precise determination of liver boundary with active contours.

After liver tissue extraction is performed, the resulting liver geometry is used as a mask for hepatic vessels segmentation. The method for segmentation of hepatic vessels in both MRI and CT images is based on vesselness filtering and local thresholding in the neighborhood of the results of vesselness filtering [26]. The vesselness filter applied is based on the work of Frangi et al. [27] and can be easily adapted to detect vessels in both CT and MRI images.

The algorithms for canine brain extraction from T1 and T2 weighted MRI images are based on morphological operations and they consist of the following steps. First, the central slice of the brain is identified by connected component analysis of eroded images. The brain tissue from the remaining slices is extracted using the similarities of adjacent slices [28,29].

Bone tissue is extracted from CT images using thresholding-based method. All of the implemented algorithms for segmentation of different objects of interest work

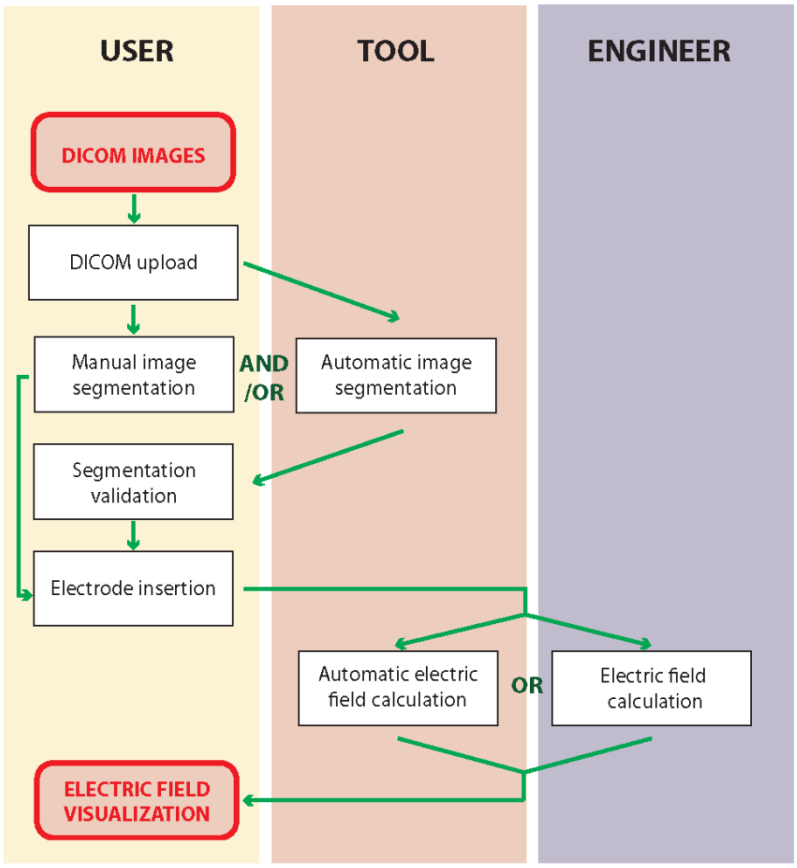

Figure 1 Diagram of the workflow of the web-based tool for visualization of the electric field distribution.

automatically and require no user input. The modular design of the tool allows additional methods to be easily added after being developed and tested. The objects that are not planned to be automatically extracted are the tumors, due to their high variability of shape, size and location. For this purpose, we have provided a tool for manual segmentation based on drawing contours by placing points on the original slices.

Segmentation validation

The results of automatic segmentation of objects of interest are displayed to the user in the form of 2D contours overlaid over the original image slices. In order to ensure robustness and quality of the model extraction from medical images, the user is asked to validate results of automatic segmentation. In this phase, the user is able to manually change the segmentation results if needed.

Correction of individual object boundaries is possible by freely moving contour points to the desired position. For this purpose, the 2D contours of segmented ob-

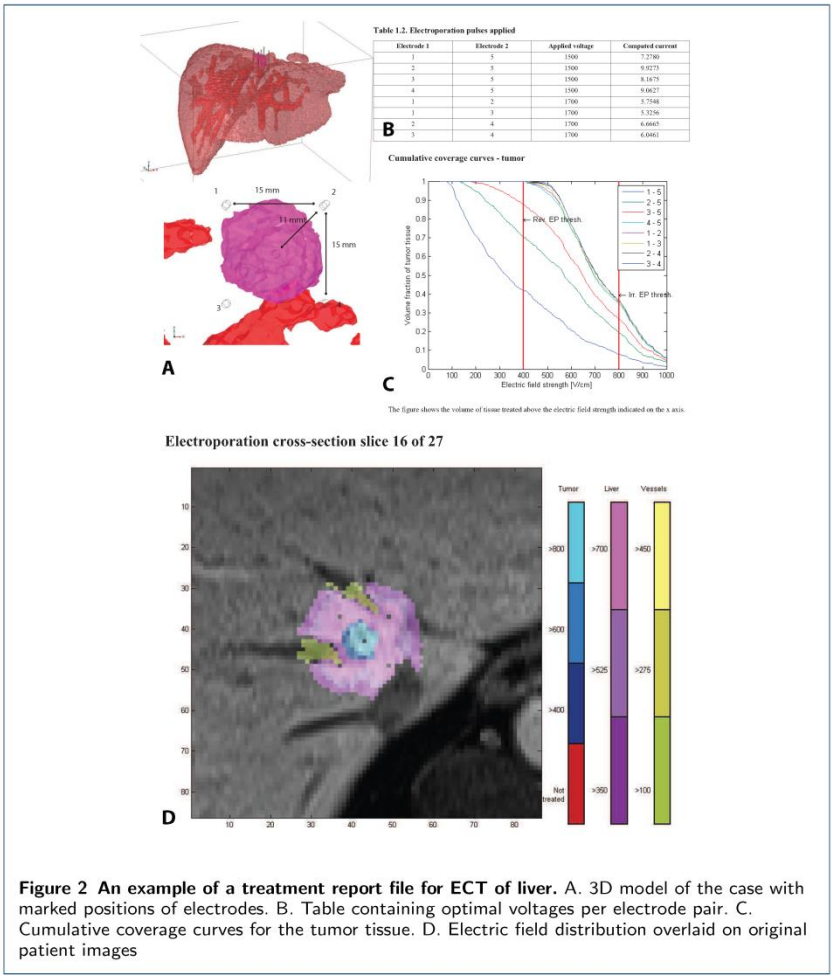

Figure 2 An example of a treatment report file for ECT of liver. A. 3D model of the case with marked positions of electrodes. B. Table containing optimal voltages per electrode pair. C. Cumulative coverage curves for the tumor tissue. D. Electric field distribution overlaid on original patient images

jects are simplified and initially reduced to 20% of the original amount of points in the contour. The reduction of contour points is based on the measure of influence of a certain contour point which is calculated based on an angle and length between adjacent edges of the contour [30]. The number of points in the 2D contour, expressed as a percentage of the original number of contour points, can also be reduced or increased by the user on the level of an individual slice during the validation process itself. When the user chooses to change the number (percentage) of points in the contour, the new points are determined based on the reduction of the original contour as described above.

In case the user has already moved some points in space prior to choosing to change the number of contour points, the changed part of the contour is first reconstructed by fitting a piecewise cubic interpolation curve through the modified points. The reduction algorithm is then performed on the contour which consists of the original points that have not been changed and the points of the fitted curve. In case there is a complete object missing from the segmentation or the user deems adjusting the

segmentation results by moving the contour points would be too laborious, he/she also has an option of erasing the segmentation results on a slice level and manually drawing the contour.
The manual drawing is supported by the manual segmentation tool described in the previous section which is also embedded in the module for manual validation.

Electrode positioning

The validated model of the target organ with tumor and other structures of interest also requires a 3D model of electrodes added before numerical modeling can be performed. The size and type of the electrodes is pre-defined by the manufacturer while the treatment as being currently performed requires them to be parallel. The user thus needs to select the type of the commercially available electrodes, the length of the active part of the electrode, and the desired trajectory of electrode entry which will be used during the actual treatment.
The commercial electrodes that are currently supported by the tool are shown in Figure 3. The choice of the entry trajectory is made by placing a starting point and an ending point in two arbitrary 2D image slices of the patient. During the definition of the electrode entry trajectory, the user is aided by the visualization of nearby structures that limit electrode access, such as large vessels in the liver or bones in the case of head and neck tumors.

Numerical modeling

Numerical modeling is currently performed using Comsol Multiphysics (Comsol AB, Stockholm, Sweden). Live link for Matlab provides an interface for Matlab and allow for complete control of the finite element method model setup and solving. To this end, we have developed code in Matlab which uses the segmentation provided by the previous steps to automatically build a model with all segmented tissues.
Electrodes are inserted into the model based on the positions on medical images specified by the user in the 'electrode positioning' module. Boundary conditions for voltage are then set on successive pairs of electrodes. For implementing different conductivity values and changing of conductivity due to electroporation [31,32], we use interpolation functions to specify the conductivity in each point of the model [33]. In this way, Matlab code allows to increase the conductivity value of the tissues in each point of the model as a function of the local electric field [31].
For mesh generation built-in meshing capabilities of Comsol Multiphysics are used. Since the model consists only of the electrodes and the bounding box of the region of interests, with the tissue parameters being handled by Matlab via lookup tables, the built-in free tetrahedral meshing algorithms have proven effective and robust. The electric field is computed iteratively until there is no further increase in conductivity. After voltages on all electrode pairs are computed, the total coverage of the target tissue and volumes of surrounding tissues covered with electric fields above the irreversible threshold are determined. Electric field distribution is also overlaid over the original medical images for easier visual representation [34].
It is important to note that the model sets the target electroporation thresholds according to pulse parameters (pulse number, duration, repetition frequency) that are most often used as standard settings in clinical applications. For ECT this means

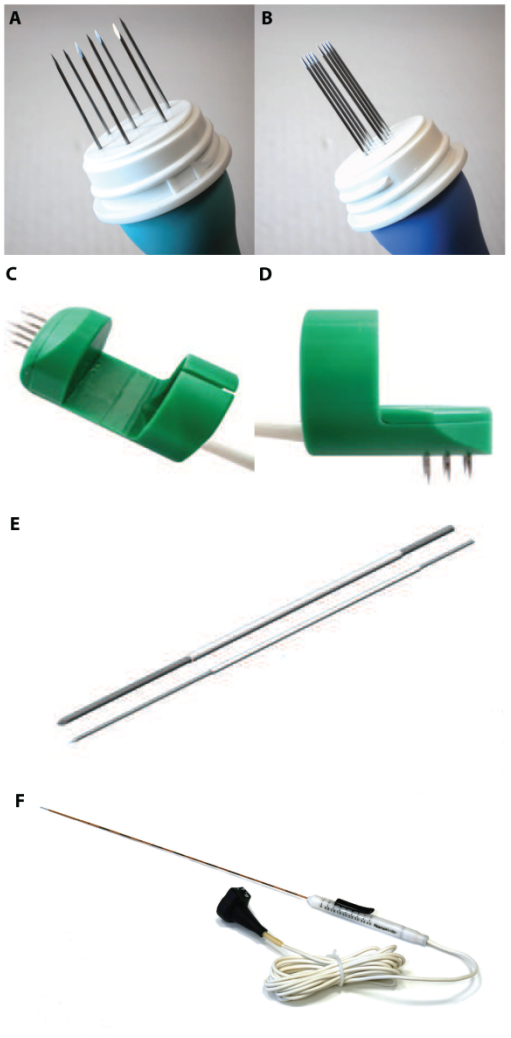

Figure 3 Commercially available electrodes. A. Hexagonal needle electrodes. B. Linear needle electrodes. C. Finger electrodes with axial needles. D. Finger electrode with perpendicular needles. E. Variable-geometry needle electrodes. F. Angiodynamics Nanoknife Variable geometry needle electrodes. All electrodes pictured in A-E are available from IGEA Srl.

8 pulses of 100 microsecond duration with repetition frequency of 1 Hz for and for IRE it is 90 pulses of 100 microsecond duration with repetition frequency of 1 Hz. In the case the user would like the pulse parameters to be different from these this issue can be resolved by direct contacting of the engineer via info@visifield.com.

Results and discussion

Web tool framework

The whole treatment planning procedure is embedded in a web-based client-server solution. The web page acts as a client graphical user interface. All of the segmentation algorithms along with numerical modeling are performed on a dedicated server running Matlab as the back-end engine. The results of the segmentation and numerical modeling along with original medical images are stored in a MySQL database and forwarded to the client side. The architecture of our web tool framework is presented schematically in Figure 4.

On the client side, Hyper-Text Markup Language (HTML) and Cascaded Stylesheets

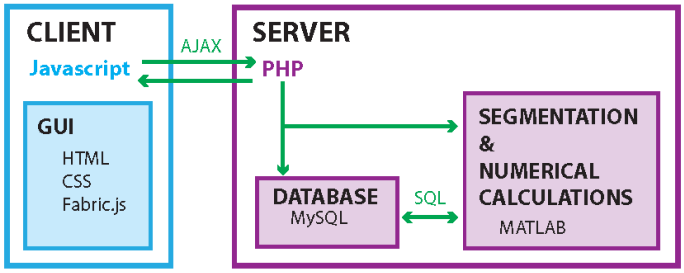

Figure 4 Schematical representation of the web tool framework with main components and technologies used in their realization.

(CSS) are used for visualization of the content (i.e. Graphical User Interface – GUI), while JavaScript (JS) is used for client-side dynamic scripting. The main part of the server side is realized using the Hypertext Preprocessor (PHP) which acts as the content back-end processor and for executing server-side processes. Also, MATLAB is currently used on the server side as the main processing back-end engine for procedures. Structured-Query Language (MySQL) is used as the database containing all the required data tables, and for indirect communication between the GUI and MATLAB (i.e. some dedicated tables are used for interaction between different software parts).

Additionally, some open-source publicly available JS libraries that are used are FABRIC.JS and jQuery. FABRIC.JS is used for client-side graphics in the manual segmentation and validation modules. jQuery is used for client-side dynamic scripting, and for performing Asynchronous JavaScript and XML (AJAX) calls from the GUI to the PHP back-end.

Graphical user interface

The tool is divided in two main working screens, shown in Figure 5: The first screen 'Cases' (Figure 5.A) permits adding new patients by uploading the DICOM images (by either dragging and dropping them into a rectangle on the screen, or by opening the classic file dialog). Existing patients are listed in the table and the currently selected patient (which is, then, available to work with in the Workspace screen) is marked. The 'Workspace' screen contains all the procedures and results of the currently selected patient. First, the user can select one of the predefined procedures (e.g. Electric field visualization in the Liver on CT images) or can create

a customized own procedure (e.g. Import DICOM Images, Automatically segment bone tissue, Validate bone tissue, Insert electrodes, Request electric field calculation, Download PDF) by dragging and dropping these individual modules to form the desired custom procedure order.
The most advanced part of the 'Workspace' is the manual segmentation/validation module (Figure 5.B), which is invoked after the automatic segmentation (or can replace it for tissues that are not yet supported by any of the automatic segmentation modules). The manual segmentation/validation module allows displaying the results of automatic segmentation (which are 2D surfaces on slices) as closed contours consisting of several points. The user can rearrange these points in order to correct any possible mistakes made by the automatic segmentation. If any objects are missed, the user can easily add new or remove existing objects by clicking on the corresponding buttons below the currently-displayed slice. Likewise, if the number of the displayed contour points is inadequate, the user can perform point refinement on the current slice and instantaneously change the number of points the back-end had generated. Zooming is also possible and the zoom (displayed as the lens next to the currently-displayed slice) is dynamically updated as the mouse moves in order to allow a precise and easily-achievable accurate segmentation/validation on the original images.
The GUI for the electrode insertion module is shown in Figure 5.C. The user can pick one of the commercially available electrodes from the drop down menu. After the choice of the electrode type has been made the user is required to specify the entry trajectory of the electrodes. This is done by marking two points in any of the two patient image slices or possibly even in the same slice. Left mouse click places the starting tip of the electrode while the right mouse click places the end point of the electrode. The described procedure needs to be done only once regardless of the final electrode number, even in cases where several individual electrodes are needed as this number will be determined by numerical modeling as the electrodes are considered to be parallel to each other.

Performance evaluation

Five independent users from four different institutions in different countries were given access to the web tool for evaluation purposes [35]. The users were not given any specific task, they were simply asked to use the tool according to their respective areas of interest. All five users have experience in medical image processing and electroporation-based treatments. The users were asked to provide feedback regarding the usage experience while we measured the times of performance of different tool components during their use. All of the users expressed the opinion that such a tool provides significant simplification of the treatment planning process, which they previously had to perform manually using different programs, taking up to 1-2 days of intense work.
The performance times of different tool components measured during evaluation by the five users are presented in Table 1, along with the level of user interaction required per individual component. The same table also provides information about which tissue types and imaging modalities each user has tested as well as the interaction type employed for each tissue/user.

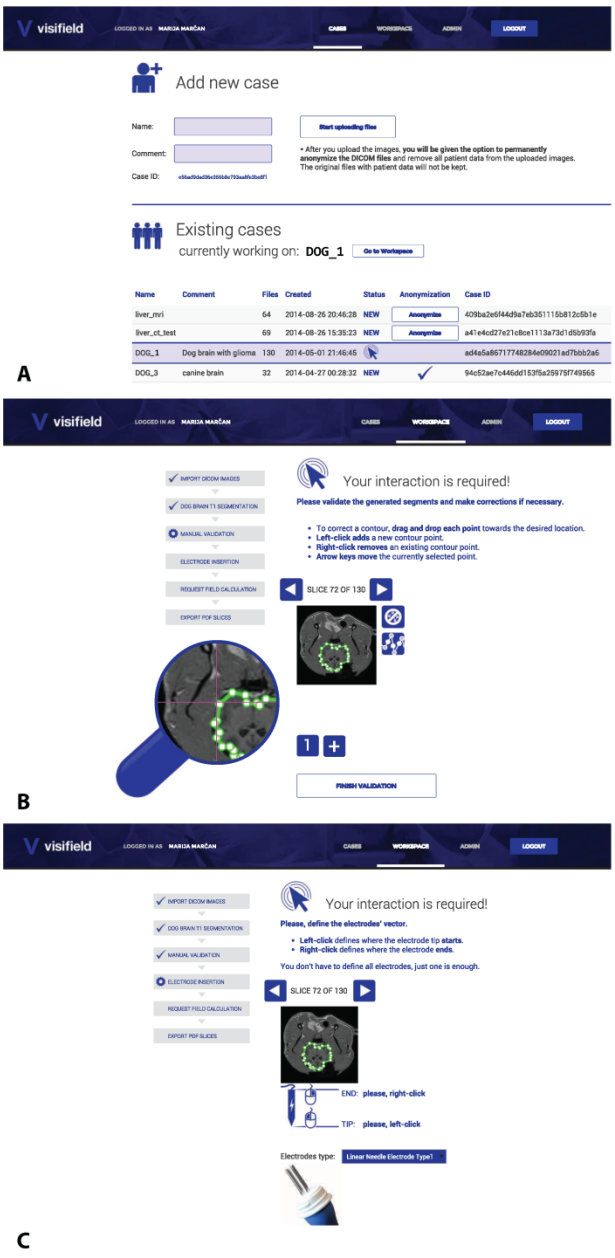

Figure 5 The main working screens of the application. A. Cases (i.e. uploading images and selecting the active patient). B. Workspace (i.e. selecting the procedure, validating segmentation results, downloading final results, etc.). C. Electrode insertion module, in which electrode type and entry point can be specified.

Table 1 Performance times of different tool components during user evaluation of the tool and level of user interaction.

Component	Level of interaction	Avg. time - User 1	Avg. time - User 2	Avg. time - User 3	Avg. time - User 4	Avg. time - User 5
Image upload	Interaction required	29.5 s	177 s	13.5 s	85 s	7.5 s
Automatic segmentation	Automatic	N/A	59 s	25 min	N/A	50.3 s
Manual segmentation	Interaction required	14 min	N/A	5 min	5 min	13 min
Manual validation	Interaction required	N/A	10 min	N/A	N/A	53 min
Tissue type /Imaging modality /Interaction level		liver tumor /MRI /manual	pelvic bone /CT /automatic	1) liver /CT /automatic; 2) prostate /MRI /manual	bone /CT /manual	1) canine brain /MRI /automatic; 2) tumor /MRI /manual

Conclusions

We have developed a web-based tool which embeds specifically-developed algorithms for medical image segmentation and numerical modeling and optimization, all for the purpose of generating patient-specific treatment plans for electroporation-based treatments. The need for treatment planning in electroporation-based treatments has already been recognized as a necessity [13, 36–38]. Since patient-specific treatment planning is not a trivial task, a tool such as the one we have presented is necessary in order to enable routine clinical use of electroporation-based treatments. So far the implemented automatic segmentation algorithms are limited to human liver and hepatic vessels, bone tissue segmentation and canine brain tissue segmentation. However, other tissue types can be segmented using the manual segmentation module. Also, it is important to note that the development of the presented tool is an iterative process and its modular design allows easy upgrade and inclusion of new algorithms for automatic segmentation according to needs of the clinical community.

In contrast to radiotherapy, electroporation-based treatments are not yet supported in medical institutions by dedicated teams of biomedical engineers or medical physicists with necessary knowledge and experience in electroporation who could prepare treatment plans. Our solution removes the burden of complicated engineering procedures from the end-user while the minimum required amount of interaction ensures robustness and validity.

Additional value of the presented solution is that it is web-based with all of the computationally intensive tasks performed on a dedicated server we provide. This concept eliminates the need to install new programs on the end-user's computer, as opposed to majority of tools for medical image segmentation that are available today. Moreover, the user can access his or her own patients and treatment plans from any computer as all the data are stored on the server. The brief yet valued evaluation by experts in the field of image processing and electroporation-based treatments has shown that the tool significantly shortens the time necessary to generate a treatment plan, from 1-2 days to a few hours. Such advance can greatly

help the expansion of electroporation-based treatments in the clinic and improve reliable treatment performance.

Competing interests
The authors declare that they have no competing interests.

Author's contributions
MM designed and implemented the algorithms for hepatic vessel segmentation and segmentation validation, and wrote the paper. DP designed and implemented the algorithms for liver MRI segmentation, implemented the entire web framework of the tool, and helped in writing the paper. BK programmed the algorithms for numerical modeling, helped optimize database access, and helped writing the paper. TF designed and implemented the algorithms for liver CT and dog brain segmentation, and helped writing the paper. DM participated in conceiving the ideas for the tool, guided the research process and critically revised and directed the manuscript. All authors read and approved the final version of the manuscript.

Acknowledgements
Publication costs were funded by the Slovenian Research Agency. This work was financially supported by the Slovenian Research Agency. The authors thank the following for their contributions to tool evaluation: Paulo Garcia, PhD of Massachusetts Institute of Technology, Peter Voigt, MD of the University Hospital of Leipzig and Giuseppe Bianchi, MD of the Rizzoli Orthopaedics Institute. Research was conducted in the scope of the Electroporation in Biology and Medicine, European Associated Laboratory. The development of the web-based tool was facilitated by use of Fabric.js and jQuery.

References
1. Kotnik, T., Kramar, P., Pucihar, G., Miklavcic, D., Tarek, M.: Cell membrane electroporation- Part 1: The phenomenon. IEEE Electrical Insulation Magazine **28**(5), 14–23 (2012)
2. Yarmush, M.L., Golberg, A., Serša, G., Kotnik, T., Miklavčič, D.: Electroporation-based technologies for medicine: principles, applications, and challenges. Annual review of biomedical engineering **16**, 295–320 (2014)
3. Mir, L.M., Orlowski, S., Belehradek, J., Paoletti, C.: Electrochemotherapy potentiation of antitumour effect of bleomycin by local electric pulses. European journal of cancer (Oxford, England : 1990) **27**(1), 68–72 (1991)
4. Sersa, G., Cemazar, M., Miklavcic, D.: Antitumor Effectiveness of Electrochemotherapy with cis-Diamminedichloroplatinum (II) in Mice. Cancer Research **55**, 3450–3455 (1995)
5. Miklavčič, D., Mali, B., Kos, B., Heller, R., Serša, G.: Electrochemotherapy: from the drawing board into medical practice. Biomedical engineering online **13**(1), 29 (2014)
6. Davalos, R.V., Mir, L.M., Rubinsky, B.: Tissue Ablation with Irreversible Electroporation. Annals of Biomedical Engineering **33**(2), 223–231 (2005)
7. Rubinsky, B., Onik, G., Mikus, P.: Irreversible electroporation: a new ablation modality–clinical implications. Technology in cancer research & treatment **6**(1), 37–48 (2007)
8. Jiang, C., Davalos, R.V., Bischof, J.C.: A Review of Basic to Clinical Studies of Irreversible Electroporation Therapy. IEEE Transactions on Biomedical Engineering **62**(1), 4–20 (2015)
9. Reberšek, M., Miklavčič, D., Bertacchini, C., Sack, M.: Cell membrane electroporation-Part 3: the equipment. IEEE Electrical Insulation Magazine **30**(3), 8–18 (2014)
10. Fini, M., Tschon, M., Ronchetti, M., Cavani, F., Bianchi, G., Mercuri, M., Alberghini, M., Cadossi, R.: Ablation of bone cells by electroporation. The Journal of bone and joint surgery. British volume **92**(11), 1614–20 (2010)
11. Fini, M., Tschon, M., Alberghini, M., Bianchi, G., Mercuri, M., Campanacci, L., Cavani, F., Ronchetti, M., Terlizzi, F.D.: Cell Electroporation in Bone Tissue. In: Kee, S.T., Gehl, J., Lee, E.W. (eds.) Clinical Aspects of Electroporation, pp. 115–127. Springer, New York, NY (2011)
12. Rubinsky, B.: Experimental Studies on Non-thermal Irreversible Electroporation in Tissue. In: Rubinsky, B. (ed.) Irreversible Electroporation. Series in Biomedical Engineering, pp. 155–181. Springer, Berlin, Heidelberg (2010)
13. Edhemovic, I., Brecelj, E., Gasljevic, G., Marolt Music, M., Gorjup, V., Mali, B., Jarm, T., Kos, B., Pavliha, D., Grcar Kuzmanov, B., Cemazar, M., Snoj, M., Miklavcic, D., Gadzijev, E.M., Sersa, G.: Intraoperative electrochemotherapy of colorectal liver metastases. Journal of surgical oncology **110**(3), 320–7 (2014)
14. Spratt, D.E., Gordon Spratt, E.a., Wu, S., DeRosa, A., Lee, N.Y., Lacouture, M.E., Barker, C.a.: Efficacy of skin-directed therapy for cutaneous metastases from advanced cancer: a meta-analysis. Journal of clinical oncology : official journal of the American Society of Clinical Oncology **32**(28), 3144–55 (2014)
15. Miklavcic, D., Beravs, K., Semrov, D., Cemazar, M., Demsar, F., Sersa, G.: The importance of electric field distribution for effective in vivo electroporation of tissues. Biophysical journal **74**(5), 2152–8 (1998)
16. Miklavcic, D., Corovic, S., Pucihar, G., Pavselj, N.: Importance of tumour coverage by sufficiently high local electric field for effective electrochemotherapy. European Journal of Cancer Supplements **4**(11), 45–51 (2006)
17. Miklavcic, D., Snoj, M., Zupanic, A., Kos, B., Cemazar, M., Kropivnik, M., Bracko, M., Pecnik, T., Gadzijev, E., Sersa, G.: Towards treatment planning and treatment of deep-seated solid tumors by electrochemotherapy. BioMedical Engineering Online **9**, 10 (2010)
18. Lecchi, M., Fossati, P., Elisei, F., Orecchia, R., Lucignani, G.: Current concepts on imaging in radiotherapy. European journal of nuclear medicine and molecular imaging **35**(4), 821–37 (2008)
19. Pavliha, D., Kos, B., Zupanič, A., Marčan, M., Serša, G., Miklavčič, D.: Patient-specific treatment planning of electrochemotherapy: procedure design and possible pitfalls. Bioelectrochemistry (Amsterdam, Netherlands) **87**, 265–73 (2012)
20. Cemazar, M., Tamzali, Y., Sersa, G., Tozon, N., Mir, L.M., Miklavcic, D., Lowe, R., Teissie, J.: Electrochemotherapy in veterinary oncology. Journal of veterinary internal medicine / American College of Veterinary Internal Medicine **22**(4), 826–31 (2008)

21. Spugnini, E.P., Citro, G., D'Avino, A., Baldi, A.: Potential role of electrochemotherapy for the treatment of soft tissue sarcoma: first insights from preclinical studies in animals. The international journal of biochemistry & cell biology **40**(2), 159–63 (2008)
22. Garcia, P.A., Pancotto, T., Rossmeisl, J.H., Henao-Guerrero, N., Gustafson, N.R., Daniel, G.B., Robertson, J.L., Ellis, T.L., Davalos, R.V.: Non-thermal irreversible electroporation (N-TIRE) and adjuvant fractionated radiotherapeutic multimodal therapy for intracranial malignant glioma in a canine patient. Technology in cancer research & treatment **10**(1), 73–83 (2011)
23. Rossmeisl, J.H., Garcia, P.A., Roberston, J.L., Ellis, T.L., Davalos, R.V.: Pathology of non-thermal irreversible electroporation (N-TIRE)-induced ablation of the canine brain. Journal of Veterinary Science **14**(4), 433 (2013)
24. Rossmeisl, J.H., Garcia, P.A., Pancotto, T.E., Roberston, J.L., Henao-Guerrero, N., Neal II, R.E., Ellis, T.L., Davalos, R.V.: Safety and Feasibility of the NanoKnife System for Irreversible Electroporation Ablative Treatment of Canine Spontaneous Intracranial Gliomas. Journal of Neurosurgery (in press), (2015)
25. Pavliha, D., Mušič, M.M., Serša, G., Miklavčič, D.: Electroporation-based treatment planning for deep-seated tumors based on automatic liver segmentation of MRI images. PloS one **8**(8), 69068 (2013)
26. Marcan, M., Pavliha, D., Music, M.M., Fuckan, I., Magjarevic, R., Miklavcic, D.: Segmentation of hepatic vessels from MRI images for planning of electroporation-based treatments in the liver. Radiology and Oncology **48**(3), 267–281 (2014)
27. Frangi, A.F., Niessen, W.J., Vincken, K.L., Viergever, M.A.: Multiscale vessel enhancement filtering. In: Wells, W.M., Colchester, A., Delp, S. (eds.) Medical Image Computing and Computer-Assisted Intervention - MICCAI '98 (1998), pp. 130–137. Springer, Cambridge, MA, USA (1998)
28. Somasundaram, K., Kalaiselvi, T.: Fully automatic brain extraction algorithm for axial T2-weighted magnetic resonance images. Computers in biology and medicine **40**(10), 811–22 (2010)
29. Somasundaram, K., Kalaiselvi, T.: Automatic brain extraction methods for T1 magnetic resonance images using region labeling and morphological operations. Computers in biology and medicine **41**(8), 716–25 (2011)
30. Latecki, L., Lakämper, R.: Convexity rule for shape decomposition based on discrete contour evolution. Computer Vision and Image Understanding **73**(3), 441–454 (1999)
31. Corovic, S., Lackovic, I., Sustaric, P., Sustar, T., Rodic, T., Miklavcic, D.: Modeling of electric field distribution in tissues during electroporation. Biomedical engineering online **12**, 16 (2013)
32. Garcia, P.a., Davalos, R.V., Miklavcic, D.: A numerical investigation of the electric and thermal cell kill distributions in electroporation-based therapies in tissue. PloS one **9**(8), 103083 (2014)
33. Aström, M., Zrinzo, L.U., Tisch, S., Tripoliti, E., Hariz, M.I., Wå rdell, K.: Method for patient-specific finite element modeling and simulation of deep brain stimulation. Medical & biological engineering & computing **47**(1), 21–8 (2009)
34. Zupanic, A., Kos, B., Miklavcic, D.: Treatment planning of electroporation-based medical interventions: electrochemotherapy, gene electrotransfer and irreversible electroporation. Physics in medicine and biology **57**(17), 5425–40 (2012)
35. Nielsen, J., Landauer, T.K.: A mathematical model of the finding of usability problems. In: Proceedings of the SIGCHI Conference on Human Factors in Computing Systems - CHI '93, pp. 206–213. ACM Press, New York, New York, USA (1993)
36. Pavliha, D., Kos, B., Marcan, M., Zupanic, A., Sersa, G., Miklavcic, D.: Planning of electroporation-based treatments using Web-based treatment-planning software. The Journal of membrane biology **246**(11), 833–42 (2013)
37. Scheffer, H.J., Nielsen, K., de Jong, M.C., van Tilborg, A.a.J.M., Vieveen, J.M., Bouwman, A.R.a., Meijer, S., van Kuijk, C., van den Tol, P.M.P., Meijerink, M.R.: Irreversible electroporation for nonthermal tumor ablation in the clinical setting: a systematic review of safety and efficacy. Journal of vascular and interventional radiology : JVIR **25**(7), 997–1011 (2014)
38. Wimmer, T., Srimathveeravalli, G., Gutta, N., Ezell, P.C., Monette, S., Maybody, M., Erinjery, J.P., Durack, J.C., Coleman, J.a., Solomon, S.B.: Planning Irreversible Electroporation in the Porcine Kidney: Are Numerical Simulations Reliable for Predicting Empiric Ablation Outcomes? CardioVascular and Interventional Radiology **38**(1), 182–90 (2015)

PAPER 4

Title: Multi-atlas segmentation of MRI images enhanced with atlas selection based on imaging properties and rater variability

Authors: MARČAN Marija, MIKLAVČIČ Damijan

Publication: IEEE Transactions on Medical Imaging

DOI: Under review; the paper was submitted on April 16th, 2015.

Year: /

Volume: /

Number: /

Pages: /

Impact factor: 3.799

Ranking:

Category name	Total journals in category	Journal rank in category	Quartile in category
computer science, interdisciplinary applications	102	10	Q1
engineering, biomedical	76	7	Q1
engineering, electrical & electronic	248	16	Q1
imaging science & photographic technology	23	2	Q1
radiology, nuclear medicine & medical imaging	122	15	Q1

Multi-Atlas Segmentation of MRI Images Enhanced with Atlas Selection Based on Imaging Properties and Rater Variability

Marija Marčan and Damijan Miklavčič*

***Abstract*—Methods of image segmentation based on registration of previously segmented images with the target image have been continuously providing good results. However, their big downside is relatively long segmentation time due to registration of each atlas with the target image, which can be shortened by selecting a subset of all atlases for the main process. Many of these atlas selection strategies include pre-registration, which is not very time-efficient, either. In this work we present a new atlas-selection strategy that requires no previous registration. The strategy is based on image meta-information that can be read directly from the DICOM header and variability of the atlas rater, which can be calculated offline and stored in the database along with the atlases. We applied the proposed method on an existing multi-atlas segmentation algorithm for prostate segmentation which originally selected the atlases solely on the presence of an endorectal coil. The method has been evaluated on a publicly available dataset of prostate images from four different institutions. Evaluation process included comparison of Dice similarity coefficients scored by multi-atlas segmentation with no atlas selection, with coil-based atlas selection and our proposed atlas-selection strategy. The results show 50% reduction of time needed for one multi-atlas based segmentation and also statistically significant improvement of the segmentation results when the atlas-selection strategy proposed in this work is used. However, the improvement in accuracy is still relatively small compared to errors introduced by registration of atlases; therefore further development in multi-atlas segmentation should be directed towards registration strategies.**

***Index Terms*—Magnetic resonance imaging (MRI), prostate, atlases, segmentation, validation, multi-atlas.**

I. Introduction

SEGMENTATION of medical images is undoubtedly a crucial part of many clinical tasks which are performed routinely. These tasks include not only diagnostics but also more complex activities such as intraoperative navigation and treatment planning. Its role in the treatment planning process is especially important in technologies for cancer treatment such as radiotherapy [1], cryotherapy [2], laser-induced interstitial thermotherapy [3], radiofrequency ablation [4] and, recently, electroporation-based treatments [5]–[7]. In the case of these technologies treatment planning not only enables routine performance of the treatment but is also key to performing the treatment successfully.

Although manual segmentation performed by an expert radiologist is today still considered to be the gold standard it is also a tedious and time-consuming task. This not only complicates the implementation of the whole treatment-planning process in the clinic but also introduces the problem of intra- and inter-rater variability [8]. Algorithms for automatic segmentation of medical images have proven to be effective in alleviating the variability and time problem [9]. Still, in order to ensure validity of results of automatic segmentation before they are used in treatment planning it would be wise, perhaps even mandatory, to use some kind of mechanism of segmentation validation and correcting by an expert clinician [8], [10], [11]. Additionally, if such validation mechanism is joined with the automatic segmentation algorithm into an integral solution it enables building a database of expert-validated segmentations which can then be used in improving the automatic segmentation algorithms. One such integrated tool that is also web-based was previously developed by our group and is used to facilitate treatment planning for electroporation-based treatments [12].

Not all automatic segmentation algorithms are convenient for improvement based on previously segmented images, e.g. the algorithms which have no parameters that could be optimized. On the other hand, some advanced algorithms rely heavily on a database of segmented cases, e.g. multi-atlas based segmentation where database images are registered to the target image and the obtained transformation deformations are propagated to respective segmented images. The final segmentation of the target image is then obtained through fusion of transformed labels [13]. Naturally, the performance of multi-atlas segmentation depends heavily on the registration and label-fusion algorithm implemented as well as the extent to which the atlases represent anatomical variability [14]. Another aspect that can influence the multi-atlas segmentation which continues to gain on its importance is the question of atlas selection. It was shown that careful selection of atlas subset decreases segmentation time and improves segmentation accuracy when compared to using all available atlases for segmentation [9], [14], [15].

Most methods of atlas selection that were implemented to-date are based on calculating image similarity between target image and atlas images [9], [15], [16]. This approach, however, requires that atlas images be registered to the target image before the image similarity measure is calculated, which is computationally equal to performing the segmentation with all atlases from the database. Another idea is to instead choose atlases based on meta-information, such as patient gender, age, clinical status etc. [14], [17]. There is also other meta-information that could be used, specifically imaging

M. Marčan and *D. Miklavčič are with the Faculty of Electrical Engineering, University of Ljubljana, SI-1000 Ljubljana, Slovenia (e-mail: marija.marcan@fe.uni-lj.si, damijan.miklavcic@fe.uni-lj.si)

Manuscript received April 14, 2015; revised xx xx, 2015.

parameters that can be read directly from the image header. Still, to the best of our knowledge such approach has not been explored, with an exception of Litjens et al. that have grouped atlases based on coil presence in their method for prostate segmentation from MRI images [18], [19].

Another aspect that could also be used in atlas selection is the variability of the rater that has segmented a certain atlas image. Although some recent works have addressed possible inaccuracy of the original atlas segmentation [20]–[22] they tie the inaccuracy to a specific case and treat one atlas segmentation as one rater. Since human raters differ in their skill level and experience it might be interesting to also try and formulate rater accuracy on the level of one specific person who introduces his/her specific variability into the atlas set.

In this work we explore the impact of atlas selection based on image meta-information and rater variability on the results of multi-atlas segmentation of MRI images. For this purpose we have developed a new framework for atlas selection that assigns each atlas a similarity value based on machine manufacturer, type, and strength, coil used and accuracy of the rater that labeled the atlas image. The framework was employed on the task of prostate segmentation from MRI images. The decision to use prostate as the target organ was made due to increased interest to use electroporation-based treatments (which are the focus of our research group) in treating prostate cancer [23], [24]. The results of multi-atlas segmentation with our proposed atlas-selection framework were compared to some previously developed multi-atlas algorithms for prostate segmentation [9], [19] in terms of accuracy and segmentation time.

II. Materials and Methods

A. Prostate segmentation from MRI images

In order to better observe the impact of our atlas selection method we have decided to implement it in previously validated multi-atlas based segmentation algorithm for prostate. In the recent years several authors have developed such algorithms [9], [18], [19], [25]–[30] which mostly vary in the choice of registration algorithm and label fusion approach. Our choice was to work with the algorithm proposed by Litjens et al. [19] since they have provided the most extensive description of the algorithm and report of validation results that enables straightforward repeatability and comparison. In addition, their algorithm was evaluated on a publicly available database from the 2012 MICCAI Grand Challenge on Prostate MRI Segmentation.

In their proposed prostate segmentation algorithm Litjens et al. perform a two-step registration of atlas images and target image: first a rigid registration and then a nonrigid registration parameterized by cubic B-splines. After applying the obtained transformations to label images they construct a baseline segmentation through majority voting and finally fuse the labels using the SIMPLE algorithm which was previously developed by Langerak et al. [26].

In our re-implementation of the algorithm we have used the Elastix package for registration as the authors have while setting the registration parameters according to detailed description provided in the original paper [19]. We have implemented the majority voting and SIMPLE algorithm in Matlab, also based on details provided by Litjens et al. Additionally, we have also performed experiments with STAPLE as the label fusion algorithm (instead of SIMPLE) [8] in order to gain additional insight into impact of our atlas selection method.

B. Atlas selection method

Our proposed atlas selection method uses two sources of information: image meta-information from MRI header and variability of the rater that segmented the atlas image. Specifically, the image meta-information used is: machine manufacturer, type, strength of the magnetic field, and whether or not an endorectal coil was used. We have chosen to use these parameters as features in our atlas selection given the available information provided in the publicly available dataset that we used for evaluation.

The variability of the rater was assessed through the leave-one-out experiment on the same publicly available dataset used for all other evaluation. Generally the best way to assess rater variability is to have multiple raters label the same case multiple times, after which ground truth can be estimated using the expectation-maximization algorithm and rater variability assessed, such as by using the STAPLE algorithm [8]. Unfortunately it is hard to obtain such data in practice. However, the underlying idea behind the multi-atlas segmentation is that the registration step results in images which have an identical intensity similarity to the target image [22]. With the assumption of a perfect registration being achieved any disagreements between the transformed label image and the estimated segmentation of the target image are in fact a product of errors in segmentation of the atlas image. This assumption about registration accuracy enables us to assess rater variability through multi-atlas segmentation where estimated target segmentation is the ground truth and transformed atlas labels are segmentations of the target image performed by individual raters. In our implementation we perform the atlas registration in the same way as described in the previous section while ground truth estimation from transformed labels is done using the STAPLE algorithm. We quantify the rater variability by calculating the Dice similarity coefficient (DSC) between the estimated ground truth and the transformed atlas label.

Since the dataset that we use does not provide the information about which rater manually labeled which atlas we assumed that each atlas was labeled by a different rater, thus treating an atlas as a rater. By performing the leave-one-out experiment we obtain DSC values per each rater per each atlas case that was left out. The final values of the variability of each rater are then calculated by averaging the DSC values of all cases per rater.

The image meta-information and rater variability are then combined to form a unique atlas similarity value in the following manner. If for a certain atlas image any of the four meta-information features (manufacturer, machine type,

TABLE I
AVAILABLE META-INFORMATION ABOUT MRI IMAGES OF THE PROSTATE FROM FOUR DIFFERENT CENTERS

Centre	Manufacturer	Field strength (T)	Endorectal coil
Haukeland University Hospital (Norway)	Siemens	1.5	Yes
Beth Israel Deaconess Medical Center (USA)	GE	3	Yes
University College London (UK)	Siemens	1.5 / 3	No
Radboud University Nijmegen Medical Centre (Netherlands)	Siemens	3	No

strength and coil) is the same as in the target image that feature is set to '1', otherwise it is set to '0'. The rater variability feature for a certain atlas is directly assigned the DSC value of the rater who performed the manual atlas labeling. The atlas similarity value is thus:

$$similarity\ value\,(atlas) = manufacturer + machine + strength + coil + variability\,(rater) \quad (1)$$

Once the similarity values of all the atlases have been calculated we rank them in descending order and select 20 best atlases [14], [30] which are used in the multi-atlas segmentation algorithm.

C. Data and experiments

The data used in the evaluation of our atlas selection method is the publicly available data from the PROMISE 12 challenge - the Prostate MR Image Segmentation challenge that was held as a part of 2012 MICCAI conference. This database contains 50 training cases with corresponding expert segmentations of prostate and 30 test cases with just the original images without the segmentation. The results of the test cases segmentation can however be submitted online to the challenge page after which they are automatically evaluated by the same metrics that were used for all participants of the challenge.
The PROMISE challenge dataset contains images which originate from four different centers and subsequently have different combinations of image meta-information features that we use in our atlas selection method. This makes it an especially convenient dataset to evaluate the impact of our atlas-selection method on segmentation results. The values of the image meta-information features for each of the four centers are presented in Table 1 [31]. The data about the type of the machine is not explicitly available so we presumed that each institution had a different machine, with the exception of UCL which, according to data about field strength, had two machines. It should also be noted that each of the four institutions provided equal number of cases which were then evenly distributed in both training and test dataset.

The evaluation of our atlas selection method was done through the leave-one-out experiments on the 50 training sample from the PROMISE dataset. We have quantified the results of each case by calculating the 3D Dice similarity coefficient (DSC). The leave one-out experiments were repeated several times, each time with different variation of the atlas-selection method. Besides selecting the 20 best atlases based on equation (1) given in the 'Atlas selection method' section we have also experimented with atlas selection based only on coil presence, as this is what was performed by Litjens et al. in their multi-atlas prostate segmentation method [19]. We have also performed the multi-atlas segmentation on all atlases, e.g. without atlas selection. In addition to varying the choice of features for atlas selection we also varied the label fusion method between SIMPLE and STAPLE. The label fusion variation was done in combination with each of the four atlas selection strategies, resulting in eight leave-one-out experiments in total.
We have also applied our atlas selection method based on (1) along with prostate segmentation method [19] to the test dataset of the PROMISE challenge. This dataset consists of 30 images from the same four institutions that provided images for the training dataset, but the reference segmentation for these images is not publicly available. We have submitted our segmentations of the test images to the PROMISE challenge web-page where they were evaluated by the organizers by the same metrics used on all the other participants of the challenge.

TABLE II
RESULTS OF LEAVE-ONE-OUT EXPERIMENTS ON TRAINING DATA FOR DIFFERENT ATLAS SELECTION AND LABEL FUSION STRATEGIES

Atlas selection + label fusion variation	Mean DSC	Median DSC	Performance time (min)
All atlases + SIMPLE	0.75	0.80	32
All atlases + STAPLE	0.72	0.76	37
Coil-based selection + SIMPLE	0.76	0.81	14
Coil-based selection + STAPLE	0.77	0.81	14
Image meta-information + rater variability + SIMPLE	0.77	0.82	14
Image meta-information + rater variability + STAPLE	0.77	0.81	14

III. RESULTS

A. Training Data

The results of the leave-one-out experiments are shown in Table 2 in the form of mean and median DSC and performance time in minutes. The results of the same experiments are also shown graphically in the form of box-plot in Figure 1. All experiments were run on the same machine, which has an 8-core Intel i7 3.40 GHz processor with 16 GB of RAM. Additionally, the registration of atlases was run in parallel using a pool of four workers with each worker assigned with one atlas at a time.

In order to gain better insight into performance of different atlas selection and label fusion strategies we have also performed the paired difference Wilcoxon signed rank tests between all of the methods. Performance of paired t-test was not used in all cases due to data being non-uniformly distributed. The results of the paired difference tests for the leave-one-out experiments on training data is shown in Table 3. The row strategies are compared to the column strategies. A table entry + denotes statistically significant superiority of the former over the latter; - denotes inferiority; NS denotes a statistically insignificant difference ($P > 0.05$). For significant differences, the respective confidence levels are given in parentheses.

B. Test Data

According to the metrics defined by the organizers of the PROMISE challenge the implemented atlas-based segmentation of the prostate in combination with our atlas selection strategy scored 74.04 out of 100, while the original atlas-based method which selected atlases only based on endorectal coil presence scored 73.3. Score is a value 1-100 calculated by the challenge organizers based on different metrics. The results are publicly displayed at http://promise12.grand-challenge.org/Results/Overview, along with the detailed score of each submission.

We have observed per-case values of the Dice similarity coefficients for the two atlas-selection methods and presented the results graphically in Figure 2.

As in the case of the training dataset we have also performed the paired difference Wilcoxon signed rank test on the results obtained on the test dataset, namely on the score values obtained by the two methods. If the test is performed on the full dataset of all 30 test cases the difference between the two methods is not statistically significant. However, through direct observation of per-case results (Figure 2.) we have established that the performance of our proposed atlas selection method is worse than that of the method based on coil presence alone mostly in the first seven cases, which all originate from the same institution. If we perform the paired difference test on the remaining 23 cases which originate from the other three institutions the results show that our proposed method is statistically significantly better, with confidence level $0.005 < P < 0.01$. The same test performed on the first seven cases that belong to a single institution show that the atlas selection method based on coil alone is statistically significantly better than our proposed method, with confidence level $P < 0.001$. The difference in performance of methods on these two subsets (one institution vs. other three institutions) is also visible from Figure 3, where we present box plots of the two methods' DSC

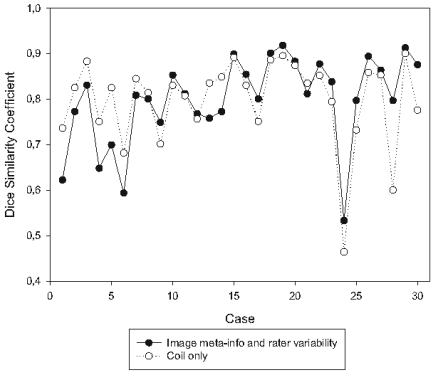

Fig. 2. Dice similarity coefficients of two different atlas selection methods in combination with a multi-atlas prostate segmentation algorithm applied on the 30 test cases.

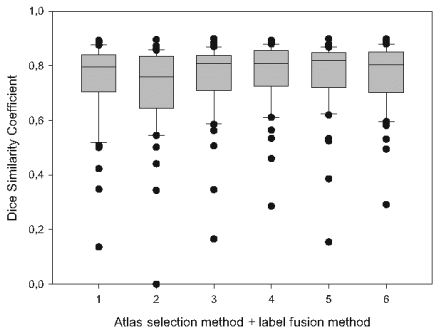

Fig. 1. Box-plot of Dice similarity Coefficients of different atlas selection and label fusion strategies applied on the leave-one out validation of prostate segmentation. 1 - No atlas selection (all atlases) + SIMPLE. 2 - No atlas selection (all atlases) + STAPLE. 3 - Coil-based atlas selection + SIMPLE. 4 - Coil-based atlas selection + STAPLE. 5 - Atlas selection based on image meta-information and rater variability + SIMPLE. 6 - Atlas selection based on image meta-information and rater variability + STAPLE.

TABLE III
RESULTS OF PAIRED DIFFERENCE WILCOXON SIGNED RANK TESTS FOR DIFFERENT ATLAS SELECTION AND LABEL FUSION STRATEGIES

	All atlases + SIMPLE	All atlases + STAPLE	Coil-based selection + SIMPLE	Coil-based selection + STAPLE	Image meta-information + rater variability + SIMPLE	Image meta-information + rater variability + STAPLE
All atlases + SIMPLE	/	NS	NS	NS	- ($P < 0.001$)	NS
All atlases + STAPLE	NS	/	NS	- ($0.001 < P < 0.005$)	NS	- ($P < 0.001$)
Coil-based selection + SIMPLE	NS	NS	/	NS	- ($0.02 < P < 0.05$)	NS
Coil-based selection + STAPLE	NS	+ ($0.001 < P < 0.005$)	NS	/	NS	NS
Image meta-information + rater variability + SIMPLE	+ ($P < 0.001$)	NS	+ ($0.02 < P < 0.05$)	NS	/	NS
Image meta-information + rater variability + STAPLE	NS	+ ($P < 0.001$)	NS	NS	NS	/

values for the whole test dataset and the two subsets.

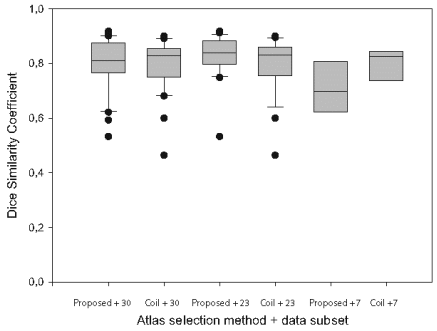

Fig. 3. Dice similarity coefficients of two different atlas selection methods in combination with a multi-atlas prostate segmentation algorithm applied on different subsets of test cases: all 30 cases, 23 cases from 3 institutions, 7 cases from the fourth institution (first 7 cases of the whole dataset of 30 test cases).

IV. DISCUSSION AND CONCLUSION

The aim of the work presented in this paper was to establish whether an atlas selection strategy based on image meta-information and variability of the rater who segmented the atlas image can improve the results of multi-atlas segmentation methods. We have applied the proposed atlas selection strategy to an existing multi-atlas prostate segmentation algorithm and evaluated its performance on a publicly available dataset of segmented prostate images from four different institutions. The dataset in question belongs to the 2012 MICCAI Grand Challenge on Prostate MRI Segmentation. The original prostate segmentation algorithm on which we applied our atlas selection strategy was also a part of the mentioned challenge, which enabled easy and transparent comparison of obtained results. The results obtained from the leave-one-out experiments on 50 images from the training set show that our proposed atlas selection strategy improves both mean and median Dice similarity coefficient for 0.02 compared to performing the segmentation with no atlas selection, i.e. using all available atlases. This difference was also shown to be statistically significant in paired difference tests ($P < 0.001$). The benefit of our atlas selection strategy over using all available atlases is even more pronounced in terms of time required for segmentation of one case, which is by using our atlas selection strategy reduced for more than 50%.

Regarding the differences between our atlas selection strategy and the strategy that was employed in the original prostate segmentation algorithm that we re-implemented for the purposes of this work (Litjens et al. 2012), observing mean and median DSC evaluated based on the training set shows no difference between two methods. A statistically significant difference in favor of our proposed method does however exist on the per-case basis ($0.02 < P < 0.05$). The difference between the two atlas selection strategies is even more visible in the results obtained from the 30 test cases. Although the results of the paired difference test applied on the whole test set show that there is no statistically significant difference, closer observation of the per-case results shown in Figure 2. raises suspicions of a possible institution bias. In Figure 2 it can be noticed that the first seven cases stand out from the rest of the results in consistent better performance of the atlas selection method based only on coil presence. Also, all of these seven cases came from the same institution, while the other 23 cases came from the other three institutions. The analysis of the paired difference in these two subsets shows a statistically significant difference in favor of the coil-only atlas selection for the first seven test cases ($P < 0.001$) and a statistically significant difference in favor of our proposed atlas selection for the rest of the subset ($0.005 < P < 0.01$). Since the paired difference was calculated using the signed rank test this had probably resulted in reported no statistically significant difference for the whole test set of 30 cases. Also, the level of the statistical difference in the two subsets is too great not to assume a certain bias towards one institution exists, although we cannot explain the reasons for this bias based on available data. Based on the performance of our proposed atlas selection strategy on the data from other three institutions as well as on the training dataset we believe the results show that our atlas selection strategy is in general superior over atlas selection

based on coil presence alone.

What can also be observed from the results is that the choice of the label fusion method, at least regarding the choice of SIMPLE or STAPLE method, has no significant influence on the final segmentation results. It would however be interesting to apply the proposed atlas selection method in combination with some other label fusion strategies, as there have been many new ones developed in the past few years [20]–[22], [32], [33]. Some of these strategies also include a way to account for registration errors based on image intensities of the original and atlas image [20], [22], which could be especially beneficial in our strategy of determining variability of the rater who segmented the atlas image and subsequent choice of atlases based on that metric. Also, the rate of improvement of segmentation results that is obtained by using our atlas selection strategy hints that the errors that occur during the registration phase still account for the majority of inaccuracy in multi-atlas based segmentation algorithms.

In summary, we have shown that selection of atlases based on image meta-information and rater variability is an elegant and efficient strategy that both improves the segmentation results and significantly reduces the time needed for multi-atlas based segmentation. We believe our strategy can be especially beneficial in cases of large databases with cases coming from many different institutions. Also, the formulation of our atlas selection strategy is such that it could include additional features that could be read directly from the DICOM header, such as the imaging protocol and contrast agent. Additionally, in the cases where multiple segmentations by the same rater exist in the database the value of rater variability can be easily recalculated offline after the addition of new cases, with no additional performance burden on the segmentation method itself. This gathering of cases and offline recalculation can be easily implemented as a web-based tool, an example of which is our previously developed tool for treatment planning of electroporation-based treatments (www.visifield.com).

ACKNOWLEDGMENT

This work was supported by the Slovenian Research Agency. Research was conducted in the scope of the Electroporation in Biology and Medicine, European Associated Laboratory. Part of this work was possible due to networking activities of COST Action TD1104 European network for development of electroporation-based technologies and treatments (EP4Bio2Med) (www.electroporation.net).

REFERENCES

[1] M. Lecchi, P. Fossati, F. Elisei, R. Orecchia, and G. Lucignani, "Current concepts on imaging in radiotherapy." *European journal of nuclear medicine and molecular imaging*, vol. 35, no. 4, pp. 821–37, Apr. 2008.

[2] T. Butz, S. K. Warfield, K. Tuncali, S. G. Silverman, E. van Sonnenberg, F. a. Jolesz, and R. Kikinis, "Pre- and Intra-operative Planning and Simulation of Percutaneous Tumor Ablation," in *Proceedings of the Third International Conference on Medical Image Computing and Computer-Assisted Intervention (MICCAI), LNCS 1935, Pittsburgh, USA*, S. L. Delp, A. M. DiGoia, and B. Jaramaz, Eds. Pittsburgh, PA, USA: Springer Berlin Heidelberg, 2000, pp. 317–326.

[3] H. J. Schwarzmaier, I. V. Yaroslavsky, A. N. Yaroslavsky, V. Fiedler, F. Ulrich, and T. Kahn, "Treatment planning for MRI-guided laser-induced interstitial thermotherapy of brain tumors - The role of blood perfusion," *Journal of Magnetic Resonance Imaging*, vol. 8, pp. 121–127, 1998.

[4] C.-C. R. Chen, M. I. Miga, and R. L. Galloway, "Optimizing electrode placement using finite-element models in radiofrequency ablation treatment planning," *IEEE transactions on bio-medical engineering*, vol. 56, no. 2, pp. 237–245, 2009.

[5] A. Zupanic, B. Kos, and D. Miklavcic, "Treatment planning of electroporation-based medical interventions: electrochemotherapy, gene electrotransfer and irreversible electroporation." *Physics in medicine and biology*, vol. 57, no. 17, pp. 5425–40, Sep. 2012.

[6] M. L. Yarmush, A. Golberg, G. Serša, T. Kotnik, and D. Miklavčič, "Electroporation-based technologies for medicine: principles, applications, and challenges." *Annual review of biomedical engineering*, vol. 16, pp. 295–320, Jul. 2014.

[7] C. Jiang, R. V. Davalos, and J. C. Bischof, "A Review of Basic to Clinical Studies of Irreversible Electroporation Therapy," *IEEE Transactions on Biomedical Engineering*, vol. 62, no. 1, pp. 4–20, 2015.

[8] S. K. Warfield, K. H. Zou, and W. M. Wells, "Simultaneous truth and performance level estimation (STAPLE): an algorithm for the validation of image segmentation." *IEEE transactions on medical imaging*, vol. 23, no. 7, pp. 903–21, Jul. 2004.

[9] S. Klein, U. a. van der Heide, I. M. Lips, M. van Vulpen, M. Staring, and J. P. W. Pluim, "Automatic segmentation of the prostate in 3D MR images by atlas matching using localized mutual information," *Medical Physics*, vol. 35, no. 4, p. 1407, 2008.

[10] A. Saad, G. Hamarneh, and T. Möller, "Exploration and visualization of segmentation uncertainty using shape and appearance prior information." *IEEE transactions on visualization and computer graphics*, vol. 16, no. 6, pp. 1366–75, 2010.

[11] M. a. Deeley, A. Chen, R. D. Datteri, J. Noble, A. Cmelak, E. Donnelly, A. Malcolm, L. Moretti, J. Jaboin, K. Niermann, E. S. Yang, D. S. Yu, and B. M. Dawant, "Segmentation editing improves efficiency while reducing inter-expert variation and maintaining accuracy for normal brain tissues in the presence of space-occupying lesions." *Physics in medicine and biology*, vol. 58, no. 12, pp. 4071–97, May 2013.

[12] D. Pavliha, B. Kos, M. Marčan, A. Županič, G. Serša, and D. Miklavčič, "Planning of electroporation-based treatments using web-based treatment-planning software," *Journal of Membrane Biology*, vol. 246, no. 11, pp. 833–842, Nov. 2013.

[13] D. Collins, C. Holmes, T. Peters, and A. Evans, "Automatic 3-D model-based neuroanatomical segmentation," *Hum. Brain Mapp.*, vol. 208, no. 1995, pp. 190–208, 1995.

[14] P. Aljabar, R. a. Heckemann, a. Hammers, J. V. Hajnal, and D. Rueckert, "Multi-atlas based segmentation of brain images: atlas selection and its effect on accuracy." *NeuroImage*, vol. 46, no. 3, pp. 726–38, Jul. 2009.

[15] T. Rohlfing, R. Brandt, R. Menzel, and C. R. Maurer, "Evaluation of atlas selection strategies for atlas-based image segmentation with application to confocal microscopy images of bee brains," *NeuroImage*, vol. 21, pp. 1428–1442, 2004.

[16] G. Sanroma, G. Wu, Y. Gao, and D. Shen, "Learning to Rank Atlases for Multiple-Atlas Segmentation." *IEEE transactions on medical imaging*, vol. 33, no. 10, pp. 1939–1953, 2014.

[17] J. M. Lötjönen, R. Wolz, J. R. Koikkalainen, L. Thurfjell, G. Waldemar, H. Soininen, and D. Rueckert, "Fast and robust multi-atlas segmentation of brain magnetic resonance images," *NeuroImage*, vol. 49, no. 3, pp. 2352–2365, 2010.

[18] Q. Gao, D. Rueckert, and P. Edwards, "An automatic multi-atlas based prostate segmentation using local appearance-specific atlases and patch-based voxel weighting," *MICCAI Grand Challenge: Prostate MR Image Segmentation 2012*, 2012.

[19] G. Litjens, N. Karssemeijer, and H. Huisman, "A multi-atlas approach for prostate segmentation in MR images," *MICCAI Grand Challenge: Prostate MR Image Segmentation 2012.*, 2012.

[20] O. Commowick, A. Akhondi-Asl, and S. K. Warfield, "Estimating a reference standard segmentation with spatially varying performance parameters: Local MAP STAPLE," *IEEE Transactions on Medical Imaging*, vol. 31, no. 8, pp. 1593–1606, 2012.

[21] A. Akhondi-Asl and S. K. Warfield, "Simultaneous truth and performance level estimation through fusion of probabilistic segmentations," *IEEE Transactions on Medical Imaging*, vol. 32, no. 10, pp. 1840–1852, 2013.

[22] A. Akhondi-Asl, L. Hoyte, M. Lockhart, and S. Warfield, "A Logarithmic Opinion Pool Based STAPLE Algorithm for the Fusion of Segmentations With Associated Reliability Weights." *IEEE transactions on medical imaging*, vol. 0062, no. 10, pp. 1–14, 2014.

[23] G. Onik and B. Rubinsky, "Irreversible Electroporation : First Patient Experience Focal Therapy of Prostate Cancer," in *Irreversible electroporation*, ser. Series in Biomedical Engineering, B. Rubinsky, Ed. Berlin, Heidelberg: Springer Berlin Heidelberg, 2010, vol. 110, pp. 235–247.

[24] M. Valerio, L. Dickinson, A. Ali, N. Ramachandran, I. Donaldson, A. Freeman, H. U. Ahmed, and M. Emberton, "A prospective development study investigating focal irreversible electroporation in men with localised prostate cancer: Nanoknife electroporation ablation trial (NEAT)," *Contemporary Clinical Trials*, vol. 39, pp. 57–65, 2014.

[25] S. Martin, V. Daanen, and J. Troccaz, "Atlas-based prostate segmentation using an hybrid registration," *International Journal of Computer Assisted Radiology and Surgery*, vol. 3, no. 6, pp. 485–492, Sep. 2008.

[26] T. R. Langerak, U. a. van der Heide, A. N. T. J. Kotte, M. a. Viergever, M. van Vulpen, and J. P. W. Pluim, "Label fusion in atlas-based segmentation using a selective and iterative method for performance level estimation (SIMPLE)." *IEEE transactions on medical imaging*, vol. 29, no. 12, pp. 2000–8, Dec. 2010.

[27] S. Martin, J. Troccaz, and V. Daanen, "Automated segmentation of the prostate in 3D MR images using a probabilistic atlas and a spatially constrained deformable model," *Medical Physics*, vol. 37, no. 4, p. 1579, 2010.

[28] J. A. Dowling, J. Fripp, S. Chandra, J. P. W. Pluim, J. Lambert, J. Parker, J. Denham, P. B. Greer, and O. Salvado, "Fast automatic multi-atlas segmentation of the prostate from 3D MR images," in *Lecture Notes in Computer Science (including subseries Lecture Notes in Artificial Intelligence and Lecture Notes in Bioinformatics)*, vol. 6963 LNCS, 2011, pp. 10–21.

[29] Y. Ou and J. Doshi, "Multi-atlas segmentation of the prostate: A zooming process with robust registration and atlas selection," *MICCAI Grand Challenge: Prostate MR Image Segmentation 2012*, pp. 1–7, 2012.

[30] T. Langerak, U. van der Heide, A. Kotte, F. Berendsen, and J. Pluim, "Improving label fusion in multi-atlas based segmentation by locally combining atlas selection and performance estimation," *Computer Vision and Image Understanding*, vol. 130, pp. 71–79, 2015.

[31] G. Litjens, R. Toth, W. van de Ven, C. Hoeks, S. Kerkstra, B. van Ginneken, G. Vincent, G. Guillard, N. Birbeck, J. Zhang, R. Strand, F. Malmberg, Y. Ou, C. Davatzikos, M. Kirschner, F. Jung, J. Yuan, W. Qiu, Q. Gao, P. E. Edwards, B. Maan, F. van der Heijden, S. Ghose, J. Mitra, J. Dowling, D. Barratt, H. Huisman, and A. Madabhushi, "Evaluation of prostate segmentation algorithms for MRI: the PROMISE12 challenge." *Medical image analysis*, vol. 18, no. 2, pp. 359–73, Feb. 2014.

[32] O. Commowick and S. K. Warfield, "Incorporating priors on expert performance parameters for segmentation validation and label fusion: A maximum a posteriori STAPLE," *Lecture Notes in Computer Science (including subseries Lecture Notes in Artificial Intelligence and Lecture Notes in Bioinformatics)*, vol. 6363 LNCS, pp. 25–32, 2010.

[33] A. J. Asman and B. a. Landman, "Robust statistical label fusion through consensus level, labeler accuracy, and truth estimation (COLLATE)," *IEEE Transactions on Medical Imaging*, vol. 30, no. 10, pp. 1779–1794, 2011.

DISCUSSION

SEGMENTATION OF HEPATIC VESSELS FROM MRI IMAGES

Development of methods for automatic segmentation of tissues which are deemed critical during electroporation based treatments, namely the hepatic vessels, from medical images was the topic of *Paper 1*. The choice of hepatic vessels as the target object for segmentation was motivated by at that time active clinical study on electrochemotherapy of liver metastases (EudraCt no. 2008-008290- 54, registered 178 at Clinicaltrials.gov no. NCT01264952), which was performed at the Institute of Oncology Ljubljana. The clinical study included treatment planning procedure which required an adequate model of the liver, tumor and hepatic vessels (Edhemovic et al. 2011). MRI was chosen as the imaging modality since the liver metastases that were treated in the clinical study are best visible in MRI images. By using the same images to segment liver, tumor and hepatic vessels additional registration errors were avoided.

As the majority of work on automatic segmentation of hepatic vessels was done on CT images I used the classical methods applied there to construct an algorithm that would work well on MRI images. The developed algorithm is based on two main approaches: filtering that enhances tubular structures and thresholding. Multiscale enhancement of tubular structures is a widely used and efficient method (Frangi et al. 1998) that is in the proposed algorithm used to locate the vessels. The final vessel boundary is then determined by performing local thresholding of the MRI image in smaller regions of interest obtained by dilation of vessel locations produced by the previous step. The thresholding method is also an established and relatively simple yet efficient approach based on minimization of intra-class variance (Otsu 1979). Besides the two main approaches the algorithm includes preprocessing and post

processing methods. The preprocessing method removes the bias that is characteristic for MRI images due to inhomogeneity of the magnetic field. Bias removal is extremely important for the local thresholding and directly influences determination of the optimal threshold. The post processing methods include region growing which serves to connect small gaps between vessel segments and morphological opening which removes very small disconnected objects.

The developed method for automatic segmentation of hepatic vessels was validated using custom-made simple phantoms and images of the patients enrolled in the clinical study of treating liver metastases by electrochemotherapy. Simple phantoms were created by inserting a glass tube filled with physiological solution into a cup filled with agarose gel. The glass tube modeled the vessel while the agarose gel modeled liver. The inserted tubes were of different diameter sizes (4 mm, 6 mm, and 8 mm) and were inserted into the gel both perpendicularly to the bottom and in a way that they leaned on the glass side. The position of the glass tubes can be seen in Figure 2. In total six phantoms with different combinations of tube size and position were used and were simultaneously imaged in an MRI device.

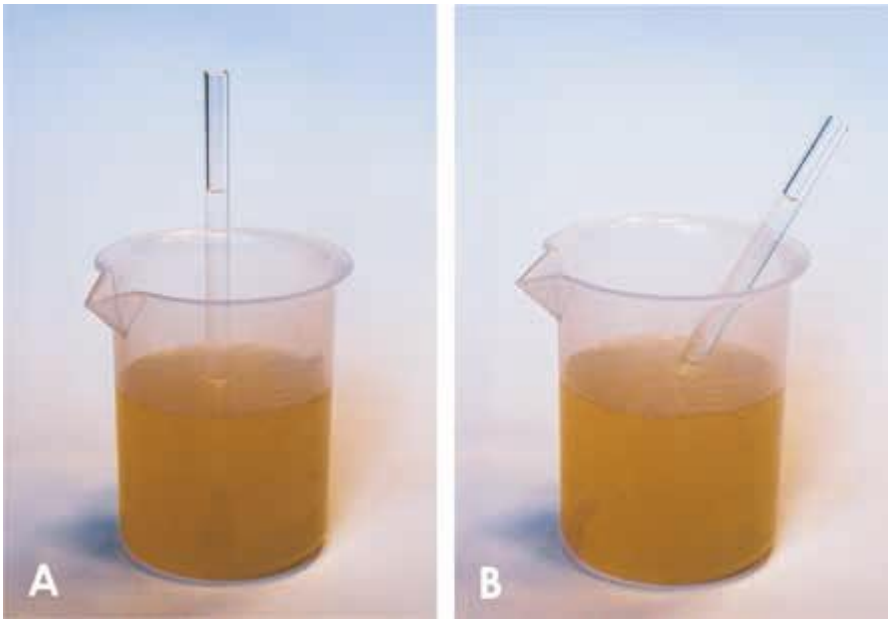

Figure 2. A simple phantom constructed for validation of hepatic vessel segmentation from MRI images. The phantom is made of agarose gel and a glass tube filled with physiological solution inserted in: (A) perpendicular position. (B) tilted position. *(The figure is originally Figure 2. from Paper 1.)*

The resulting images were segmented by the developed algorithm and compared to the expected size of the vessel in axial slices which was determined based on the mathematical equation for area of the circle. The results presented in Figure 3 indicate the developed method is able to accurately determine the edge of the vessel.

The validation on medical images of real patients was performed for six cases from the clinical study. The series chosen for segmentation were the same as the ones used for segmentation of liver in earlier work (Pavliha, Mušič, et al. 2013) - T1-weighted axial images taken 20 min after injection of Primovist® (Bayer Group, Germany) contrast agent. Hepatic vessels were previously manually segmented from the images by an experienced radiologist, thus providing the gold standard for the evaluation of the proposed algorithms. The metrics chosen for evaluation included sensitivity, average symmetric surface distance (ASSD) and Hausdorff distance, which were determined per vessel segment. To express the metrics on the case level the median of all metric values obtain per vessel segment were calculated. These results are shown in Table 1.

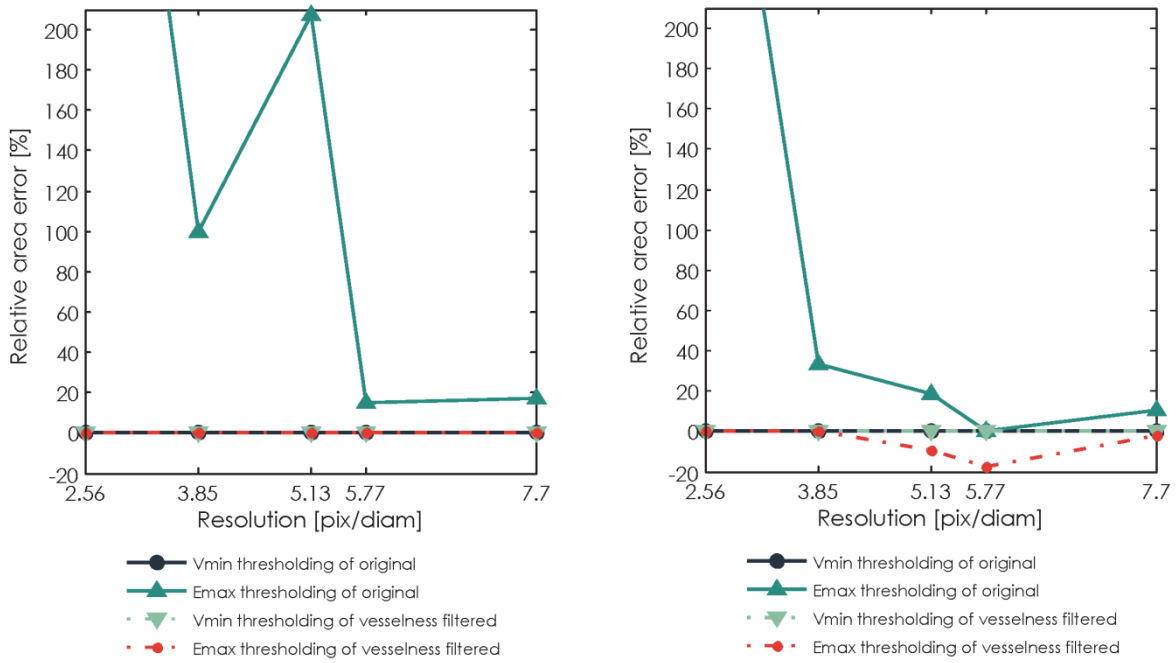

Figure 3. Median accuracy of segmented area of phantom as a function of resolution for different segmentation methods: variance minimization thresholding of the original image, entropy maximization thresholding of the original image, vesselness filtered image thresholded by variance minimization thresholding, and vesselness filtered image thresholded by entropy maximization thresholding. A. Tube in perpendicular position. B. Tube in tilted position. *(The figure is originally Figures 4. and 5. from Paper 1.)*

Table 1. Results of segmentation of all hepatic vessels from six clinical cases. Segmentation was performed by the method based on local thresholding. Results show median sensitivity (SEN), median average symmetric surface distance and median Hausdorff distance. *(The table is originally Table 3. from Paper 1.)*

CASE	Number of objects	Pixel resolution [mm]	Median SEN	Median ASSD [pix]	Median ASSD [mm]	Median Hausdorff distance [pix]	Median Hausdorff distance [mm]
1	305	0.684	100,0	1,0	0,7	2,2	1,5
2	347	0.684	100,0	1,2	0,8	3,2	2,2
3	328	0.684	100,0	1,1	0,8	3,2	2,2
4	327	1.188	89,9	0,7	0,8	2,8	3,4
5	400	1.188	90,0	0,6	0,8	2,2	2,7
6	454	1.188	100,0	0,9	1,1	3,0	3,6
OVERALL (mean)			**96,7**	**0,9**	**0,8**	**2,8**	**2,6**

Of the metrics used for algorithm evaluation most prominent indicators of method suitability for treatment planning of electroporation based treatments are ASSD and Hausdorff distance, which indicate mean expected error and the maximum expected error produced by the segmentation method. The values of these errors averaged over all six clinical cases were 0.8 mm for ASSD and 2.6 mm for Hausdorff distance. The average sensitivity of the method was shown to be 96.7 which indicates good method performance in locating the hepatic vessels. However, in order to determine whether the method is robust enough to be used in generating reliable treatment plans for electroporation-based treatments, a deeper understanding of influence of vessels on the electric field distribution had to be obtained first.

INFLUENCE OF VESSELS ON THE OUTCOME OF ELECTROPORATION-BASED TREATMENTS

Recent practice in performing treatment planning for electroporation-based treatments has grown to take into account different tissues that are in the vicinity of the tumor along with their electrical conductivity. However, the vessels were usually not modeled as separate objects with the justification that their conductivity is accounted for in the bulk tissue conductivity (Šel et al. 2005; Cukjati et al. 2007). Although it was suspected that large vessels, such as those found in the liver, might have their own individual and significant effect on the distribution of the electric field, there was no definite quantification of the extent of that

effect. The first attempts at gaining insight into the effect were made only recently (Golberg et al. 2015).

In the second part of my PhD, which is described in Paper 2, I set out to give an answer whether ignoring the vessels that are situated near the tumor can have adverse effects on the treatment outcome. In other words, I wanted to establish whether the vessels can affect the electric field distribution in such a way that would cause the coverage of the tumor to be smaller than if no vessels were present. I also wanted to determine for which vessel sizes and distances from the tumor could this effect occur.

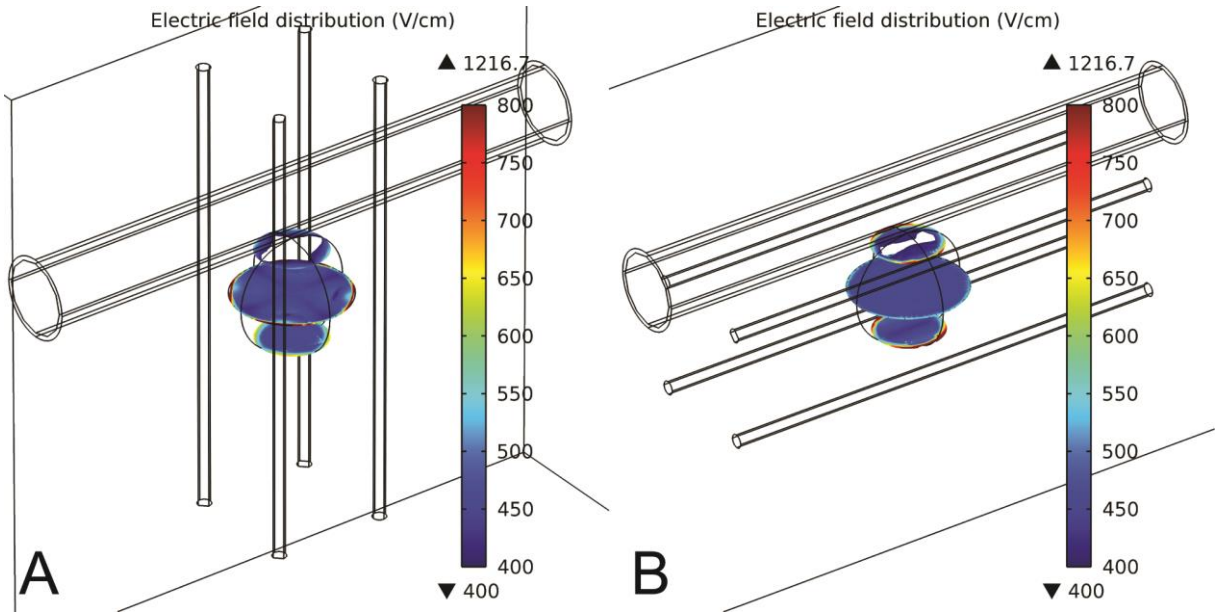

Figure 4. 2D sliced color map of the electric field distribution for a case where a significant difference in tumor coverage is observed as a result of the presence of the blood vessel. The color map is presented for a simplified model of ECT of a 10 mm tumor with a 4 electrode configuration and in the presence of a 7 mm vessel which is 0 mm away from the tumor. The color maps are shown for two vessel positions: A. Vessel perpendicular to the electrodes. B. Vessel parallel to the electrodes. The slices for which the color map is shown span the plane parallel to the vessel. The relative position of the planes along the third axis (the one which the plane does not span) is the same in both cases and fixed at -4 mm, 0 mm, and 4 mm away from the tumor center. *(The figure is originally Figure 7. from Paper 2.)*

In order to achieve the above goal I have created a numerical model consisting of a sphere and a cylinder, where the sphere represented tumor and the cylinder represented a vessel. I varied the sizes of both tumor and vessel, as well as the distance between them and the position of the vessel regarding the electrodes. For each tumor size I first determined the

optimal treatment parameters while disregarding the vessel. After that I performed another calculation with the same parameters only this time with vessel included in the model.

The results of my calculations show that ignoring the vessels that are in tumor vicinity while calculating optimal treatment parameters can indeed cause incomplete coverage of the tumor by a sufficiently high electric field. An example of this effect is shown in Figure 4.

The effect of the vessels varies with sizes of both tumor and vessel and the distance between them. In general, the effect will be present in cases of a vessel with 3 mm diameter or larger which is 3 mm away from the tumor or closer. As expected, the effect is more pronounced for larger vessels and smaller distances, which can be observed in Figure 5 and Figure 6. More important conclusion that can be drawn by observing these two figures is that an adverse effect of the vessels is a lot more pronounced when a treatment is performed without an electrode that is inserted inside the tumor, i.e. the central electrode. Below results shown in Figure 5 correspond to the case without the central electrode while Figure 6 shows the results for the case with the central electrode.

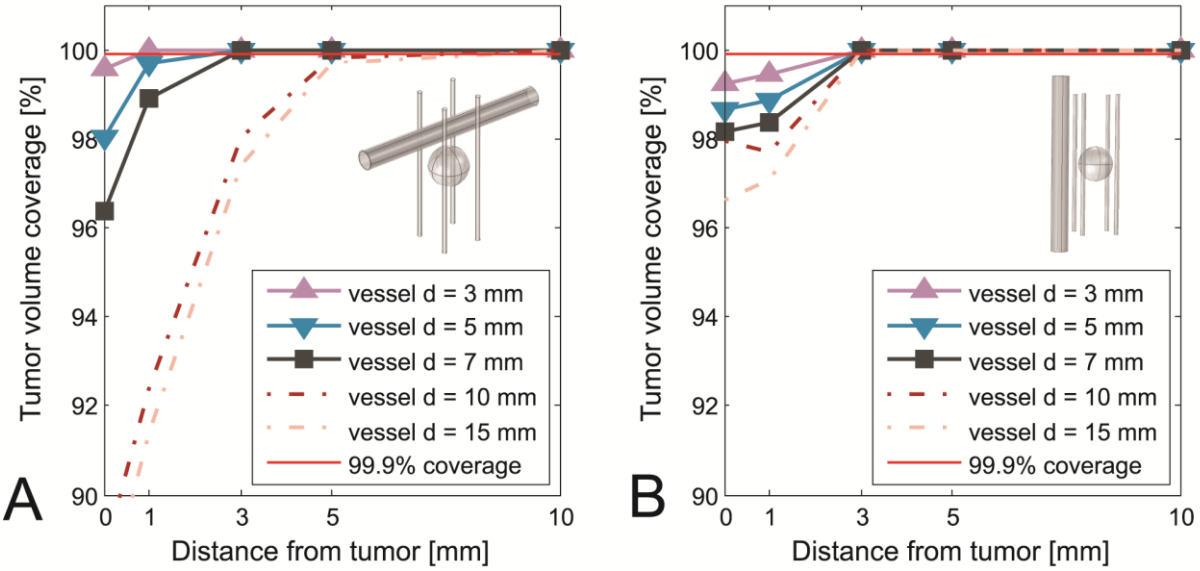

Figure 5. Tumor coverage for ECT of simplified model of 10 mm tumor with 4 electrodes. The coverage is plotted against different distances between vessel and tumor, and with respect to different vessel positions and sizes. A. Vessel perpendicular to the electrodes. B. Vessel parallel to the electrodes. *(The figure is originally Figure 3. from Paper 2.)*

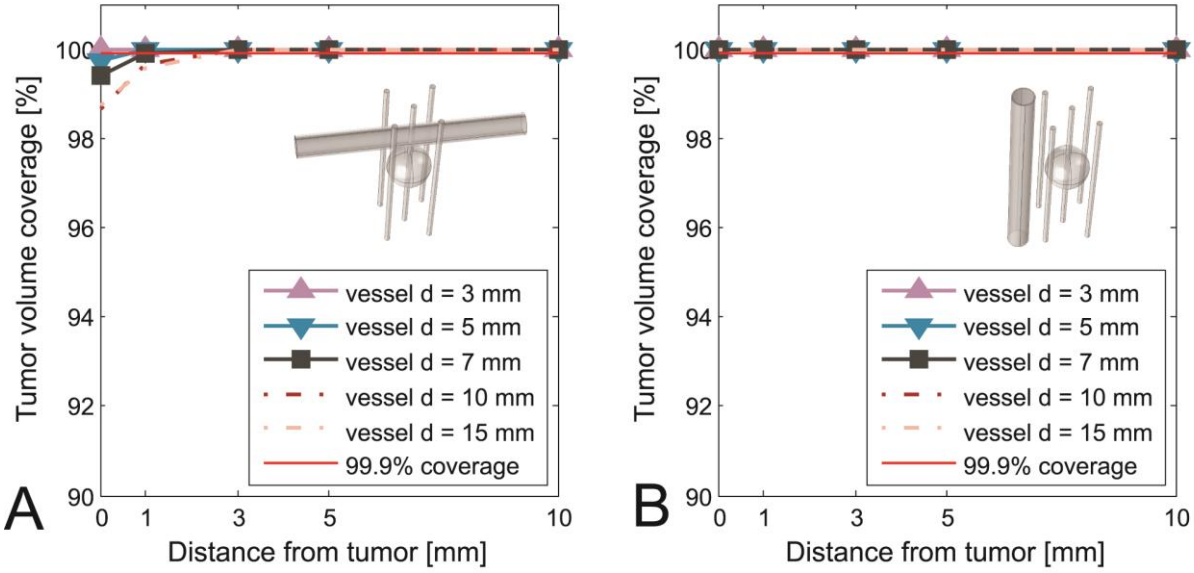

Figure 6. Tumor coverage for ECT of simplified model of 10 mm tumor with 5 electrodes. The coverage is plotted against different distances between vessel and tumor, and with respect to different vessel positions and sizes. A. Vessel perpendicular to the electrodes. B. Vessel parallel to the electrodes. *(The figure is originally Figure 4. from Paper 2.)*

Besides performing theoretical numerical calculations I have also performed a series of experiments on models based on real patient images of the liver where the vessels were close to the tumor. In these experiments I have first taken vessels into account while determining optimal treatment parameters, after which I would introduce variants of the error of my vessel segmentation algorithm that I have previously determined. Namely, I performed left, right, up and down shifts an enlargement and shrinking of the vessels where the value of these deformations was 1 pixel or 3 pixels. These values are in fact integer values of average symmetric surface distance and Hausdorff distance respectively, the error metrics I used to evaluate my segmentation algorithm in the previous chapter. By observing the changes in the electric field distribution after introducing the error into vessel geometry but keeping the treatment parameters unchanged I was able to determine the robustness of my proposed method for automatic vessel segmentation. The obtained results follow the ones reported for the theoretical model above: the segmentation method is robust enough not to affect the tumor coverage with possible errors, but only in the case the central electrode is used during treatment.

EDITING AND VALIDATION OF RESULTS OF THE AUTOMATIC SEGMENTATION

Recent advances in the field of medical image segmentation are producing new, more accurate and faster algorithms now more than ever. Moreover, methods for automatic segmentation are appearing that are deemed accurate enough to bridge the problem of intra-rater and inter-rater variability which appears in manual segmentation (Warfield et al. 2004). Still, in the applications where the cost of possible segmentation error is high (such as any treatment planning) the human factor can still not be completely eliminated. In such cases results of automatic segmentation can be used as a starting point for trained experts who can then examine and correct the results if necessary (Deeley et al. 2013).

Having the treatment planning process for electroporation-based treatments encapsulated in a web-based tool provided a perfect platform for integration of segmentation validation and editing mechanisms. The general idea of such a tool was to provide the clinicians with an easy way to adjust the segmented contours while still giving them enough control over the level of detail and the amount of change they wanted to make. To this end I have designed an editing tool that represents the segmentation results in the form of connected contour points which are overlaid over original 2D image slices. The choice of 2D was made since it is the view clinicians usually use in other imaging applications and is therefore most straightforward to them. The user can adjust the contour by simply clicking on a point and dragging it to a new position. He/she can also delete or add new points. The implementation of the editing and validation module in the web-based tool for treatment planning is shown in Figure 7.

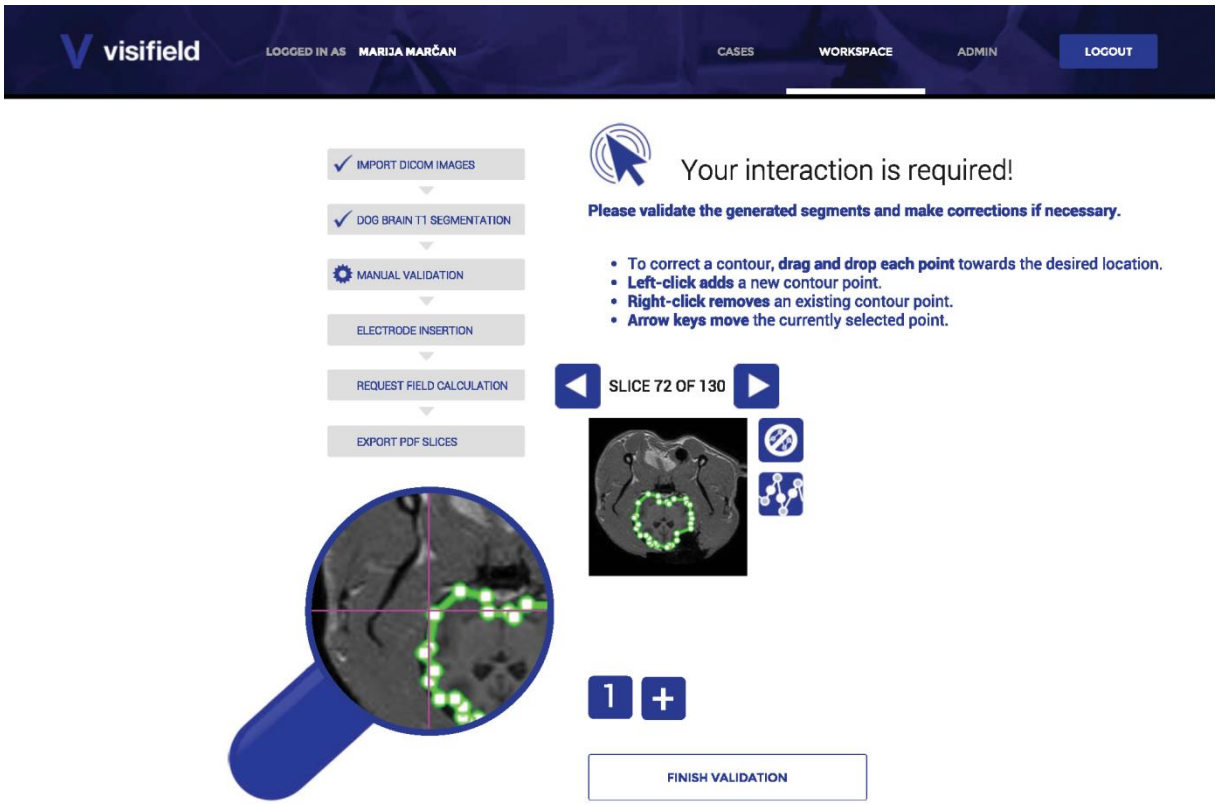

Figure 7. Segmentation editing implemented inside a web-based tool for electroporation treatment planning. *(The figure is originally Figure 5.B from Paper 3.)*

The specificity of this module is the way in which it enables the user to control the level of detail and amount of change. Since showing all points of the segmented contour would be too crowded and confusing, the user is initially shown only 20% of all the contour points. The decision of which points to show is made by iterative calculation of point weight and contour reduction. Point weight is a value that describes the importance a certain point has for contour form and is calculated based on an angle and length between the two edges of the contour adjacent to that point (Latecki & Lakämper 1999). The user can change the level of contour detail, i.e. *refine* the contour at any time by changing the percentage value of the total number of points, after which new points to be shown are calculated based on the same method described above. The refinement of the contour is performed on the level of one slice.

A specific case of contour point reduction is performed in the case the user has already changed some part of the contour. Since new points to be shown are always calculated based

on an existing full contour that is stored in the database, if that contour has been changed on some level of detail the database contour needs to be updated before new point reduction can be made. To this end I have implemented a cubic spline interpolation method that reconstructs the contour between the points the user has moved while all other points of the full contour remain unchanged.

Performance of the proposed validation and editing tool has so far been evaluated by five experts from four different institutions. Evaluation was performed as a part of the whole treatment planning procedure and the users were able to use any medical images for that purpose. Although the initial feedback regarding the editing and validation tool is positive further elaborate study should be made where the tool could be compared to some other editing methods.

SEGMENTATION ALGORITHM IMPROVEMENT BASED ON DATABASE OF VALIDATED SEGMENTED IMAGES

Including the segmentation validation as a mandatory step in the treatment planning workflow also results in a continuously growing database of expert segmentations. Such databases are valuable as they can be used for development of new or improvement of existing algorithms, a benefit I also wanted to explore in my work. The underlying assumption for my work was that not only pairs of original images and accurate segmentations can influence better future segmentations, but also other data which can be stored along with the images, such as imaging meta-information contained in DICOM header.

Since the algorithm for automatic segmentation of the vessels did not rely on any fixed parameters that could be optimized based on new cases I have implemented a segmentation method for prostate, an organ which is also of high interest for electroporation-based treatment. The implemented method is multi-atlas based (Litjens et al. 2012), where one atlas is a pair of original image and its segmentation. Although the method has shown promising results and was applied for segmentation of different organs its main downside remains long performance time due to the need to register each atlas image to the target image that is being segmented. In the past various methods for selecting a subset of most similar atlases were explored with the aim of reducing segmentation time and improving the results (Rohlfing et al. 2004; Wu et al. 2007; Aljabar et al. 2009; Langerak et al. 2013). However, none

of the proposed selection methods explored the possibility of utilizing imaging meta-information.

In my work I have formulated a framework for atlas selection based on manufacturer of the imaging machine, strength of the imaging machine, and presence of endorectal coil. Such choice of parameters was made with accordance to the publicly available testing dataset, which was a part of a grand challenge in prostate segmentation from MRI (Litjens et al. 2014) and as such did not disclose full image meta-information. The dataset was still highly appropriate for testing of my atlas selection method as it contained images from four different institutions which had overlapping properties. Besides choosing the atlases based on image meta-information I have also included rater variability into the framework formulation in order to try and account for less-than-perfect human raters.

I have compared my proposed atlas selection method with segmentation performed on all available atlases and with atlas selection based only on coil selection. In addition, I have combined all of the atlas selection strategies with two different label fusion methods in order to eliminate possible bias due to choice of label fusion strategy. The results, shown in Table 2, indicate better performance of my atlas selection method over the no-selection strategy in both segmentation results and time. Better performance was also confirmed in the subsequent paired difference statistical tests, even for atlas selection based only on coil presence.

Table 2. Results of leave-one-out experiments on training data for different atlas selection and label fusion strategies. *(The table is originally Table 2. from Paper 4.)*

Atlas selection + label fusion variation	Mean DSC	Median DSC	Performance time (min)
All atlases + SIMPLE	0.75	0.80	32
All atlases + STAPLE	0.72	0.76	37
Coil-based selection + SIMPLE	0.76	0.81	14
Coil-based selection + STAPLE	0.77	0.81	14
Image meta-information + rater variability + SIMPLE	0.77	0.82	14
Image meta-information + rater variability + STAPLE	0.77	0.81	14

The presented results were obtained from a relatively small set of available images (only 50) compared to a possible database of images that could be collected through routine use of the web-based treatment planning tool. Having a larger dataset of images from many different institutions would emphasize the advantages of the proposed atlas selection method even more. Also, the method has space for improvement through inclusion of other imaging parameters, such as contrast agent and imaging protocol.

CONCLUSION

The main focus of the work presented in this doctoral dissertation was to bring treatment planning for electroporation-based treatments of deep-seated tumors closer to routine use in the clinic by ensuring fast and reliable creation of 3D models based on medical images. Automatizing of the process of medical image segmentation allows it to be encapsulated together with the numerical modeling procedures into a tool that can be used to generate treatment plans without the need to possess elaborate engineering knowledge.

The presented thesis began with research and development of an automatic segmentation method of hepatic vessels from MRI images as a support to a clinical study of electrochemotherapy of colorectal liver metastases. The developed method was validated using both phantoms and medical images of the patients. Additionally, in order to better determine the impact of possible segmentation errors on the outcome of the electroporation-based treatment, a sensitivity study was performed. The study observed the impact of vessels in general and evaluated errors of the proposed segmentation method on the distribution of the electric field in the tumor. The distribution of the electric field is in direct correlation with treatment success, as the prerequisite for success is to cover the whole tumor by a sufficiently high electric field. The results of the sensitivity study show that the proposed vessel segmentation method is robust enough to be used in automatic treatment-planning for electroporation-based treatment of liver tumors which are situated near the vessels. It has also shown that vessels need to be included in calculation while performing treatment planning.

Although a certain medical image segmentation method may in general be robust enough, the risk of making an error in the process of treatment planning is too large to completely eliminate the human factor. For this reason the scope of this work also included development

of a method for validation and editing of the results of the automatic segmentation by the experts. The developed method was tailored to current use preferences of clinical radiologists but is also intuitive to use by experts from other fields. The method has already been integrated into the existing web-based tool for treatment-planning and is being used by users from several institutions (www.visifield.com).

Collecting the validated and edited segmentation results created by experts in the previous stage of this work results in a continuously growing database of expert segmentations. Such database is a valuable asset in development of any new segmentation algorithm and can also be used to close the segment-validate loop by improving the existing algorithms. To this end I have devised a strategy which can utilize not only original images and their segmentations but also all other image meta-information in order to produce better segmentations of new cases. The approach has been evaluated on the example of multi-atlas segmentation of prostate and shows advantages over conventional variation of that segmentation method in both segmentation results and performance time.

In conclusion, I believe that proposed methods and obtained results presented in this doctoral dissertation have set an important milestone in efforts to make the treatment planning process more easy to use for clinicians and also more reliable for the patients.

ORIGINAL CONTRIBUTIONS

SEGMENTATION OF CRITICAL STRUCTURES FOR ELECTROPORATION-BASED TREATMENTS OF DEEP-SEATED SOLID TUMORS

An algorithm for segmentation of critical structures (tubular structures like major vessels in the liver) provides the methods for numerical modeling of electroporation-based treatments with an accurate, patient-specific geometry, resulting in patient-specific treatment plans. Patient-specific treatment plans are a necessary prerequisite for performing electroporation-based treatments of deep-seated solid tumors. Segmentation algorithms that require minimum user input significantly reduce the time needed for generation of one electroporation-based treatment plan. Also, simplification of the electroporation-based treatment planning procedure from the clinician's point of view creates a more stimulating environment for attempts to use electroporation-based treatments for deep-seated solid tumors in new areas of the human body. In my work I have developed a new algorithm for automatic segmentation of hepatic vessels from MRI images. The accuracy of the segmentation algorithm was validated with respect to manual radiologist segmentation.

EFFECT OF NEARBY VESSEL STRUCTURES ON THE ELECTRIC FIELD DISTRIBUTION IN THE TUMOR

Extraction of patient’s anatomy through segmentation of medical images inevitably produces some errors. In order to ensure the robustness of treatment planning, it is necessary to evaluate the potential effect of such errors on the electric field distribution. In this part of my work I have focused on determining the effect of errors in automatic segmentation of hepatic vessels on the electric field distribution in electroporation-based treatments in the liver. In order to do this I first performed a numerical analysis on a simple ‘sphere and cylinder’ model

for tumors and vessels of different sizes and relative positions. Second, I performed an analysis of two models extracted from medical images of real patients in which I introduced variations of an error of the automatic vessel segmentation method.

AN ERGONOMIC METHOD FOR SEGMENTATION VALIDATION AND CORRECTIONS

Decades of development of medical image segmentation field have shown that it is still not possible to fully eliminate the assistance of humans from the segmentation procedure. Along with demands for segmentation method robustness set as high as they are for treatment planning, it is obvious that the human opinion needs to be included in order to ensure valid 3D models. The human opinion can be applied after the initial segmentation procedure as a form of a validation mechanism in order to ensure the necessary level of reliability. In order to facilitate this process of validation I have devised a method which requires minimum user input in order to reduce interaction time and user stress. Such mechanism of segmentation validation not only helps ensure validity of the treatment plans but also provides valuable feedback regarding segmentation algorithm performance.

EFFECTS OF NEW VALIDATED SEGMENTATIONS ON SEGMENTATION ALGORITHM IMPROVEMENT

Gathering of feedback through validations and corrections of segmentation by users results in creation of a database of segmented cases. Such database can be used as a source for gaining deeper insight about algorithm performance and algorithm improvement. While human segmentations are initially considered as true segmentations or ground truth and in general more reliable than machine segmentation, human segmentation is not perfect and is also prone to errors. Measures named intra-rater variability and inter-rater variability are often assessed for segmentation methods of various organs and tissues in order to assess the segmentation method quality. In my work I have thus developed an approach to systematically incorporate knowledge about rater variability and imaging parameters of existing segmentations in the database in order to produce better segmentations of new, unknown cases.

REFERENCES

Aljabar, P. et al., 2009. Multi-atlas based segmentation of brain images: atlas selection and its effect on accuracy. *NeuroImage*, 46(3), pp.726–38.

Al-Sakere, B. et al., 2007. Tumor ablation with irreversible electroporation. *PloS one*, 2(11), p.e1135.

Butz, T. et al., 2000. Pre- and Intra-operative Planning and Simulation of Percutaneous Tumor Ablation. In S. L. Delp, A. M. DiGoia, & B. Jaramaz, eds. *Proceedings of the Third International Conference on Medical Image Computing and Computer-Assisted Intervention (MICCAI)*. Pittsburgh, PA, USA: Springer Berlin Heidelberg, pp. 317–326.

Chen, C.-C.R., Miga, M.I. & Galloway, R.L., 2009. Optimizing electrode placement using finite-element models in radiofrequency ablation treatment planning. *IEEE transactions on bio-medical engineering*, 56(2), pp.237–245.

Corovic, S. et al., 2013. Modeling of electric field distribution in tissues during electroporation. *Biomedical engineering online*, 12, p.16.

Corovic, S., Zupanic, A. & Miklavcic, D., 2008. Numerical modeling and optimization of electric field distribution in subcutaneous tumor treated with electrochemotherapy using needle electrodes. *IEEE Transactions on Plasma Science*, 36(4 PART 3), pp.1665–1672.

Cukjati, D. et al., 2007. Real time electroporation control for accurate and safe in vivo non-viral gene therapy. *Bioelectrochemistry*, 70(2), pp.501–507.

Davalos, R. V., Mir, L.M. & Rubinsky, B., 2005. Tissue ablation with irreversible electroporation. *Annals of Biomedical Engineering*, 33(2), pp.223–231.

Deeley, M. a et al., 2013. Segmentation editing improves efficiency while reducing inter-expert variation and maintaining accuracy for normal brain tissues in the presence of space-occupying lesions. *Physics in medicine and biology*, 58(12), pp.4071–97.

Deng, X. & Du, G., 2008. Editorial: 3d segmentation in the clinic: a grand challenge II liver tumor segmentation. In *Proceedings of MICCAI workshop on 3D segmentation in the clinic: a grand challenge II*. New York, New York, USA, pp. 1–12.

Edhemovic, I. et al., 2011. Electrochemotherapy: a new technological approach in treatment of metastases in the liver. *Technology in cancer research & treatment*, 10(5), pp.475–485.

Edhemovic, I. et al., 2014. Intraoperative electrochemotherapy of colorectal liver metastases. *Journal of Surgical Oncology*, 110(3), pp.320–327.

Frangi, A.F. et al., 1998. Multiscale vessel enhancement filtering. In W. M. Wells, A. Colchester, & S. Delp, eds. *Medical Image Computing and Computer-Assisted Intervention - MICCAI '98 (1998)*. Cambridge, MA, USA: Springer Berlin Heidelberg, pp. 130–137.

Garcia, P. a et al., 2011. Non-thermal irreversible electroporation (N-TIRE) and adjuvant fractionated radiotherapeutic multimodal therapy for intracranial malignant glioma in a canine patient. *Technology in cancer research & treatment*, 10(1), pp.73–83.

Garcia, P. a, Davalos, R. V & Miklavcic, D., 2014. A numerical investigation of the electric and thermal cell kill distributions in electroporation-based therapies in tissue. *PLoS ONE*, 9(8), p.e103083.

Golberg, A. et al., 2015. Tissue heterogeneity in structure and conductivity contribute to cell survival during irreversible electroporation ablation by "electric field sinks." *Scientific Reports*, 5, p.8485.

Heller, L.C. & Heller, R., 2010. Electroporation gene therapy preclinical and clinical trials for melanoma. *Current gene therapy*, 10(4), pp.312–317.

Ivorra, A. & Rubinsky, B., 2007. In vivo electrical impedance measurements during and after electroporation of rat liver. *Bioelectrochemistry*, 70(2), pp.287–295.

Jiang, C., Davalos, R. V & Bischof, J.C., 2015. A Review of Basic to Clinical Studies of Irreversible Electroporation Therapy. *IEEE Transactions on Biomedical Engineering*, 62(1), pp.4–20.

Klein, S. et al., 2008. Automatic segmentation of the prostate in 3D MR images by atlas matching using localized mutual information. *Medical physics*, 35(4), pp.1407–1417.

Kos, B. et al., 2010a. Robustness of treatment planning for electrochemotherapy of deep-seated tumors. *Journal of Membrane Biology*, 236(1), pp.147–153.

Kos, B. et al., 2010b. Robustness of treatment planning for electrochemotherapy of deep-seated tumors. *The Journal of membrane biology*, 236(1), pp.147–53.

Kotnik, T. et al., 2012. Cell membrane electroporation- Part 1: The phenomenon. *IEEE Electrical Insulation Magazine*, 28(5), pp.14–23.

Langerak, T.R. et al., 2013. Multiatlas-based segmentation with preregistration atlas selection. *Medical physics*, 40(9), p.091701.

Latecki, L. & Lakämper, R., 1999. Convexity rule for shape decomposition based on discrete contour evolution. *Computer Vision and Image Understanding*, 73(3), pp.441–454.

Lecchi, M. et al., 2008. Current concepts on imaging in radiotherapy. *European journal of nuclear medicine and molecular imaging*, 35(4), pp.821–37.

Litjens, G. et al., 2014. Evaluation of prostate segmentation algorithms for MRI: the PROMISE12 challenge. *Medical image analysis*, 18(2), pp.359–73.

Litjens, G., Karssemeijer, N. & Huisman, H., 2012. A multi-atlas approach for prostate segmentation in MR images. *MICCAI Grand Challenge: Prostate MR Image Segmentation 2012*.

Marcan, M. et al., 2014. Segmentation of Hepatic Vessels from Mri Images for Planning of Electroporation-Based Treatments in the Liver. *Radiology and Oncology*, 48(3), pp.1–15.

Marty, M. et al., 2006. Electrochemotherapy – An easy, highly effective and safe treatment of cutaneous and subcutaneous metastases: Results of ESOPE (European Standard Operating Procedures of Electrochemotherapy) study. *European Journal of Cancer Supplements*, 4(11), pp.3–13.

Miklavcic, D. et al., 2006. Importance of tumour coverage by sufficiently high local electric field for effective electrochemotherapy. *European Journal of Cancer Supplements*, 4(11), pp.45–51.

Miklavcic, D. et al., 1998. The importance of electric field distribution for effective in vivo electroporation of tissues. *Biophysical journal*, 74(5), pp.2152–8.

Miklavcic, D. et al., 2010. Towards treatment planning and treatment of deep-seated solid tumors by electrochemotherapy. *Biomedical engineering online*, 9, p.10.

Miklavčič, D. et al., 2014. Electrochemotherapy: from the drawing board into medical practice. *Biomedical engineering online*, 13(1), p.29.

Miklavčič, D. et al., 2012. Electrochemotherapy: Technological advancements for efficient electroporation-based treatment of internal tumors. *Medical and Biological Engineering and Computing*, 50(12), pp.1213–1225.

Mir, L.M. et al., 1991. Electrochemotherapy potentiation of antitumour effect of bleomycin by local electric pulses. *European journal of cancer*, 27(1), pp.68–72.

Mir, L.M. et al., 2006. Standard operating procedures of the electrochemotherapy: Instructions for the use of bleomycin or cisplatin administered either systemically or locally and electric pulses delivered by the CliniporatorTM by means of invasive or non-invasive electrodes. *European Journal of Cancer Supplements*, 4(11), pp.14–25.

Neal, R.E. et al., 2012. Experimental characterization and numerical modeling of tissue electrical conductivity during pulsed electric fields for irreversible electroporation treatment planning. *IEEE Transactions on Biomedical Engineering*, 59(4), pp.1076–1085.

Neumann, E. et al., 1982. Gene transfer into mouse lyoma cells by electroporation in high electric fields. *The EMBO journal*, 1(7), pp.841–5.

Orlowski, S. et al., 1988. Transient electropermeabilization of cells in culture. *Biochemical Pharmacology*, 37(24), pp.4727–4733.

Otsu, N., 1979. A Threshold Selection Method from Gray-Level Histograms. *IEEE Transactions on Systems, Man, and Cybernetics*, 9(1), pp.62–66.

Pavliha, D., Mušič, M.M., et al., 2013. Electroporation-based treatment planning for deep-seated tumors based on automatic liver segmentation of MRI images. B. Rubinsky, ed. *PloS one*, 8(8), p.e69068.

Pavliha, D. et al., 2012. Patient-specific treatment planning of electrochemotherapy: Procedure design and possible pitfalls. *Bioelectrochemistry*, 87, pp.265–273.

Pavliha, D., Kos, B., et al., 2013. Planning of electroporation-based treatments using web-based treatment-planning software. *Journal of Membrane Biology*, 246(11), pp.833–842.

Pavselj, N. et al., 2005. The course of tissue permeabilization studied on a mathematical model of a subcutaneous tumor in small animals. *IEEE transactions on bio-medical engineering*, 52(8), pp.1373–81.

Pucihar, G. et al., 2011. Equivalent pulse parameters for electroporation. *IEEE transactions on bio-medical engineering*, 58(11), pp.3279–88.

Reberšek, M. et al., 2014. Cell membrane electroporation-Part 3: the equipment. *IEEE Electrical Insulation Magazine*, 30(3), pp.8–18.

Rohlfing, T. et al., 2004. Evaluation of atlas selection strategies for atlas-based image segmentation with application to confocal microscopy images of bee brains. *NeuroImage*, 21(4), pp.1428–1442.

Rubinsky, B., Onik, G. & Mikus, P., 2007. Irreversible electroporation: a new ablation modality--clinical implications. *Technology in cancer research & treatment*, 6(1), pp.37–48.

Saad, A., Hamarneh, G. & Möller, T., 2010. Exploration and visualization of segmentation uncertainty using shape and appearance prior information. *IEEE transactions on visualization and computer graphics*, 16(6), pp.1366–75.

Sano, M.B. et al., 2010. Towards the creation of decellularized organ constructs using irreversible electroporation and active mechanical perfusion. *Biomedical engineering online*, 9(1), p.83.

Scheffer, H.J. et al., 2014. Irreversible electroporation for nonthermal tumor ablation in the clinical setting: a systematic review of safety and efficacy. *Journal of vascular and interventional radiology : JVIR*, 25(7), pp.997–1011.

Schwarzmaier, H.J. et al., 1998. Treatment planning for MRI-guided laser-induced interstitial thermotherapy of brain tumors - The role of blood perfusion. *Journal of Magnetic Resonance Imaging*, 8(1), pp.121–127.

Serša, G., Čemažar, M. & Miklavčič, D., 1995. Antitumor effectiveness of electrochemotherapy with cis-diamminedichloroplatinum(II) in mice. *Cancer Research*, 55(15), pp.3450–3455.

Šel, D. et al., 2005. Sequential finite element model of tissue electropermeabilization. *IEEE Transactions on Biomedical Engineering*, 52(5), pp.816–827.

Vovk, U., Pernuš, F. & Likar, B., 2007. A review of methods for correction of intensity inhomogeneity in MRI. *IEEE Transactions on Medical Imaging*, 26(3), pp.405–421.

Warfield, S.K., Zou, K.H. & Wells, W.M., 2004. Simultaneous truth and performance level estimation (STAPLE): an algorithm for the validation of image segmentation. *IEEE transactions on medical imaging*, 23(7), pp.903–21.

Withey, D.J. & Koles, Z.J., 2008. A Review of Medical Image Segmentation : Methods and Available Software. *International Journal of Bioelectromagnetism*, 10(3), pp.125 – 148.

Wong, K.-P., 2005. Medical image segmentation: Methods and applications in functional imaging. In J. Suri, D. Wilson, & S. Laxminarayan, eds. *Handbook of Biomedical Image Analysis – Volume 2: Segmentation Models Part B*. Topics in Biomedical Engineering International Book Series. Kluwer Academic/Plenum Publishers, pp. 111–182.

Wu, M. et al., 2007. Optimum template selection for atlas-based segmentation. *NeuroImage*, 34(2), pp.1612–1618.

Yarmush, M.L. et al., 2014. Electroporation-Based Technologies for Medicine: Principles, Applications, and Challenges. *Annual Review of Biomedical Engineering*, 16(1), pp.295–320.

Zhang, L., Widera, G. & Rabussay, D., 2004. Enhancement of the effectiveness of electroporation-augmented cutaneous DNA vaccination by a particulate adjuvant. In *Bioelectrochemistry*. pp. 369–373.

Zupanic, A., Kos, B. & Miklavcic, D., 2012. Treatment planning of electroporation-based medical interventions: electrochemotherapy, gene electrotransfer and irreversible electroporation. *Physics in medicine and biology*, 57(17), pp.5425–40.

Županič, A., Čorović, S. & Miklavčič, D., 2008. Optimization of electrode position and electric pulse amplitude in electrochemotherapy. *Radiology and Oncology*, 42(2), pp.93–101.

Županič, A. & Miklavčič, D., 2010. Optimization and Numerical Modeling in Irreversible Electroporation Treatment Planning A Brief Overview of Irreversible Electroporation Basics. In B. Rubinsky, ed. *Technology in cancer research & treatment*. Springer-Verlag Berlin Heidelberg, pp. 255–260.